Dissertation

submitted to the

Combined Faculty of Natural Sciences and Mathematics

of the Ruperto Carola University Heidelberg, Germany

for the degree of

Doctor of Natural Sciences

Presented by

Minakshi Gandhi, M. Sc. Biotechnology

Born in: Malkapur, Maharashtra India

Oral examination: 28th August 2019

This page has been intentionally left blank

Role of long non-coding RNA *lincNMR* in nucleotide metabolism in cancer

Referees:

Prof. Dr. Peter Angel

Prof. Dr. Sven Diederichs

This page has been intentionally left blank

TABLE OF CONTENTS

TABLE OF CONTENTS i

PUBLICATIONS vii

POSTER PRESENTATION viii

AWARDS AND GRANTS ix

ABSTRACT xi

ZUSAMMENFASSUNG xiii

LIST OF FIGURES xv

LIST OF TABLES xvi

ABBREVIATIONS xvii

1. INTRODUCTION 1

1.1 Liver Cancer 1

1.1.1 Epidemiology 1

1.1.2 Risk factors 1

1.1.3 Pathogenesis 2

1.1.4 Diagnosis, prognosis and treatment 2

1.2 Non-coding RNAs 3

1.2.1 Background and discovery 3

1.2.2 Long non-coding RNAs – classification 3

1.2.3 Long non-coding RNA – characterization and expression regulation 4

1.2.4 Long non-coding RNAs – in regulation of hallmarks of cancer 5

1.2.5 Long non-coding RNAs – as drivers of hepatocarcinogenesis 5

1.2.6 Long non-coding RNAs – molecular mechanisms in HCC 5

1.3 Cell Proliferation, Senescence and Nucleotide Metabolism 6

1.3.1 Cell cycle regulation in normal liver 6

1.3.2 Deregulation of proliferation and cell cycle in HCC 7
1.3.3 Cellular Senescence 7
1.3.4 Nucleotide Metabolism 8
1.3.5 Nucleotide metabolism in cell proliferation 8
1.3.6 Long non coding RNAs – Senescence and Nucleotide Metabolism 9
2. AIMS OF MY DOCTORAL PROJECT 11
3. MATERIALS 13
3.1 Reagents and chemicals 13
3.2 Kits and consumables 17
3.2.1 Kits 17
3.2.2 Consumables 17
3.3 Buffers and solutions 18
3.4 Equipments and devices 20
3.5 Nucleic acid sequences 22
3.5.1 siPOOL sequences 22
3.5.2 RT - qPCR primer sequences 30
3.5.3 Sequences of 5’ and 3’ RACE primer 32
3.5.4 Sequences of biotinylated DNA oligos 32
3.6 Biological material 33
3.6.1 Human cancer cell lines 33
3.6.2 Antibodies 33
3.6.3 Plasmids 34
3.7 Softwares 34
3.8 Online tools and databases used in this study 35
4. METHODS 37
4.1 Human cancer cell lines 37
4.1.1 Growth and propagation of human cancer cell lines 37

4.1.2 Cryopreservation of cells lines 38
4.1.3 Thawing of cryo - preserved cells 38
4.1.4 Cell line authentication and mycoplasma test 38
4.2 Transfections 38
4.2.1 siPOOL transfections 38
4.2.2 Plasmid transfections 38
4.3 RNA isolation, reverse transcription and quantitative PCR 39
4.3.1 RNA isolation using TRIzol 39
4.3.2 RNA isolation using kits 39
4.3.3 DNase digestion of total RNA 39
4.3.4 DNase digestion of RNA isolated using kits 40
4.3.5 Reverse transcription 40
4.3.6 qPCR primer design 40
4.3.7 qPCR 40
4.4 Protein isolation, quantitation, western blot 41
4.4.1 Protein lysate preparation 41
4.4.2 Bicinchoninic Acid (BCA) assay 41
4.4.3 Sodium Dodecyl Sulfate - Polyacrylamide Gel Electrophoresis (SDS-PAGE) 41
4.4.4 Western Blot 42
4.5 Plasmid isolation, purification and sequencing 42
4.5.1 Generation of plasmids in Gateway vector system 42
4.5.2 Genomic DNA isolation 43
4.5.3 Transformation of bacteria 43
4.5.4 Plasmid DNA isolation 43
4.6 Basic characterization of *lincNMR* 44
4.6.1 Subcellular fractionation 44
4.6.2 Rapid Amplification of cDNA ends (RACE) 45
4.7 Cellular function of *lincNMR* 45

4.7.1 Cell viability assay 45
4.7.2 Cell proliferation assay 45
4.7.3 Cell cycle analysis 46
4.7.4 Senescence associated β-GAL assay 46
4.8 Molecular Function 46
4.8.1 Triple label SILAC-MS 46
4.8.2 *In vivo* RNA Antisense Purification - Mass Spectrometry (*In vivo* RAP - MS) 47
4.8.3 Crosslinking RNA Immunoprecipitation (UV - RIP) 47
4.8.4 dNTP measurement assay 48
4.8.5 dNTP bathing assay 49
4.8.6 Luciferase reporter assay 49
4.8.7 Chick Chorioallantoic Membrane (CAM) Assay 49
4.9 Statistical analysis, softwares, databases and online tools 49
4.9.1 T-TEST 49
4.9.2 Software, databases and online tools 50
5. RESULTS 51
5.1 Transcriptome-wide expression analysis of lncRNAs in liver cancer 51
5.2 Basic characterization of *lincNMR* 54
5.2.1 *lincNMR* is a long non-coding RNA 54
5.2.2 *lincNMR* is a predominantly cytoplasmic lncRNA 56
5.3 Cellular function of *lincNMR* 57
5.3.1 Depletion of *lincNMR* invokes a strong proliferation defect in multiple cancer cell lines 57
5.3.2 Silencing of *lincNMR* causes a cell cycle arrest in G0/G1 phase of cell cycle 59
5.3.3 Loss of *lincNMR* triggers an induction of senescence in multiple cancer cell lines 59
5.4 Molecular function of *lincNMR* 61
5.4.1 RAP-MS to identify direct protein binding partner*s of lincNMR* 61
5.4.2 *lincNMR* directly binds to YBX1 protein, which regulates cell survival 62

5.4.3 Validation of *lincNMR* - YBX1 interaction using UV - RIP 63
5.4.4 Silencing of YBX1 mimics the phenotype induced by *lincNMR* depletion 64
5.4.5 *LincNMR* directly binds to YBX1 and regulates its transactivational activity 65
5.4.6 Total cellular proteome after *lincNMR* depletion using triple-label SILAC approach 66
5.4.7 Loss of *lincNMR* causes downregulation of key enzymes in nucleotide metabolism 67
5.4.8 Silencing of RRM2, TK1 and TYMS also mimics the phenotype induced by *lincNMR* loss 69
5.4.9 *LincNMR* and YBX1 share common target genes regulating nucleotide metabolism 70
5.4.10 *LincNMR* target genes are regulated and associated with poor survival in liver cancer 70
5.4.11 Depletion of *lincNMR* leads to reduced dNTP levels in liver cancer 73
5.4.12 Extracellular supply of dNTPs rescues the phenotype induced by depletion of *lincNMR* ... 74
5.5 Potential clinical significance of *lincNMR* in cancer 75
5.5.1 *lincNMR* is induced and regulated in multiple cancer entities 75
5.5.2 *lincNMR* is also expressed in multiple human cancer cell lines 76
5.5.3 *lincNMR* induced knockdown and growth inhibitory phenotype is stable until 168 h 77
5.5.4 Depletion of *lincNMR* leads to decreased tumor size and growth *in vivo* 78
6. DISCUSSION 79
7. FURTHER EXPERIMENTAL DIRECTIONS FOR THIS PROJECT 88
8. ACKNOWLEDGEMENTS 92
9. APPENDIX 95
9.1.1 LncRNA expression data from liver cancer patient dataset from TANRIC 95
9.1.2 List of 49 lncRNAs screened for expression in 9 liver cancer cell lines 101
9.1.3 Genbank submission of *lincNMR* sequences 102
9.1.4 List of candidates identified in *lincNMR* RAP-MS 103
9.1.5 Proteome after *lincNMR* depletion 104
10. REFERENCES 111
DECLARATION 124

PUBLICATIONS

List of publications during my time as a PhD student

Gandhi M, Gross M, Holler J, Patil N, Leupold J, Munschauer M, Hartigan C, Schenone M, Allgayer H, Baek K, Diederichs S. *"lincNMR* regulates Nucleotide Metabolism via a YBX1 - RRM2 Axis in Cancer" **Nature Communications** (Manuscript under review – original article)

Gandhi M, Caudron-Herger M, Diederichs S
"RNA motifs and combinatorial prediction of interactions, stability and localization of noncoding RNAs" **Nature Structure and Molecular Biology (2018) 25(12):1070-1076** (Review)

Nötzold L, Frank L, **Gandhi M**, Polycarpou-Schwarz M, Gross M, Gunkel M, Beil N, Erfle H, Harder N, Rohr K, Trendel J, Krijgsveld J, Longerich T, Schirmacher P, Boutros M, Erhardt S, Diederichs S: "The long non-coding RNA LINC00152 is essential for cell cycle progression through mitosis in HeLa cells." **Scientific Reports 2017 7(1):2265** (Original article)

Goyal A, Fiškin E, Gutschner T, Polycarpou-Schwarz M, Gross M, Neugebauer J, **Gandhi M**, Caudron-Herger M, Benes V, Diederichs S
"A cautionary tale of sense-antisense gene pairs: independent regulation despite inverse correlation of expression."
Nucleic Acid Research. 2017 45(21):12496-12508 (Original article)

POSTER PRESENTATION

List of conferences where I contributed through this project with a poster during my PhD

MAY 29th – JUN 3rd 2019: Cold Spring Harbor, NY USA

84th CSHL Symposium on RNA Control and Regulation

Minakshi Gandhi, Matthias Gross, Jessica Holler, Nitin Patil, Joerg Leupold, Matthias Munschauer, Heike Allgayer, Kim Baek, Eric Lander, Sven Diederichs

***lincNMR* regulates Nucleotide Metabolism via a YBX1 - RRM2 Axis in Cancer**

FEB 25th – MAR 1st 2018: Keystone, CO USA

Non Coding RNAs: Forms, Function Physiology

Minakshi Gandhi, Matthias Gross, Mathias Munschauer, Eric Lander, Sven Diederichs

Depletion of the long non-coding RNA *SINCR1* inhibits cell proliferation and induces senescence in liver cancer cells

OCT 11th – 14th 2017: Regensburg, Germany

SFB 960 Symposium: The Biology of RNA - Protein Complexes

Minakshi Gandhi, Matthias Gross, Mathias Munschauer, Eric Lander, Sven Diederichs

Depletion of the long non-coding RNA *SINCR1* inhibits cell proliferation and induces senescence in liver cancer cells

JUL 05th – 07th 2017: Weil der Stadt, Germany

German Cancer Research Center (DKFZ) PhD Retreat **Minakshi Gandhi,** Mathias Munschauer, Eric Lander, Sven Diederichs

The tumor-induced lncRNA *SINCR1* controls cell proliferation and induces senescence in liver cancer

NOV 22nd 2015: Kloester Schoental, Germany

Functional & Structural Genomics – Research Program B Retreat

Minakshi Gandhi, Sven Diederichs

In vivo RNA affinity purification to elucidate lncRNA - protein networks

AWARDS AND GRANTS

Following is the list of awards / grants I received during PhD

2019: **CSHL Scholarship / Registration Bursary**

84th Symposium on RNA Control and Regulation at Cold Spring Harbor Laboratory, NY USA

2017: Best Poster Award

SFB 960 Symposium: The Biology of RNA-Protein Complexes, Regensburg, BY Germany

2017: Travel Grant

SFB 960 Symposium: The Biology of RNA-Protein Complexes, Regensburg, BY Germany

2017: Best Poster Award

DKFZ PhD Retreat, Weil der Stadt, BW Germany

2014: Full Doctoral Scholarship, Deutscher Akademischer Austauschdient (DAAD)

German Academic Exchange Service (DAAD), Bonn, NRW Germany

2014: External training award from Graduate School of Life Sciences, University of Wuerzburg

To participate in FELASA – B: "Basic Animal handling" in Berlin, BB Germany

This page has been intentionally left blank

ABSTRACT

Whole transcriptome analysis of the human genome has revealed that the majority of the genome gives rise to non-protein-encoding or simply non-coding RNAs (ncRNAs). Long non-coding RNAs (lncRNAs) ranging from 200 nt to >100 kb represent a large subgroup of ncRNAs. They have emerged as critical players for not only regulating various physiological and developmental processes but also various cancers including liver cancer. Global cancer statistics report of 2018 has shown liver cancer to be the fourth leading cause of cancer-related deaths worldwide and has predicted it to be the sixth most commonly diagnosed cancer. Notably, advanced stage liver cancer has a poor overall survival rate of less than 20 % - thus warranting further investigations into the understanding of molecular mechanisms driving hepatocarcinogenesis, contributing to the discovery of improved diagnostic, prognostic and treatment modalities.

Here, I performed a transcriptome-wide profiling of lncRNAs in liver cancer and identified a novel lncRNA, which I named *lincNMR* (long intergenic non-coding RNA - Nucleotide Metabolism Regulator). *LincNMR* was induced six-fold in hepatocellular carcinoma compared to normal liver tissue. Depletion of *lincNMR* in multiple liver cancer cell lines invoked a strong proliferation defect and lead to an induction of senescence. This phenotype was also observed in multiple breast and lung cancer cell lines suggesting cancer-wide role of *lincNMR*. Silencing of *lincNMR* caused a strong depletion of the key dNTP synthesizing enzymes RRM2, TK1 and TYMS implicating *lincNMR* in regulation of nucleotide metabolism. Notably, dNTP levels were significantly decreased in liver cancer cells upon the loss of *lincNMR*. Importantly, the proliferation defect induced by downregulation of *lincNMR* could be rescued by bathing the cells in exogenous pools of extracellular dNTPs. An *in vivo* RNA Antisense Purification combined with mass spectrometry (RAP-MS) approach identified YBX1 as a direct interaction partner of *lincNMR*. Furthermore, I show YBX1 as a regulator of RRM2, TK1 and TYMS gene expression and found *lincNMR* to control the transactivational activity of YBX1 as measured in luciferase assays. Lastly, I established the relevance of *lincNMR* for tumor growth *in vivo* using the Chick Chorioallantoic Membrane (CAM) model. *LincNMR*-depleted tumors were significantly smaller in size and weight. In summary, I discovered a novel lncRNA, *lincNMR*, which regulates tumor cell proliferation through a YBX1-RRM2-TK1-TYMS axis governing nucleotide metabolism.

This page has been intentionally left blank

ZUSAMMENFASSUNG

Die vollständige Transkriptomanalyse des menschlichen Genoms erwies, dass ein Großteil des Genoms zu nicht-proteinkodierenden beziehungsweise nicht-kodierenden RNAs (ncRNAs) umgeschrieben wird. Lange, nicht-kodierende RNAs (lncRNAs) im Bereich von 200 nt bis >100 kb stellen eine große Untergruppe von ncRNAs dar. Sie sind nicht nur wichtige Akteure in verschiedenen physiologischen und entwicklungsbezogenen Prozessen, sondern auch Regulatoren verschiedener Krebsarten, wie Leberkrebs. Der globale Krebsstatistikbericht von 2018 hat gezeigt, dass Leberkrebs die vierthäufigste Ursache für krebsbedingte Todesfälle weltweit, sowie die sechsthäufigste diagnostizierte Krebsart ist. Zudem weist Leberkrebs im fortgeschrittenen Stadium eine sehr niedrige Gesamtüberlebensrate von weniger als 20 % auf. Dies rechtfertigt weitere Untersuchungen zum Verständnis der molekularen Mechanismen, welche die Hepatokarzinogenese antreiben. Die daraus gewonnenen Erkenntnisse tragen zur Entdeckung verbesserter Diagnose- Prognose- und Behandlungsmethoden bei.

In der vorliegenden Arbeit habe ich eine Transkriptomprofilierung von lncRNAs in Leberkrebs durchgeführt und eine neue lncRNA identifiziert, die ich *lincNMR* (long intergenic non-coding RNA-Nucleotide Metabolism Regulator) genannt habe. *LincNMR* lag im hepatozellulären Karzinom im Vergleich zu normalem Lebergewebe sechsfach induziert vor. Die Depletion von *lincNMR* verursachte einen starken Proliferationsdefekt in diversen Leberkrebszelllinien und führte zu einer Induktion der Seneszenz. Dieser Phänotyp wurde auch in mehreren Brust- und Lungenkrebszelllinien beobachtet, was auf eine krebsweite Rolle von *lincNMR* hindeutet. Die Stilllegung von *lincNMR* führte zu einer starken Abnahme der wichtigsten dNTP-synthetisierenden Enzyme RRM2, TK1 und TYMS. Dies impliziert eine Regulation des Nukleotidstoffwechsels durch *lincNMR*. Insbesondere waren die dNTP-Spiegel in Leberkrebszellen nach dem Verlust von *lincNMR* signifikant gesenkt. Hervorzuheben ist, dass der durch die Runterregulierung von lincNMR induzierte Proliferationsdefekt durch Zugabe von extrazellulären dNTPs zu den Zellen aufgehoben werden konnte. Eine Kombination aus *in vivo* RNA Antisense Aufreinigung und Massenspektrometrie (RAP-MS) identifizierte YBX1 als direkten Interaktionspartner von *lincNMR*. Zudem zeige ich, dass YBX1 die Genexpression von RRM2, TK1 und TYMS reguliert. Dass wiederum lincNMR die Transaktivierungsaktivität von YBX1 steuert, erwies die Durchführung eines Luciferase-Assays. Schließlich untersuchte ich die Relevanz von *lincNMR* für das Tumorwachstum *in vivo* mittels eines Hühnerei-Chorion-Allantoic-Membran (CAM)-Tests. Größe und Gewicht von lincNMR-depletierten Tumoren waren im Vergleich zu nicht-depletierten Tumoren signifikant reduziert. Zusammenfassend

habe ich eine neuartige lncRNA, *lincNMR*, entdeckt, welche die Proliferation von Tumorzellen über die nukleotidstoffwechselsteuernde YBX1-RRM2-TK1-TYMS-Achse reguliert.

LIST OF FIGURES

Figure 1: Schematic: Transcriptome-wide lncRNA profiling in liver cancer 52
Figure 2: *lincNMR* emerged as a candidate with the strongest impact on cell viability 53
Figure 3: Basic characterization of *lincNMR* 55
Figure 4: *lincNMR* is non-coding and predominantly cytoplasmic 56
Figure 5: Depletion of *lincNMR* invokes a proliferation defect in multiple cancer cell lines 58
Figure 6: Silencing of *lincNMR* caused a cell cycle arrest in G0/G1 phase 59
Figure 7: Loss of *lincNMR* triggers an induction of senescence and SASP 60
Figure 8: Schematic: *LincNMR in vivo* RNA Antisense Purification (RAP-MS) 61
Figure 9: YBX1 has a strongest association with survival in liver cancer patients 62
Figure 10: Direct interaction between *lincNMR* - YBX1 validated by UV – RIP 63
Figure 11: Depletion of YBX1 mimics phenotype induced by *lincNMR* depletion 64
Figure 12: *LincNMR* regulated the transactivation activity of YBX1 in liver 65
Figure 13: Schematic overview and reproducibility of triple-label SILAC experiment 66
Figure 14: Panther overrepresentation analysis reveals enrichment of key cell cycle terms 67
Figure 15: Loss of *lincNMR* causes depletion of enzymes regulating nucleotide metabolism 68
Figure 16: Depletion of *RRM2*, *TK1* and *TYMS* mimicks the phenotype induced by *lincNMR* loss 69
Figure 17: Loss of YBX1 also regulates *lincNMR* target genes RRM2, TK1 and TYMS 70
Figure 18: *RRM2*, *TK1* and *TYMS* are expressed and regulated in liver cancer 71
Figure 19: Impact of *lincNMR* target genes on survival in liver cancer 72
Figure 20: Correlation of expression between *lincNMR* and its targets in liver cancer patients 72
Figure 21: Depletion of *lincNMR* leads to reduced dNTP levels 73
Figure 22: Exogenous supply of dNTPs rescues the phenotype induced by *lincNMR* loss 74
Figure 23: *lincNMR* is induced in multiple cancer entities 75
Figure 24: *lincNMR* is also expressed in multiple human cancer cell lines 76
Figure 25: *lincNMR*-induced phenotype using siPOOLs is stable until day 7 after transfection 77
Figure 26: Loss of *lincNMR* leads to decreased tumor weight and size in vivo 78
Figure 27: Multiscatter plot for phosphoproteomics dataset as a quality control reproducibility 88
Figure 28: Depletion of *lincNMR* leads to strong induction of UBE2O phosphorylation 89
Figure 29: *lincNMR* levels correlates with *UBE2O* where UBE2O expression is linked to survival in liver cancer patients 90

LIST OF TABLES

Table 1. List of reagents and chemicals used in this study 13
Table 2. List of kits used in this study 17
Table 3. List of consumables used in this study 17
Table 4. Buffers and solutions recipes used in this study 18
Table 5. List of equipments and devices used in this study 20
Table 6. List of siPOOLs used in this study 22
Table 7. List of RT - qPCR primers used in this study 30
Table 8. List of primers used for 5' and 3' RACE experiments 32
Table 9. Sequences of biotinylated DNA oligos used for *lincNMR* RAP-MS 32
Table 10. Cell line, origin, growth medium and biosafety level 33
Table 11. List of antibodies used in this study 33
Table 12. List of plasmids used in this study 34
Table 13. List of softwares used in this study 34
Table 14. List of web tools used in this study 35
Table 15. LncRNA expression data of 217 lncRNAs with FC > 5 and p-value < 0.001 95
Table 16: RT-qPCR expression data for 49 lncRNAs in multiple HCC cell lines 101
Table 17: Sequences of *lincNMR* 5' and 3' RACE Clones submitted to Genbank 102
Table 18: List of candidates from *lincNMR* RAP-MS 103
Table 19: List of deregulated proteins post *lincNMR* loss (p < 0.001, data = *log2* ratios) 104

ABBREVIATIONS

Abbreviation	Full form
%	Percentage
°C	Degree Celsius
µg	Microgram
µl	Microliter
µM	Micromolar
aa	Amino acid
AASLD	American Association for the Study of Liver Diseases
ADC	Adenocarcinoma
AFP	α-fetoprotein
AML	Acute Myeloid Leukemia
AS	Antisense
ATCC	American Type Culture Collection
BCA	Bicinchoninic Acid
bp	Base pair(s)
BrdU	Bromodeoxyuridine
BSA	Bovine Serum Albumin
CAGE	Cap Analysis of Gene Expression
CAM	Chick Chorioallantoic Membrane
cDNA	Complementary DNA
CDS	Coding sequence
ceRNA	Competing endogenous RNA
ChIP	Chromatin Immunoprecipitation
ChIP-seq	Chromatin Immunoprecipitation sequencing
CML	Chronic Myelogenous Leukemia
CPC	Coding Potential Calculator
CSHL	Cold Spring Harbor Laboratory
CT	Cycle Threshold
dATP	Deoxyadenosine 5'-triphosphate
dCTP	Deoxycytidine 5'-triphosphate
dGTP	Deoxyguanine 5'-triphosphate
DKFZ	German Cancer Research Center

DMEM	Dulbecco's Modified Eagle's Medium
DMSO	Dimethyl Sulfoxide
DNA	Deoxyribonucleic Acid
dNTP	Deoxyribonucleotide triphosphate
DPPM	Disorders of Purine and Pyrimidine Metabolism
dsDNA	Double-stranded DNA
dTMP	Deoxythymidine monophosphate
DTT	Dithiothreitol
dTTP	Deoxythymidine 5'-triphosphate
dUMP	Deoxyuridine monophosphate
E. coli	Escherichia coli
ECL	Enhanced Chemiluminescence
EDTA	Ethylenediaminetetraacetic acid
EGFP	Enhanced Green Fluorescent Protein
ENCODE	ENCyclopedia Of DNA Elements
FACS	Fluorescence activated cell sorting
FBS	Fetal Bovine Serum
FPKM	Fragment per kilo base per million mapped reads
g	Gram
g	Gravitational force
GAPDH	Glyceraldehyde-3-Phosphate Dehydrogenase
GWAS	Genome-Wide Association Studies
h	Hour(s)
H_2O	Dihydrogen Monoxide, water
HBV	Hepatitis B Virus
HCC	Hepatocellular Carcinoma
HCV	Hepatitis C Virus
HEPES	(4-(2-hydroxyethyl)-1-piperazineethanesulfonic acid)
HLB	Hypotonic Lysis Buffer
HOTAIR	HOX Antisense Intergenic RNA
HOXC	Homeobox C cluster
HOXD	Homeobox D cluster
HPLC	High Performance Liquid Chromatography

HRP	Horseradish Peroxidase
HU	Hydroxyurea
HULC	Highly Upregulated in Liver Cancer
IL-1a	Interleukin 1a
IL-1b	Interleukin 1b
IL-6	Interleukin 6
kb	Kilobases
KCl	Potassium Chloride
kDa	Kilodalton
kg	Kilogram
LB	Luria Bertani
LC-MS/MS	Liquid Chromatography – Mass Spectrometry
LIHC	Liver Hepatocellular Carcinoma (TCGA cohort)
lincNMR	Long intergenic non-coding RNA Nucleotide Metabolism Regulator
lincRNA	Long intergenic non-coding RNA
lncRNA	Long non-coding RNA
M	Molar
MALAT1	Metastasis Associated Lung Adenocarcinoma Transcript 1
mg	Milligram
$MgCl_2$	Magnesium Chloride
min(s)	Minute(s)
miRNA	MicroRNA
ml	Milliliter
mM	Millimolar
mRNA	Messenger RNA
MS	Mass Spectrometry
MW	Molecular Weight
MWS	Modified Wuarin-Schibler
n	Number of replicates
NaCl	Sodium Chloride
NAFLD	Non-Alcoholic Fatty Liver Disease
NASH	Nonalcoholic Steatohepatitis
NCI	National Cancer Institute

ncRNA	Non-coding RNA
Neg Ctrl	Negative Control
ng	Nanogram
NGS	Next Generation Sequencing
nt	Nucleotides
OIS	Oncogene Induced Senescence
opti-MEM	Minimum Essential Medium
ORF	Open Reading Frame
P	p-value
PAGE	Polyacrylamide Gel Electrophoresis
PBS	Phosphate-Buffered Saline
PCR	Polymerase Chain Reaction
pH	Negative decimal logarithm of the hydrogen ion concentration
PI	Propidium Iodide
PLK1	Polo like kinase 1
Pol II	Polymerase II
PPIA	Peptidylprolyl isomerase A
R	Correlation coefficient
RACE	Rapid Amplification of cDNA Ends
RAP	RNA Antisense Purification
RBP	RNA binding proteins
RefSeq	The Reference Sequence Database
RIP	RNA Immunoprecipitation
RIPA	Radioimmunioprecipitation assay buffer
RISC	RNA-induced silencing complex
RNA	Ribonucleic Acid
RNAi	RNA interference
RNR	Ribonucleotide Reductase
rpm	Revolutions per minute
RPMI	Roswell Park Memorial Institute Medium
RPS	RNA Precipitation Solution
RRM2	Ribonucleotide Reductase Regulatory Subunit M2
rRNA	Ribosomal RNA

RS	Replicative Senescence
RSEM	RNA-Seq by Expectation Maximization
RT	Room Temperature
RT-qPCR	Reverse Transcription - quantitative PCR
SASP	Senescence Associated Secretary Phenotype
SA-β-Gal	Senescence Associated β Galactosidase
SAHF	Senescence Associated Heterochromatic Foci
SDS	Sodium Dodecyl Sulfate
SDS-PAGE	Sodium Dodecylsulfate-PAGE
sec	Second(s)
SEM	Standard Error of Mean
SILAC	Stable Isotope Labelling by Amino Acids
siPOOL	siRNA Pool
siRNA	Small interfering RNA
snRNA	Small nuclear RNA
ss	Single-stranded
TANRIC	The Atlas of non-coding RNA in Cancer
TBS	Tris-buffered saline
TBS-T	Tris-buffered saline and Tween 20
TCGA	The Cancer Genome Atlas
TERC	Telomerase RNA Component
THF	Tetrahydrofolate
TK1	Thymidine Kinase 1
TP53	Tumor Protein p53
tRNA	Transfer RNA
TSS	Transcription Start Site
TYMS	Thymidylate Synthetase
UV	Ultraviolet
VCL	Vinculin
WB	Western Blot
WRAP53	WD Repeat-Containing Antisense To TP53
XGAL/BCIG	5-bromo-4-chloro-3-indolyl-β-D-galactopyranoside
XIST	X-Inactive Specific Transcript

This page has been intentionally left blank

1. INTRODUCTION

Since this project mainly investigates liver cancer, I start by introducing this disease with a focus on risk factors, pathology including current diagnostic, prognostic and treatment modalities. As the second major topic of this project is the function of non-coding RNAs, I delve into our understanding of their role and relevance in health and diseases including in liver cancer and their potential to regulate multiple hallmarks of cancer including cell proliferation. Lastly, I provide an overview of nucleotide metabolism pathways in the context of cancer cell proliferation and cellular senescence.

1.1 Liver Cancer

1.1.1 Epidemiology

Liver cancer is the fourth leading cause of cancer related deaths worldwide and is predicted to be the sixth most commonly diagnosed cancer in 2018 [1]. Almost 800,000 new cases are being reported every year making it the fifth most commonly diagnosed cancer in men and ninth in women. It is more prevalent in males as compared to females due to a more pronounced inflammatory response [2]. Liver cancer comprises of multiple malignancies like hepatocellular carcinoma (HCC), cholangiocarcinoma (intrahepatic bile duct sarcoma) and hepatoblastoma [3, 4]. Of all liver cancers diagnosed, HCC accounts for 75 % - 85 % of the cases followed by cholangiocarcinoma. Although the five year overall survival of HCC patients has improved over the last years, it is still not better than 20% [2, 5].

1.1.2 Risk factors

Major risk factors contributing to hepatocarcinogenesis include increased alcohol intake, liver cirrhosis, obesity, diabetes, infection with hepatitis B and C viruses (HBV and HCV) and exposure to aflatoxins. In 80 % – 90 % of patients, chronic liver disease and cirrhosis are the underlying causes of progression to hepatocarcinogenesis [2]. Over a half of the reported global HCC cases are attributed to an HBV infection with a prevalence in Asia and Africa whereas about 30% of global HCC cases are due to only HCV infection with highest incidences in northern and middle Africa [6]. Obesity and type-2 diabetes are strongly associated with development of non-alcoholic fatty liver disease (NAFLD) which can progress into Nonalcoholic steatohepatitis (NASH) and cirrhosis which eventually progresses into HCC [7]. In western countries, up to 50 % of the reported HCC cases are attributed to alcohol abuse where up to 38 % are due to NAFLD [7, 8]. Other reported risk factors for HCC include hemochromatosis, α-1 antitrypsin deficiency and Wilson's disease [9].

1.1.3 Pathogenesis

Hepatocarcinogenesis is a complex multistep process in which a chronic liver injury leads to development of cirrhotic liver which further eventually progresses into liver cancer. Cirrhotic liver consists of dead tissue incapable of regeneration, which is a major factor in hepatocyte turnover in otherwise healthy liver [6]. Continuous liver damage as a result of increased deposition of fibrous tissue contributes to disturbed liver architecture as well as function [10]. Overall, malignant transformation is a long process that takes up to 30 years or more from cirrhotic liver to formation of dysplastic nodules and eventually to HCC.

1.1.4 Diagnosis, prognosis and treatment

As per the American Association for the Study of Liver Diseases (AASLD) guidelines, initial diagnosis of HCC is based on elevated serum levels of α-fetoprotein (AFP), radiological tests and a biopsy. Recent studies have shown insufficiency of AFP levels for HCC diagnosis because AFP levels are also elevated in intrahepatic cholangiocarcinoma as well as in some cases of metastasized colon cancer [11, 12]. Due to limitations in diagnostic modalities, HCC is often diagnosed in advanced stage when patients are already symptomatic and liver function is significantly impaired, which strongly contributes to a poor five year overall survival rate of less than 20%. Treatment of HCC is decided based on the tumor grade, number of nodules and the degree of liver function impairment. Most well established systemic strategies for cancer treatment fail to be effective in the terminal stage of HCC and are primarily used as a palliative course of treatment. Due to the challenges discussed above, course of treatment for HCC remains limited to loco-regional procedures such as partial liver resection, tumor ablation and liver transplantation [13, 14]. At the moment, the only FDA approved primary line of treatment for terminal stage HCC is a multi-kinase inhibitor Sorafenib (Nexavar) which improves average survival of patients from 7.9 to 10.7 months with manageable side-effects [15, 16]. Sorafenib functions by inhibiting angiogenesis, proliferation, migration and resistance to apoptosis by targeting the Ras-Raf-MAP2K-MAPK pathway [16]. Recently, a multi-kinase inhibitor Regorafenib, normally used for the treatment of gastrointestinal and colorectal cancer, demonstrated a survival benefit in HCC patients and thus was approved as a second line of therapy for HCC [17, 18].

1.2 Non-coding RNAs

1.2.1 Background and discovery

In 1958, Francis Crick proposed that genetic information flows from DNA to RNA, which serves as a template for translation into proteins [19]. This was defined to be the central dogma of molecular biology. Later in 1961, Jacob and Monod demonstrated the need of an RNA intermediate which was termed messenger RNA or mRNA. Although according to central dogma of molecular biology, RNA was simply a messenger molecule translating genetic information from DNA to proteins, it quickly became evident that not all RNA molecules acted as messenger RNAs and coded for proteins. Early work from the Zamenick lab demonstrated that RNA was involved in protein synthesis not as a messenger molecule but as an adaptor molecule for amino acids which were later called transfer RNAs (tRNAs) [20]. Similarly, a link between rRNAs and ribosomes was also established around the same time [21]. These were the first RNA molecules with non-protein-coding functions. Following the discovery of rRNAs and tRNAs, several other groups of small RNAs such as small nuclear RNAs (snRNAs) and small nucleolar RNAs (snoRNAs) were discovered. snRNAs play a role in RNA splicing [22, 23] whereas snoRNAs are involved in rRNA processing [24]. After the discovery of ribozymes it was abundantly clear that RNAs were functionally involved in roles other than protein synthesis [25, 26]. Subsequently, next generation sequencing (NGS) technologies revealed that the majority of the genome gave rise to non-protein-coding transcriptome or simply non-coding RNAs (ncRNAs) [27]. These non-coding RNAs could be divided into two major groups by virtue of their length - small and long RNA non-coding RNAs. The most extensively studied group of small non-coding RNA molecules are microRNAs (miRNAs), which are 20 - 22 nt in length and depending on the degree of complementarity to their miRNA binding site regulate the expression of their target RNA through the RNA-induced silencing complex (RISC) by either degrading the RNA or by inhibiting their translation into proteins, thus regulating post transcriptional gene expression using the RNA interference mechanism (RNAi) [28, 29]. In contrast to miRNAs, long non-coding RNAs (lncRNAs) are a highly heterogeneous class of biomolecules and function via different mechanisms upon interaction with not only RNA but also with DNA and proteins.

1.2.2 Long non-coding RNAs – classification

Long non-coding RNAs are defined as RNA molecules longer than 200 bases in length with minimal or no protein coding potential and more aptly can be defined as RNA transcripts that are functional as RNAs beyond translation and do not belong to any other non-coding RNA groups such as small (miRNA, piRNA,

snoRNA), functional or structural RNAs (tRNA, rRNA, snRNA) [27]. Other than being classified by length, lncRNAs can also further be grouped into sense, antisense, bidirectional, intergenic or intronic transcripts based on the genomic orientation of the nearest protein-coding gene [27, 30-32]. LncRNAs transcribed from intergenic regions are called long intergenic non-coding RNAs (lincRNAs) whereas intragenic transcripts overlap with a protein-coding gene. Almost 60 % of lncRNA transcripts fall into the intergenic category where they arise from independent promoters or divergently from a bidirectional promoter [33]. Intragenic lncRNAs can further be classified as sense or anti-sense transcripts depending on their orientation with respect to the protein-coding gene. They can either arise from external promoters or internal promoters of the genes they overlap. Transcripts arising from internal promoters are the second largest group of lncRNAs accounting for 30 % of total annotated transcripts [34]. Additionally lncRNAs are further classified based on the functional roles in cancer, like proto-oncogenic [35, 36] or tumor suppressive [37, 38].

1.2.3 Long non-coding RNA – characterization and expression regulation

Similar to mRNAs, expression of lncRNAs is subjected to epigenetic and transcriptional regulation [39-42]. Active (H3K4me3 and H3K36me3) and repressive (H3K27me3) histone marks around the transcription start site (TSS) define the transcription status of a lncRNA. LncRNAs are also shown to display a much denser methylation status as compared to their mRNA counterparts [42]. LncRNAs are transcribed by RNA polymerase II and subjected to subsequent post-transcriptional processing involving 5'-capping and 3'-polyadenylation [34, 43]. In comparison to the mRNA counterparts, lncRNAs are less expressed in general but display high tissue specificity [27, 44, 45] and can localize to a specific compartment in the cell depending on the biological function [46, 47]. Nuclear lncRNAs can act on transcriptions factors [35] or as guides for chromatin modifying complexes [48] whereas cytoplasmic lncRNAs often play a role in post-transcriptional gene expression regulation by either acting as competing endogenous RNAs (ceRNAs) / microRNA sponges [49] or regulating the stability of mRNAs [50]. Being a heterogeneous class of molecules, lncRNAs play diverse functional roles by either interacting with DNA, RNA or proteins in recruitment of chromatin modifying complexes [36] or transcription factors [35], controlling mRNA stability [50] or acting as competing endogenous RNAs [49]. Irrespective of limited sequence conservation across different organisms, diverse expression patterns and complexity, lncRNAs have been shown to help us understand developmental complexities of higher evolved organisms due to their significant functional roles in regulating multiple biological processes [30, 51, 52].

1.2.4 Long non-coding RNAs – in regulation of hallmarks of cancer

A growing number of publications emphasizes the importance of the role of lncRNAs in a multitude of physiological and pathological processes [47, 53, 54]. Although lncRNAs were initially viewed as background noise, it is now evident that they play an important role in the regulation of various biological processes and their deregulation has been linked to multiple cancers [47, 55].

LncRNAs act as drivers of carcinogenesis by regulating one or multiple hallmarks of cancer [56-58]. Several well investigated examples include lncRNAs regulating viability (*GAS5* and *PANDA*) [59-61], proliferation (*CTBP1-AS, PVT1*) [62-64], growth suppression (*MIR31HG* and *NKILA*) [65, 66], migration (*LincRNA-p21, BANCR and MALAT1*) [67-69], angiogenesis (*HULC* and *MALAT1*) [70, 71], and cellular immortality (*NBAT1*, *TERRA* and *TINCR*) [72-74].

1.2.5 Long non-coding RNAs – as drivers of hepatocarcinogenesis

Due to their frequent association with deregulation of hallmarks processes in cancer, lncRNAs have gained and maintained special attention also in liver cancer research.

LncRNA *HOTAIR* is expressed not only in HepG2 cells but also induced in HCC tumor tissues where upregulation of *HOTAIR* is also associated with earlier relapse and tumor progression [75-77]. LncRNAs *LINC00152, ZEB-AS1* and *LINC01225* function as oncogenes by accelerating motility and invasiveness in HCC cells [78-80]. LncRNAs such as *TUC338* [81] and *MALAT1* [82] also modulate drug resistance and sensitivity in HCC cells through pathways involving cell cycle arrest, apoptosis and DNA repair.

Frequent deregulation, up- or downregulation, tissue- and cancer-specific expression of lncRNAs make them attractive targets for a multitude of clinical applications like diagnosis, prognosis or treatment of cancer. Using expression as an attribute, lncRNAs such as *PVT1*, *uc002mbe.2*, *CCHE1* and *CRNDE* distinguish tumor tissues from the normal tissue [83-86]. Additionally, some lncRNAs such as *JPX, XIST, SNHG15, SNHG20, GAS5, CARLo-5* and *SNHG3* have potential to be used as prognostic markers due to their correlation with overall survival and difference between low and high risk HCC [84, 87-92].

1.2.6 Long non-coding RNAs – molecular mechanisms in HCC

LncRNAs modulate gene expression in HCC through complex regulatory networks. LncRNA *GIHCG* promotes progression of HCC through upregulation of DNA methylation and H3K27me3 levels [93] whereas lncRNA *ZNFX1-AS1* [94] suppresses cell growth in HCC by modulation of miR-9 methylation. *Linc00441* promotes HCC progression through H3K27 modifications [95]. Some lncRNAs such as *CCAT2*

[96] and *HOTAIR* [97] function as transcriptional regulators and promote EMT via modulation of transcription factors Slug and Snail in HCC. LncRNA *uc.338* accelerates growth in HCC via transcriptional modulation of CDKN1A [98].

LncRNAs regulate hepatocarcinogenesis by interacting with plethora of biomolecules due to their heterogeneous nature. LncRNA-protein and lncRNA-RNA interactions play a key role in lncRNA functions in HCC. LncRNA *HNF1A-AS1* promotes HCC upon repressing p21 on its interaction with EZH2 whereas lncRNA *SNHG12* - miR-199a/b-5p - MLK3 - NF-κB signaling promotes tumorigenesis and metastasis in HCC cells [99]. LncRNA *HULC* and *MALAT1* work together to promote CSC proliferation in HCC cells [100].

1.3 Cell Proliferation, Senescence and Nucleotide Metabolism

Normal cells and tissues control cell proliferation by modulation of growth promoting signals that regulate the entry into the cell cycle thereby ensuring the maintenance of tissue homeostasis, architecture and function. Cell cycle is a complex cascade of events resulting in a division of a cell into two daughter cells. The eukaryotic cell cycle is divided into two phases: interphase and mitosis or M phase. Interphase is the longest phase of the cell cycle consisting of three steps G1, S and G2 phase. G1 phase is the first gap phase where the cell grows in size and organelles are duplicated whereas in S phase (also called as synthesis phase), cell synthesizes a new copy of the cell's DNA using the DNA replication machinery. In G2 phase (a second gap phase), cell prepares for M phase / cell division by reorganizing its contents. Continuously proliferating cells complete G2 phase and undergo cell division in M phase whereas cells that don't divide exit enter a non-dividing phase called G0.

In sections below, I further discuss the aspects important for the regulation and deregulation of cell cycle in normal liver and in HCC.

1.3.1 Cell cycle regulation in normal liver

Under normal conditions, hepatocytes are fully differentiated and do not proliferate. But upon injury, they are able to exit G0 state and enter the cell cycle to undergo cell division. Progression of hepatocytes through different cell cycle phases is controlled by the expression and activity of cyclin-CDK complexes. Additionally, CDK inhibitors bind to cyclins to regulate their activity in a specific cell cycle phase. Cell cycle inhibitors are divided into two families Cip/Kip and Ink4. Members of Cip/Kip families p21, p27 and p57 bind to the ATP binding pocket of all CDKs and inhibit CDK/cyclin complex function

whereas INK4 inhibitors p16, p15, p18 and p19 bind and alter the conformation of the CDK4/6 complex and in result impair cyclin D binding [101].

Upregulation of CDK inhibitors results in a cell cycle arrest. In the absence of external growth stimuli, p27 maintains hepatocytes in the quiescent state by restricting cyclin/CDK activity [102-104]. In this state, hepatocytes still express membrane receptors which could be activated by cytokines or growth factors resulting in expression of early phase genes and cell cycle re-entry through cyclin D expression and consecutive phosphorylation of pRb by the cyclin D / CDK4 complex.

1.3.2 Deregulation of proliferation and cell cycle in HCC

Deregulation of the cell cycle plays a central role in various cancers including hepatocarcinogenesis through uncontrolled cell proliferation, resistance to cell death, evasion of growth suppressors and genomic instability. Development of HCC is a multi-step process in which different risk factors contribute to multiple cycles of hepatocyte damage, death and regeneration which leads to accumulation of collagen in the tissue leading to liver fibrosis [105]. Over a period of time, fibrotic liver turns cirrhotic and eventually transforms into pre-cancerous and cancerous lesions. WNT, MET or AKT pathways are most frequently deregulated individually or in combination in up to 20 % - 80 % of HCC cases [106, 107]. Most often, the first and most common cellular alteration observed in HCC is telomere shortening. Telomere shortening affects cell cycle checkpoint regulation thus affecting hepatocyte proliferation [108]; the limited replication potential due to shortening of telomeres is known as replicative senescence (RS).

1.3.3 Cellular Senescence

Cellular senescence was first described by Hayflick and Moorehead in context of human primary fibroblasts as cells having limited lifespan in cell culture [109]. Cellular senescence can be triggered by diverse stimuli such as oncogene induction, oxidative stress and DNA damage [110]. Though the senescent cells do not divide, they display pronounced characteristics such as a change in cell shape to flattened morphology, increase in cell size, induction of expression of cell cycle inhibitors and increased senescence-associated β-galactosidase activity detectable at low pH. Most senescent cells display compaction of heterochromatin known as Senescence Associated Heterochromatic Foci (SAHF). As an additional marker, senescent cells display a Senescence Associated Secretary Phenotype (SASP), characterized by production and secretion of regulatory factors including interleukins, angiogenic factors, cytokines, growth factors and matrix metalloproteinases [111, 112]. SASP regulates the

functions of tissues and organs by recruiting immune cells and remodeling of extracellular matrix [113, 114]. Induction of senescence is an attractive therapeutic modality due to its potential in regulating cancer cell proliferation by irreversible cell cycle arrest [115-118].

The onset of cellular senescence leads to the deregulation of genes associated with G1 phase progression inducing a cell cycle arrest in G1 phase and failure to progress into the S phase. Among other *bona fide* proliferation markers, negatively regulated G1/S phase transition genes include the genes driving dNTP biosynthesis [119-123]. As characterized by multiple markers listed above, senescent cells remain metabolically active and undergo cellular alterations including but not limited to pathways of nucleotide, glucose, mitochondrial and lipid metabolism [124].

1.3.4 Nucleotide Metabolism

Cellular deoxyribonucleotide triphosphates (dNTPs) are essential for a wide variety of biological processes [125]. Disturbance of dNTP synthesis results in genotoxicity impacting genome integrity and stability, mutagenesis, mitochondrial health and disorders of purine and pyrimidine metabolism (DPPM) [126-128]. On the other hand, increased dNTP pools have been associated with uncontrolled DNA replication with reduced fidelity and deregulation of cell cycle [129, 130]. This implies that a balance of intracellular levels of dNTP pools is essential to prevent multiple diseases associated with DPPM like obesity, diabetes and cancer [128, 130, 131].

1.3.5 Nucleotide metabolism in cell proliferation

Highly proliferative cells increase DNA and RNA biosynthesis to maintain the pace with accelerated cell division [132, 133]. This is supported by increased synthesis of nucleotide biosynthesis genes in late G1 phase of the cell cycle [134] using either of the two pathways: *de novo* nucleotide biosynthesis pathway and salvage pathway [135].

The *de novo* biosynthesis pathway is highly energy-intensive and generates purine and pyrimidines from raw materials like glucose, glutamine, aspartate and $HCO3^-$ [136]. Due to high energy requirements, cells have developed a more energy-efficient route to synthesize dNTPs, called nucleoside salvage pathway [137]. The salvage pathway essentially recycles nitrogen bases and nucleosides arising from nucleotide breakdown and diet to synthesize dNTPs [136].

Ribonucleotides obtained from either pathway are reduced to dNTPs with the help of a key enzyme called ribonucleotide reductase (RNR) [138, 139]. RNR consists of a tetrameric complex with two

catalytic subunits (RRM1) and two small regulatory subunits (RRM2) [139]. Of note, RRM2 subunits regulate and are rate limiting enzymes for dNTP synthesis during S phase whereas RRM1 is present throughout the cell cycle [140].

Both pathways of dNTP biosynthesis are utilized for thymidine biosynthesis in cells. The salvage pathway involves usage of the enzyme Thymidine Kinase 1 (TK1) for thymidine triphosphate formation which is critical for the process of DNA replication. Expression of TK1 is significantly reduced in senescent cells [141]. TK1 phosphorylates thymidine to generate dTMP, a precursor of thymidine triphosphate (dTTP) pools [142]. dTTP synthesis using the salvage pathway is not sufficient to sustain mitochondrial DNA replication [143] and thus *de novo* dTMP synthesis pathway is often utilized for thymidine nucleotide biosynthesis. This involves the conversion of dUMP to dTMP catalyzed by tetrahydrofolate (THF)-dependent enzymes including Thymidylate Synthetase (TYMS) [144]. TYMS catalyzes the methylation of deoxyuridylate to deoxythymidylate using 10-methylenetetradehydrofolate as a cofactor, which maintains dTMP pools essential for DNA replication and repair. Depletion of TYMS results in deoxyuridine misincorporation into nuclear DNA leading to genome instability [145].

1.3.6 Long non coding RNAs – Senescence and Nucleotide Metabolism

Expression of a multitude of lncRNAs have been reported to be deregulated in senescence but only a handful have been functionally linked to the pathways driving senescence.

Some examples of lncRNAs modulating senescence include *ANRIL*, *MIR31HG*, *FAL-1*, *PANDA*, *VAD, SALNR*, *UCA1*, *HOTAIR* and *7SL*. Overall, it has been reported that nuclear lncRNAs (*ANRIL*, *MIR31HG*, *FAL-1*, *PANDA, VAD and SALNR*) function through transcriptional repression / transcriptional activation / modulating protein localization / telomere remodeling pathways whereas cytoplasmic lncRNAs (*UCA1*, *HOTAIR* and *7SL*) modulate the senescence pathways by regulation of mRNA stability and translation turnover of its targets.

ANRIL has been identified to interact with SUZ12 and CBX7 (components of PRC2 and PRC1 complexes) to promote epigenetic silencing of CDKN2A/CDKN2B loci and thereby impair senescence. Downregulation of ANRIL has been associated with induction of cell cycle inhibitors p14, p15 and p16 further aiding to support its role in senescence [146-148]. *MIR31HG* has been shown to transcriptionally repress $p16^{INK4A}$ by interacting with both the PRC1 and PRC2 complexes [149]. Focally amplified lncRNA on chromosome 1 (*FAL-1*) interacted with and stabilized BMI1 (a PRC1 component) while repressing *p21* expression and promoting senescence [150]. *PANDA* has been shown to act as a scaffold between SAFA

(transcriptional regulator scaffold attachment factor A), PRC1 and PRC2 interactions in proliferating cells whereas, in senescent cells, SAFA-PRC complex disruptions promoted the expression of *PANDA* where *PANDA* interacted with transcription NF-YA and suppressed the expression of proliferation genes thus playing a dual role in regulation of cell proliferation and senescence [61]. LncRNA *VAD* has been shown to be induced in OIS and to activate transcription of CDKN2B locus contributing to senescent phenotype [151]. *SALNR* was found to be over expressed in RS and OIS has been shown to interact with NF90 (nuclear factor 90) to prevent biogenesis of senescence-associated miRNAs [152-154]. Overexpression of *UCA1* has been attributed with stabilizing *p16* mRNA by sequestering hnRNPA1 in RAS induced senescence [155]. Depletion of *HOTAIR* has been reported to suppress senescence in cancer [156] whereas *7SL* has been reported to enhance the translation turnover of p53 by binding to 3' UTR of *p53* mRNA leading to cell cycle arrest and senescence by competing with HuR [157, 158].

While there have been multiple reports of lncRNAs regulating pathways governing senescence, there are no reports of lncRNAs in the context of regulation of nucleotide metabolism pathways so far.

2. AIMS OF MY DOCTORAL PROJECT

HCC has been reported to cause more than 740,000 deaths annually and is the fourth leading cause of cancer-related deaths worldwide. The treatment options for HCC are limited with a poor overall survival of less than 20 %, thus warranting further investigations into molecular mechanisms underlying hepatocarcinogenesis. The era of high-throughput sequencing has aided in the discovery of lncRNAs regulating hallmarks of cancer, but there are no reported studies of lncRNAs so far investigating the regulation of cancer cell proliferation through nucleotide metabolism pathways.

Thus the aim of my doctoral research project is to investigate and uncover novel mechanisms driving hepatocarcinogenesis from a lncRNA perspective.

The aims of this project can be sub-divided into the following objectives:

- to identify novel lncRNAs induced and regulated in hepatocellular carcinoma
- to screen for an impact on cell viability after depletion of selected lncRNAs
- to select a novel lncRNA candidate for further investigation based on the strength of phenotype
- to perform in-depth characterization of the selected novel lncRNA in terms of -
    - basic characterization: coding potential, gene boundaries and subcellular localization
    - cellular function
    - and molecular function

This page has been intentionally left blank

3. MATERIALS

Parts of the text and figures presented in this chapter are revised versions of the figures and text submitted for publication as an original research article:

Gandhi et al., *"lincNMR* regulates Nucleotide Metabolism via a YBX1 - RRM2 Axis in Cancer"
Nature Communications (manuscript under review)

3.1 Reagents and chemicals

Table 1. List of reagents and chemicals used in this study

Reagent/ Chemical	Supplier	Catalogue Number
4,4,5,5-D4 L-Lysine-2hcl	Fisher Scientific	11305402
Acetic Acid	Lager	12847
Acetone	Sigma-Aldrich	32201-1L
Ampicilin Sodium Crystalline	Sigma	A9518-25G
Anti-FLAG M2 Magnetic Beads	Sigma	M8823
Anti-Mouse Igg For IP (HRP)	Abcam	ab131368
Benzonase	Santa Cruz	sc-202391
Beta-Mercaptoethanol	Sigma-Aldrich	M6250
Bovine Serum Albumin (Bsa)	Sigma	A9418-10G
Bp Clonase Ii Enzyme	Thermofisher	11789020
Bromphenol Blue	Serva	15375.02
Chlorofom	Lager	12938
Chloroform : Isoamylalcohol 24:1	Th. Geyer	SA/00025666/000100
Crystal Violet	Serva	27335.01
Dialyzed FBS	Life Technologies	88212
Dimethyl Sulphoxide	Applichem	A3672,0100
Dmem (High Glucose Medium)	Life Technologies	41965062
Dnase I Recombinant, Solution	Roche	4716728001
Dntp Set, 100 Mm Solutions	Thermo Fisher	R0182
Dream Taq Dna-Polymerase	Fermentas	EP0702
Dtt	Roche	10708984001

Dynabeads Streptavidin Beads	Life Technologies	65002
Ecl(Tm) Prime	Ge Life Science	GERPN2236
Edta	Gebru	10341000
Ethanol	Dkfz Catalogue	873
Ethidium Bromide	Carl Roth	2218.1
Fcs	Life Technologies	10270106
Formaldehyde	Sigma-Aldrich	F8775-4X25ML
Generule 100 Bp DNA Ladder	Fermentas	SM0241
Generuler 100 Bp Plus DNA Ladder	Fermentas	SM0322
Glutaraldehyde	Serva	23116.01
Glycerol	Sigma-Aldrich	G9012
Glycine	Gerbu	1023
Glycogen	Carl Roth	HP51.1
Hydrogen Peroxide 30%	Sigma-Aldrich	H1009-100ML
Isopropanol	Lager	13404
L-Arginine-Hcl, 13C6	Life Technologies	88210
L-Arginine-Hcl, 13C6, 15N4	Life Technologies	89990
Le Agarose	Biozym	840004
Lipofectamine 2000	Life Technologies	11668019
Lipofectamine Rnaimax	Invitrogen	13778150
L-Lysine-2hcl, 13C6, 15N2	Thermo Fisher	88209
L-Proline	Thermo Fisher	88211
Magnesium Chloride	Roth	KK36.3
Matrigel Matrix High Conc. A75(Hc)	Corning	354262
Methanol	Lager	12693
N, N'-Dimethylformamide	Th.Geyer	39756.02
N-Dodecyl B-D-Maltoside	Sigma-Aldrich	D4641
Np - 40	Applichem	A1694,0250
Opti-Mem Reduced Serum Medium	Invitrogen	31985047
Pageruler Prestained Protein Ladder	Fermentas	26616
Pbs	Sigma	D8537-6X500ML

Penicilin-Streptomycin Solution	Sigma	P0781-100ML
Phos-Stop	Roche	4906837001
Pierce Bca Protein Assay Reagent B	Thermo Fisher	23224
Pmsf	Sigma Aldrich	78830-5G
Potassium Chloride	13096	Lager
Powersybr Green PCR MM, 5ml	Life Technologies	4367659
Propidium Iodide	Sigma-Aldrich	P4170
Protease Inhibitor	Roche Diagnostics	11873580001
Protein G Magnetic Beads	Cell Signaling	9006S
Proteinase K Solution	Life Technologies	AM2546
Random Hexamer Primer	Fermentas	SO142
Revertaid Reverse Transcriptase	Fermentas	EP0442
Ribolock Rnase Inhibitor	Thermo Scientific	EO0381
Ribolock Rnase Inhibitor (40 U/µl)	Thermo Fischer	EO0384
Riboruler High Range	Thermo Fisher	11893993
Riboruler Low Range	Thermo Fisher	SM1821
Rnase A	Sigma/Roche	10109169001
Roti-Phenol / Chlorofom / Isoamyl	Lager	13294
Rotiphorese® Gel Acrylamide Solution	Carl Roth	3029.1
Rpmi 1640 Medium	Life Technologies	21875091
Sds (Sodium Dodecyl Sulphate)	Roth	2326.2
Silac Rpmi 1640 Medium	Life Technologies	A2494401
Skim Milk Powder	Sigma-Aldrich	70166-500G
Sodium Acetate Solution (3 M), Ph 5.2	Thermo Scientific	R1181
Sodium Chloride		12781
Sodium Deoxycholate	Sigma-Aldrich	D6750-10G
Superase In (20 U/Ml)	Life Technologies	AM2696
Supersignal West Picosubstrate	Fisher Scientific	34580X4
Tcep	Sigma	646547
Temed	Carl Roth	2367.3
Thymidine	Sigma-Aldrich	T9250

Tri Reagent	Sigma	T9424-200ML
Trisma Base	Lager	12681
Triton X-100	Gerbu	2000, 1000
Trypsin 0.05%	Life Technologies	25300054
Trypsin 0.25 %	Life Technologies	25200056
TURBO DNA-Free™ Kit	Thermo	AM1907
TURBO Dnase (2 U / µl)	Life Technologies	AM2238
Turbofect Transfection Reagent	Fisher Scientific	15325016
Tween 20	Mp Biomedicals	M4904
Ultrapure Distilled Water	Invitrogen	10977049
Urea	Th. Geyer	SA/U0631/000500

3.2 Kits and consumables

3.2.1 Kits

Table 2. List of kits used in this study

Kit	Supplier	Catalogue Number
Axyprep Plasmid Miniprep Kit	Axygen	AP-MN-P-250
Celltiter Glo Luminescent Cell Viability Assay	Promega	G7572
Dual Luciferase Reporter Assay System	Promega	E1910
Genejet Gel Extraction Kit	Thermo Scientific	K0691
Genelute Genomic DNA Kit	Sigma-Aldrich	G1N10
Pcr Mycoplasma Test Kit	Promocell	PK-CA91-1048
Pierce Silac Protein Quantitation	Thermo Fisher	89982
Purelink Hipure Plasmid Midiprep	Life Technologies	K210005
Qiagen Mirneasy Mini Kit	DKFZ Lager	217004
Silac Protein Quantitation Kit – Rpmi 1640	Life Technologies	89982
Smarter RACE Cdna Amplication	Clontech	634859
Topo Ta Cloning Kit, Dual Promoter	Life Technologies	450640

3.2.2 Consumables

Table 3. List of consumables used in this study

Item	Company	Catalogue Number
10 cm Dishes, 96 X 20mm	TPP	Multiple
15 cm Dishes, 146x21 Mm	TPP	Multiple
15 ml, 50 Ml Falcon Tubes	TPP	Multiple
2 ml Cryotubes	Greiner Bio-One	126278
6-, 12-, 24 - Well Plates	TPP	Multiple
96 - Well Plate	Greiner Bio-One	650101
96 - Well Plate, Black Clear Bottom	Greiner Bio-One	655076
Combitips Advanced, 0.2 ml	NeoLab	E-6401
Cover Glass	VWR	HECH1001/12
Cryo Vials	Greiner Bio-One	122263

GeneJet PCR Purification Kit	Thermo Fisher	K0702
GenElute Mammalian Genomic DNA Miniprep Kit	Sigma-Aldrich	G1N350
MicroAmp Fast Optical 96-Well Reaction Plate	ABI	4346907
MicroAmp Optical Adhesive Film	Life Technologies	4311971
Millex-HV 0.45 µm	Neolab	SLHV033RS
Nitrocellulose Membrane 0.45 µm	VWR	10600002
NucleoSpin Plasmid	Macherey-Nagel	740588.25
Parafilm	DKFZ-Lager	12728
PCR Tubes 0.2 mL	Biozym	710980
Reaction Tube 1.5 mL	Eppendorf	12682
Reaction Tube 2 mL	Eppendorf	12776
Scalpels	DKFZ-Lager	13493
Sterile Filter Tips (1-50 mL)	Nerbe Plus	Multiple
Sterile Filter Tips (1-1000 µL)	Nerbe Plus	Multiple

3.3 Buffers and solutions

Table 4. Buffers and solutions recipes used in this study

Buffer	Recipe
1.5X Hybridisation Buffer	15 mM Tris-HCL pH 7.5, 7.5 mM EDTA, 750 mM LiCl, 0.75% DDM, 0.3% SDS, 0.15% Sodium Deoxycholate, 6M Urea, 3.75 mM TCEP
1X Wash Buffer (RAP-MS)	10 mM Tris-HCL pH 7.5, 5 mM EDTA, 500 mM LiCl, 0.5% DDM, 0.2% SDS, 0.1% Sodium Deoxycholate, 4M Urea, 2.5mM TCEP
200X DNase Salt Solution	500 mM MgCl2, 100mM CaCl2
Medium for Breast and Lung cell lines	DMEM, 10% FCS, no P/S
Cell culture medium for CAM experiment	RPMI-1640, 10% FCS, 1% P/S
Cell culture medium for Liver cell lines	RPMI-1640, 10% FCS, no P/S
dNTP mix	10 mM dATP, 10 mM dGTP, 10 mM dCTP, 10 mM dTTP
High Salt Wash Buffer (CLIP)	0.1% SDS, 0.5% Sodium Deoxycholate, 0.5% NP-40, 0.05

	M Nacl, 0.010 M KCl, 0.005 M Na2HPO4, 0.0005 M KH2PO4
Hypotonic Lysis Buffer (HLB)	10 mM Tris (pH 7.5), 10 mM NaCl, 3 mM MgCl2, 0.3% (vol/vol) NP-40, 10% (vol/vol) Glycerol
LB Agar	2.5% Luria Broth Base, 1.5% agar
LB Medium	2.5% Luria Broth Base
Low Salt Wash Buffer (CLIP)	0.1% SDS, 0.5% Sodium Deoxycholate, 0.5% NP-40, 0.01 M Nacl, 0.002 M KCl, 0.001 M Na2HPO4, 0.0001 M KH2PO4
Modified Wuarin-Schibler Buffer (MWS)	10 mM Tris-HCl (pH 7.0), 4 mM EDTA, 0.3 M NaCl, 1 M Urea, 1% (vol/vol) NP-40
Proteinase K Buffer (CLIP)	125 mM Tris-Cl pH 7.8, 62.5 mM NaCl, 12.5 mM EDTA
RIPA Buffer	50 mM Tris-HCl pH 7.5, 150 mM NaCl, 1% Triton X-100, 0.5% Na-Deoxycholate, 0.1% SDS, 1% DTT
RNA Elution Buffer (RAP-MS)	20 mM Tris-HCL pH 8.0, 10mM EDTA , 2% NLS, 2.5mM TCEP,
RNA Loading Dye	95% Formamide, 0.05% SDS, 0.05% Bromphenol blue, 4.9% TE-buffer
RNA Precipitation Solution (RPS)	3 M Sodium Acetate (pH 5.5), 9.5 ml of Ethanol
SDS PAGE Running Buffer (10X)	0.25 M Tris-base, 1.92 M Glycine, 1% SDS
SDS PAGE Solution B	1.5 M Tris-base, 0.4% SDS
SDS PAGE Solution C	0.5 M Tris-base, 0.4% SDS
TBE Buffer	0.89 M Tris, 0.89 M Boric acid, 0.5 M EDTA (pH 8.0)
TBS Buffer	247 mM Tris, 1.37 M NaCl, 26.8 mM KCl, 0.05% Tween-20
Total Cell Lysis buffer (CLIP and RAP-MS)	10 mM Tris HCL pH 7.5, 500 mM Lithium Chloride, 0.5% Dodecyl Maltoside, 0.2% SDS, 0.1% Sodium Deoxycholate
Western Blot Loading Buffer (6X)	58% SDS PAGE Solution C, 25% Glycerol, 8% SDS, 0.01% Bromphenol Blue, 0.6 M DTT
Western Blot Transfer Buffer (10X)	0.25 M Tris-base. 1.92 M Glycine, fresh 1X buffer contains 20% Methanol

3.4 Equipments and devices

Table 5. List of equipments and devices used in this study

Equipment Name	Company
Applied Biosystems StepOnePlus Cycler	Applied Biosystems
BD FACSCantoTM II	Beckton Dickinson
BioPhotometer Plus	Eppendorf
Cell Counter Neubauer	Roth
Cell Incubator Labotect C200	Labotect
Dynamag 15	Life Technologies
Dynamag 2	Life Technologies
Fluoroskan Ascent FL	Thermo Scientific
FLUOstar Omega Microplate Reader	BMG Labtech
Gilson Pipetman Pipette Set	Gilson
Heraeus B5042H Heater	Heraeus
Heraeus Fresco 17 Centrifuge	Thermo Scientific
Heraeus Labofuge 400	Thermo Scientific
Heraeus Megafuge 16R Centrifuge	Thermo Scientific
Heraeus Pico 17 Centrifuge	Thermo Scientific
INFORS HT - Ecotron (Bacterial Shaker)	INFORS HAT
INTAS UV Gel Imager	INTAS
Intelli – Mixer	NeoLab
Isotemp 202 (Waterbath)	Thermo Scientific
Kisker Maxigel (20x20 cm) Electrophoresis System	Kisker
Leica DM IRB Microscope	Leica
LTQ Orbitrap XL Mass Spectrometer	Thermo Scientific
Metal – Block - Thermostate MBT - 250	Kleinfeld
Mini Trans - Blot Electrophoretic Transfer Cell	Bio-Rad
Mini - Protean Minigel System Bio - Rad	Bio-Rad
Multistep Pipette (Multipette stream)	Eppendorf
MultiSUB Choice Tray (15x15 cm)	Kisker

Multiwell Pipette (pipet lite)	Rainin
Nalgene 5100-0036 Cryo 1°C	Thermo Fisher
NanoDrop 2000 Spectrophotometer	Thermo Scientific
Olympus CellR Microscope	Olympus
Orbital Shaker DOS-10L	NeoLab
PCR Thermal Cycler PTC-200	Bio-Rad
PowerPac Basic, Power Supply	Bio-Rad
PowerPac HC, Power Supply	Bio-Rad
Research Pipette 100 – 1000 µl	Eppendorf
Research Pipette 2 – 20 µl	Eppendorf
Research Pipette 20 – 200 µl	Eppendorf
Rocking Shaker	Kisker
Sartorius pH Meter PB - 11	Sartorius
Spectra Max M5e	Molecular Devices
SterilGARD III Advance Cell Culture Hood	The Baker Company
Thermo Scientific Savant DNA120	Thermo
UV Stratalinker 1800	Stratagene
Vortex Mixer	NeoLab
Whatman Nitrocellulose Blotting Membrane	Whatman

3.5 Nucleic acid sequences

3.5.1 siPOOL sequences

Table 6. List of siPOOLs used in this study

siPOOL Name	siRNA No.	Sense sequence	Antisense sequence
siPOOL-NC	1	UGUACGCGUCUCGCGAUUU	AAAUCGCGAGACGCGUACA
	2	UAUACGCGGUACGAUCGUU	AACGAUCGUACCGCGUAUA
	3	UUCGCGUAAUAGCGAUCGU	ACGAUCGCUAUUACGCGAA
	4	UCGGCGUAGUUUCGACGAU	AUCGUCGAAACUACGCCGA
	5	UCGCGUAAGGUUCGCGUAU	AUACGCGAACCUUACGCGA
	6	UCGCGAUUUUAGCGCGUAU	AUACGCGCUAAAAUCGCGA
	7	UCGCGUAUAUACGCUACGU	ACGUAGCGUAUAUACGCGA
	8	UUUCGCGAACGCGCGUAAU	AUUACGCGCGUUCGCGAAA
	9	UCGUAUCGUAUCGUACCGU	ACGGUACGAUACGAUACGA
	10	UUAUCGCGCGUUAUCGCGU	ACGCGAUAACGCGCGAUAA
	11	UCUCGUAGGUACGCGAUCU	AGAUCGCGUACCUACGAGA
	12	UCGUACUCGAUAGCGCAAU	AUUGCGCUAUCGAGUACGA
	13	UUUGCGAUACCGUAACGCU	AGCGUUACGGUAUCGCAAA
	14	UGCGUAAGGCAUGUCGUAU	AUACGACAUGCCUUACGCA
	15	UUAUCGGCAGUUCGCCGUU	AACGGCGAACUGCCGAUAA
	16	UAGCGCGACAUCUAUCGCU	AGCGAUAGAUGUCGCGCUA
	17	UCGUCGUAUCAGCGCGUUU	AAACGCGCUGAUACGACGA
	18	UACGCGAAACUGCGUUCGU	ACGAACGCAGUUUCGCGUA
	19	UCGACGAUAGCUAUCGCGU	ACGCGAUAGCUAUCGUCGA
	20	UCGCGUAAUACGCGAUCGU	ACGAUCGCGUAUUACGCGA
	21	UCGCGAUAAUGUUACGCGU	ACGCGUAACAUUAUCGCGA
	22	UUAACGCGCUACGCGUAUU	AAUACGCGUAGCGCGUUAA
	23	UCGCGUAUAGGUAACGCGU	ACGCGUUACCUAUACGCGA
	24	UUACGCGAUCACGUAACGU	ACGUUACGUGAUCGCGUAA
	25	UUAUCGCGCGUCGCGUAAU	AUUACGCGACGCGCGAUAA
	26	UUACGUACUAGUGCGUACU	AGUACGCACUAGUACGUAA

	27	UAUACGCCGGUUGCGUAGU	ACUACGCAACCGGCGUAUA
	28	UUCGCGUGCAUAGCGUAAU	AUUACGCUAUGCACGCGAA
	29	UACGCGACCUAAUCGCGAU	AUCGCGAUUAGGUCGCGUA
	30	UCGUACGCUGAACGCGUAU	AUACGCGUUCAGCGUACGA
si-*lincNMR*-A	1	GACAATCCTTAGACTTCTT	AAGAAGTCTAAGGATTGTC
	2	CGCCCACTCTCACCCGGAA	TTCCGGGTGAGAGTGGGCG
	3	CAGCAATTATCACCAATCT	AGATTGGTGATAATTGCTG
	4	CGAGATAGGAGGCCCATAA	TTATGGGCCTCCTATCTCG
	5	GACAAAGAAGGACAAATAT	ATATTTGTCCTTCTTTGTC
	6	GGGAACGCTGCCATGAATT	AATTCATGGCAGCGTTCCC
	7	GCTATACCCTGCGTTTTGA	TCAAAACGCAGGGTATAGC
	8	CCCATTGGGATGTTCATTA	TAATGAACATCCCAATGGG
	9	CAAACAGATCCAATCACAA	TTGTGATTGGATCTGTTTG
	10	GAGCCTTCATTCAAACTAA	TTAGTTTGAATGAAGGCTC
	11	GTGAAAAGCATATGGTAAT	ATTACCATATGCTTTTCAC
	12	GCTTGATTTAACCACGCCA	TGGCGTGGTTAAATCAAGC
	13	GCAGCACCGGTGTTCTTCA	TGAAGAACACCGGTGCTGC
	14	GTACACCATGGTCAATATA	TATATTGACCATGGTGTAC
	15	GATAAATGAAAGAGTAGTA	TACTACTCTTTCATTTATC
	16	CTCTCCTGGGTTCCGGTAA	TTACCGGAACCCAGGAGAG
	17	CGCCACAGTGCATACATAT	ATATGTATGCACTGTGGCG
	18	GACCTAGAGGGATCAGCTT	AAGCTGATCCCTCTAGGTC
	19	GAACATTAAGGACGAGATA	TATCTCGTCCTTAATGTTC
	20	CCGTCCAGGACCTCAAACA	TGTTTGAGGTCCTGGACGG
	21	CCCGATGCTGAGTTCACGA	TCGTGAACTCAGCATCGGG
	22	CCAGTAAGAAAGCCTGGTT	AACCAGGCTTTCTTACTGG
	23	CACCTTACTGAGCTTCAAA	TTTGAAGCTCAGTAAGGTG
	24	CCTGTTGGAATTACACCTT	AAGGTGTAATTCCAACAGG
	25	CCCTCTTGGATCTGGCTCT	AGAGCCAGATCCAAGAGGG
	26	GGATCGTGGCGAAGTCTAT	ATAGACTTCGCCACGATCC
	27	CAGATTAAGAAGAACCAAA	TTTGGTTCTTCTTAATCTG

	28	GGACTTCGTCCAAGCCTTT	AAAGGCTTGGACGAAGTCC
	29	GTCAATTTTAAACAGGTTA	TAACCTGTTTAAAATTGAC
	30	CATGTTATTGTTGATAATT	AATTATCAACAATAACATG
si-*lincNMR*-B	1	CCAATCTAGATTATGAGAT	ATCTCATAATCTAGATTGG
	2	GGACGACCTCTTCCTATAT	ATATAGGAAGAGGTCGTCC
	3	GTTCATTAGAACTCTGAAA	TTTCAGAGTTCTAATGAAC
	4	CCTCAAACAGATCCAATCA	TGATTGGATCTGTTTGAGG
	5	GCCTTTCCGTCCAGGACCT	AGGTCCTGGACGGAAAGGC
	6	CCACCTTACTGAGCTTCAA	TTGAAGCTCAGTAAGGTGG
	7	CGGTAAGAAGAGATTCCAA	TTGGAATCTCTTCTTACCG
	8	GAGATTTCAGGAAAGAGAA	TTCTCTTTCCTGAAATCTC
	9	CCTCTCCTGGGTTCCGGTA	TACCGGAACCCAGGAGAGG
	10	GTGTACAGTATAATGATAA	TTATCATTATACTGTACAC
	11	GTCCGACCTAGAGGGATCA	TGATCCCTCTAGGTCGGAC
	12	CCATGGGACAGCCCTCTGA	TCAGAGGGCTGTCCCATGG
	13	CTCTCACTCTCTTATGGAA	TTCCATAAGAGAGTGAGAG
	14	CAGTGCATACATATGTCAA	TTGACATATGTATGCACTG
	15	GCTGGGAACGCTGCCATGA	TCATGGCAGCGTTCCCAGC
	16	CGGAACCTTTCATCTCTTA	TAAGAGATGAAAGGTTCCG
	17	GAATAGTACGTTAGACAAA	TTTGTCTAACGTACTATTC
	18	GGCAACGTTGACTTCCAGT	ACTGGAAGTCAACGTTGCC
	19	CTGCAAGGACTTCGTCCAA	TTGGACGAAGTCCTTGCAG
	20	CTGCTTACAACCATGCTGA	TCAGCATGGTTGTAAGCAG
	21	GATGGTTACCAGTTAGAAA	TTTCTAACTGGTAACCATC
	22	GCCTGTTGGAATTACACCT	AGGTGTAATTCCAACAGGC
	23	GAGATAGGAGGCCCATAAT	ATTATGGGCCTCCTATCTC
	24	GCCATGAATTGGGCTTGGT	ACCAAGCCCAATTCATGGC
	25	GAAGAACCAAAGCAGAATA	TATTCTGCTTTGGTTCTTC
	26	CACCATGGTCAATATAGTT	AACTATATTGACCATGGTG
	27	CAGATCTTGTGGAATCTAA	TTAGATTCCACAAGATCTG
	28	CACCTTGGATCGTGGCGAA	TTCGCCACGATCCAAGGTG

	29	GCGAAGTCTATAGAGGTCA	TGACCTCTATAGACTTCGC
	30	GCCCATTGGGATGTTCATT	AATGAACATCCCAATGGGC
si-YBX1	1	GGATATGGTTTCATCAACA	TGTTGATGAAACCATATCC
	2	CCAGTTCAAGGCAGTAAAT	ATTTACTGCCTTGAACTGG
	3	CTGAGTAAATGCCGGCTTA	TAAGCCGGCATTTACTCAG
	4	GCCTAGAGAGGACGGCAAT	ATTGCCGTCCTCTCTAGGC
	5	CCTGTTAATAAAGGTCTTA	TAAGACCTTTATTAACAGG
	6	CCCAACAACGCCGGCCCTA	TAGGGCCGGCGTTGTTGGG
	7	GAAATTCCAGCAATAAGAA	TTCTTATTGCTGGAATTTC
	8	CCCTCCTGTGCAGGGAGAA	TTCTCCCTGCACAGGAGGG
	9	GAGATGAGACCCAAGGTCA	TGACCTTGGGTCTCATCTC
	10	GGCTTACCATCTCTACCAT	ATGGTAGAGATGGTAAGCC
	11	GGTAATAACAAACGTGTTT	AAACACGTTTGTTATTACC
	12	GCCCTCCTCGCCAAAGACA	TGTCTTTGGCGAGGAGGGC
	13	GCCCGTTGACCAGATAAAT	ATTTATCTGGTCAACGGGC
	14	GGCGAAGGTTCCCACCTTA	TAAGGTGGGAACCTTCGCC
	15	GGGCGTCGACCACAGTATT	AATACTGTGGTCGACGCCC
	16	GATTGGAGCTGAAGACCTA	TAGGTCTTCAGCTCCAATC
	17	CCACGCAATTACCAGCAAA	TTTGCTGGTAATTGCGTGG
	18	GCGGAGGCAGCAAATGTTA	TAACATTTGCTGCCTCCGC
	19	CTAAACCACAAGATGGCAA	TTGCCATCTTGTGGTTTAG
	20	GCCGATCCACCAGCTGAGA	TCTCAGCTGGTGGATCGGC
	21	GGTAGACCAGTGAGGCAGA	TCTGCCTCACTGGTCTACC
	22	CAATGTAAGGAACGGATAT	ATATCCGTTCCTTACATTG
	23	CACCAAGGAAGATGTATTT	AAATACATCTTCCTTGGTG
	24	GCAGACCGTAACCATTATA	TATAATGGTTACGGTCTGC
	25	CGACGCAGACGCCCAGAAA	TTTCTGGGCGTCTGCGTCG
	26	GGTACCGCCGCAACTTCAA	TTGAAGTTGCGGCGGTACC
	27	GACCTAAAGTGCTTGCTTT	AAAGCAAGCACTTTAGGTC
	28	CCAGGGTGCAGGAGAACAA	TTGTTCTCCTGCACCCTGG
	29	CCATCATCCGGTTTAGTCA	TGACTAAACCGGATGATGG

	30	GTCATCCAACAAGAAGAAA	TTTCTTCTTGTTGGATGAC
si-RRM2	1	CATTAAAATGAAAGGCTTT	AAAGCCTTTCATTTTAATG
	2	GCCAGATAGAAGACAGGTT	AACCTGTCTTCTATCTGGC
	3	GGCACTTTACAAACAAATA	TATTTGTTTGTAAAGTGCC
	4	GTGTTACCAACTAGCCACA	TGTGGCTAGTTGGTAACAC
	5	GTTATTGTTACCTAAAGTT	AACTTTAGGTAACAATAAC
	6	CAATGGCAGTCTTGGCTTT	AAAGCCAAGACTGCCATTG
	7	CTGTCTCTCATTAGCTGAA	TTCAGCTAATGAGAGACAG
	8	CTACAAGTTGTTCATTCTA	TAGAATGAACAACTTGTAG
	9	GCCGTTTCATTTTATTTCT	AGAAATAAAATGAAACGGC
	10	GTGCTGGTAGTATCACCTT	AAGGTGATACTACCAGCAC
	11	CAAGTATTTCAGTCTCAAA	TTTGAGACTGAAATACTTG
	12	GCCCTTACTTGGCTGATTT	AAATCAGCCAAGTAAGGGC
	13	GAATAATGCACAAGTCTTA	TAAGACTTGTGCATTATTC
	14	CACAAGGCGATAATAGCTT	AAGCTATTATCGCCTTGTG
	15	GCCTCACTGCTTCAACGCA	TGCGTTGAAGCAGTGAGGC
	16	CTCTGTAATATGATACATT	AATGTATCATATTACAGAG
	17	CTTAAACTTTAGTAGGAAA	TTTCCTACTAAAGTTTAAG
	18	CCCTTTAGTGAGCTTAGCA	TGCTAAGCTCACTAAAGGG
	19	GAAAGGGAAACAAGTATTT	AAATACTTGTTTCCCTTTC
	20	CACCATGAATTGTCCGTAA	TTACGGACAATTCATGGTG
	21	GGGATTAAACAGTCCTTTA	TAAAGGACTGTTTAATCCC
	22	GGGAAACAAGTATTTCAGT	ACTGAAATACTTGTTTCCC
	23	GGGATAAAGGAATCTCTCA	TGAGAGATTCCTTTATCCC
	24	CACTAAGTGACTAAAGTAA	TTACTTTAGTCACTTAGTG
	25	GCTAAGGTAGTATTGTAAA	TTTACAATACTACCTTAGC
	26	CATTTATTGTATAGACAAT	ATTGTCTATACAATAAATG
	27	GAGAAGCCGTTTCATTTTA	TAAAATGAAACGGCTTCTC
	28	GTGAGGTACAGGCGGAAGT	ACTTCCGCCTGTACCTCAC
	29	CTGCAGCTCTCGCCGCTGA	TCAGCGGCGAGAGCTGCAG
	30	GCTTGGTCGACAAGGAGAA	TTCTCCTTGTCGACCAAGC

si-TK1	1	CCGGGAAGACCGTAATTGT	ACAATTACGGTCTTCCCGG
	2	CCGAGAGCGTGGTGAAGCT	AGCTTCACCACGCTCTCGG
	3	CCCAGCCACTCCAGGAGGA	TCCTCCTGGAGTGGCTGGG
	4	CCGTAATTGTGGCTGCACT	AGTGCAGCCACAATTACGG
	5	GCTTCCGGGAAGCCGCCTA	TAGGCGGCTTCCCGGAAGC
	6	GGCTTAGGCCTCTCTGCCT	AGGCAGAGAGGCCTAAGCC
	7	CCATGGCCAACGCCGGGAA	TTCCCGGCGTTGGCCATGG
	8	GGTGATCAAGTATGCCAAA	TTTGGCATACTTGATCACC
	9	GGATTCACGCCCTCTTGTT	AACAAGAGGGCGTGAATCC
	10	GAGCCTTGGCCCACACTGA	TCAGTGTGGGCCAAGGCTC
	11	GGAACAACAGCATCTTTCA	TGAAAGATGCTGTTGTTCC
	12	CTGCGGCTTTCACTGCTGA	TCAGCAGTGAAAGCCGCAG
	13	GCCTACTGGACGCTGCCCT	AGGGCAGCGTCCAGTAGGC
	14	GCATTAACCTGCCCACTGT	ACAGTGGGCAGGTTAATGC
	15	GGCTTTCACTGCTGAGTTT	AAACTCAGCAGTGAAAGCC
	16	CCGCTTGGTGGCCTGGGAT	ATCCCAGGCCACCAAGCGG
	17	CCAACTGAGGGACCTGCGA	TCGCAGGTCCCTCAGTTGG
	18	GGGAAGCCGCCTATACCAA	TTGGTATAGGCGGCTTCCC
	19	CCTTCCTACCTCTGGTGAT	ATCACCAGAGGTAGGAAGG
	20	GCCTTCTGGGAACTCTCCT	AGGAGAGTTCCCAGAAGGC
	21	GTGCCTGGTGATCAAGTAT	ATACTTGATCACCAGGCAC
	22	CTGCTTAAAGCTTCCCTCT	AGAGGGAAGCTTTAAGCAG
	23	CGGTGTGCATGGAGTGCTT	AAGCACTCCATGCACACCG
	24	GGCAGATCCAGGTGATTCT	AGAATCACCTGGATCTGCC
	25	CTACCCACTGGTCTGCTTA	TAAGCAGACCAGTGGGTAG
	26	CACCAACCTTGCTGGGACT	AGTCCCAGCAAGGTTGGTG
	27	CACGCCCTCTTGTTTCCTT	AAGGAAACAAGAGGGCGTG
	28	CCTGCATGCTGCCCAGCCA	TGGCTGGGCAGCATGCAGG
	29	GCTTATGAAATTAACTAAT	ATTAGTTAATTTCATAAGC
	30	GGAACACCATGGAGGCACT	AGTGCCTCCATGGTGTTCC
si-TYMS	1	TGCCAGTTCTTTCCATAAT	ATTATGGAAAGAACTGGCA

	2	GCTATTCCCTCAAATCTGA	TCAGATTTGAGGGAATAGC
	3	CCCACGTACTTATAAAGAA	TTCTTTATAAGTACGTGGG
	4	CGGGCCTGAAGCCAGGTGA	TCACCTGGCTTCAGGCCCG
	5	GGTTATGAACTTTAAAGTT	AACTTTAAAGTTCATAACC
	6	CCTGAAGCCAGGTGACTTT	AAAGTCACCTGGCTTCAGG
	7	GGCAAATGTAACTGTGCCA	TGGCACAGTTACATTTGCC
	8	GGGAGCTGAGTAACACCAT	ATGGTGTTACTCAGCTCCC
	9	TGCATTTCAATCCCACGTA	TACGTGGGATTGAAATGCA
	10	CATGATGTAGAGTGTGGTT	AACCACACTCTACATCATG
	11	GTCCGTGACCTATCAGTTA	TAACTGATAGGTCACGGAC
	12	GAGTAACACCATCGATCAT	ATGATCGATGGTGTTACTC
	13	GTTAACTCACTGAGGGTAT	ATACCCTCAGTGAGTTAAC
	14	GGTGAATTTCACAAGCTAT	ATAGCTTGTGAAATTCACC
	15	TTCCATAATAAAAGGCTTT	AAAGCCTTTTATTATGGAA
	16	CAATCCCACGTACTTATAA	TTATAAGTACGTGGGATTG
	17	ACTGAGGGTATCTGACAAT	ATTGTCAGATACCCTCAGT
	18	CACAAGCTATTCCCTCAAA	TTTGAGGGAATAGCTTGTG
	19	CTGAGGGAGCTGAGTAACA	TGTTACTCAGCTCCCTCAG
	20	TGTAGAGTGTGGTTATGAA	TTCATAACCACACTCTACA
	21	GAACTTTAAAGTTATAGTT	AACTATAACTTTAAAGTTC
	22	GGATGTTGCCACTGGCAAA	TTTGCCAGTGGCAACATCC
	23	GGCTTTGAGTTAACTCACT	AGTGAGTTAACTCAAAGCC
	24	TGTATGTGCTCTTAGCAAA	TTTGCTAAGAGCACATACA
	25	GCCACTGGCAAATGTAACT	AGTTACATTTGCCAGTGGC
	26	GCTGAGTAACACCATCGAT	ATCGATGGTGTTACTCAGC
	27	AGGAGAATGAAATGTATGT	ACATACATTTCATTCTCCT
	28	GGGTATCTGACAATGCTGA	TCAGCATTGTCAGATACCC
	29	CGCTACAGCCTGAGAGATT	AATCTCTCAGGCTGTAGCG
	30	CGATCATGATGTAGAGTGT	ACACTCTACATCATGATCG
si-HULC	1	CATATGTATCTTTGGAAGA	TCTTCCAAAGATACATATG
	2	GGAATTGGAGCCTTTACAA	TTGTAAAGGCTCCAATTCC

	3	GACCATGCAGGAACTCTGA	TCAGAGTTCCTGCATGGTC
	4	GGTGGAACTCATGATGGAA	TTCCATCATGAGTTCCACC
	5	GCAAGAAGTTTCCTGGCAA	TTGCCAGGAAACTTCTTGC
	6	CTGAAGTAAAGGCCGGAAT	ATTCCGGCCTTTACTTCAG
	7	GACATTTCAACCTCCAGAA	TTCTGGAGGTTGAAATGTC
	8	CTGAATTATGTTGTTATCA	TGATAACAACATAATTCAG
	9	GCCTTTACAAGGGAATGAA	TTCATTCCCTTGTAAAGGC
	10	GTACTTTCTCCCTGAATTA	TAATTCAGGGAGAAAGTAC
	11	GAGACAAGAGCTCTCTTTA	TAAAGAGAGCTCTTGTCTC
	12	GGAAGAAACTCTGAAGTAA	TTACTTCAGAGTTTCTTCC
	13	CAGACCAAAGCATCAAGCA	TGCTTGATGCTTTGGTCTG
	14	GCCGGAATATTCTTTGTTT	AAACAAAGAATATTCCGGC
	15	CCTGGCAATAAACTAAGCA	TGCTTAGTTTATTGCCAGG
	16	CTGTGGCAAATTTGTACTT	AAGTACAAATTTGCCACAG
	17	GGAACACAAATTAAGTGTT	AACACTTAATTTGTGTTCC
	18	GGAAGAGTCGTCACGAGAA	TTCTCGTGACGACTCTTCC
	19	GGAACTCTGATCGTGGACA	TGTCCACGATCAGAGTTCC
	20	GTGTTCAACCTGTGGCAAA	TTTGCCACAGGTTGAACAC
	21	CCAATCTGCAAGCCAGGAA	TTCCTGGCTTGCAGATTGG
	22	CTGAAACTAGAATTAAACA	TGTTTAATTCTAGTTTCAG
	23	GTCACGAGAACCAGACCAT	ATGGTCTGGTTCTCGTGAC
	24	CCACGTGAGGATACAGCAA	TTGCTGTATCCTCACGTGG
si-PLK1	1	GGCAACCAAAGTCGAATAT	ATATTCGACTTTGGTTGCC
	2	CCGAAACCGAGTTATTCAT	ATGAATAACTCGGTTTCGG
	3	GACTTCGTGTTCGTGGTGT	ACACCACGAACACGAAGTC
	4	CCCGCACTATGGTGGACAA	TTGTCCACCATAGTGCGGG
	5	CCATGGAAATATCCATTCA	TGAATGGATATTTCCATGG
	6	CGGCCAGCAACCGTCTCAA	TTGAGACGGTTGCTGGCCG
	7	CCGTGAGTTCCCATCCCAA	TTGGGATGGGAACTCACGG
	8	GGTCGACTGCCACCTCAGT	ACTGAGGTGGCAGTCGACC
	9	GGGTATCAGCTCTGTGATA	TATCACAGAGCTGATACCC

	10	GGGCCCATACTGGTTGGCT	AGCCAACCAGTATGGGCCC
	11	GACCATTCCACCAAGGTTT	AAACCTTGGTGGAATGGTC
	12	CCCAACTCCTTGATGAAGA	TCTTCATCAAGGAGTTGGG
	13	CGGGCAAGATTGTGCCTAA	TTAGGCACAATCTTGCCCG
	14	GGGTTGCTGTGTAAGTTAT	ATAACTTACACAGCAACCC
	15	GGCACTGAGTCCTACCTCA	TGAGGTAGGACTCAGTGCC
	16	CCCTCACAGTCCTCAATAA	TTATTGAGGACTGTGAGGG
	17	GGCAGCGTGCAGATCAACT	AGTTGATCTGCACGCTGCC
	18	CCATATGAATTGTACAGAA	TTCTGTACAATTCATATGG
	19	GCCAGTACCTGCACCGAAA	TTTCGGTGCAGGTACTGGC
	20	CCCTGTGTGGGACTCCTAA	TTAGGAGTCCCACACAGGG
	21	CCATTAACGAGCTGCTTAA	TTAAGCAGCTCGTTAATGG
	22	GCCTCATCCTCTACAATGA	TCATTGTAGAGGATGAGGC
	23	CACTGCCCGCCCAACCATT	AATGGTTGGGCGGGCAGTG
	24	CTGAGCCTGAGGCCCGATA	TATCGGGCCTCAGGCTCAG
	25	CGATACTACCTACGGCAAA	TTTGCCGTAGGTAGTATCG
	26	CTTAATGACGAGTTCTTTA	TAAAGAACTCGTCATTAAG
	27	GCTGCACAAGAGGAGGAAA	TTTCCTCCTCTTGTGCAGC
	28	CCATCTTCTGGGTCAGCAA	TTGCTGACCCAGAAGATGG
	29	CACCAGCACGTCGTAGGAT	ATCCTACGACGTGCTGGTG
	30	GGATCAAGAAGAATGAATA	TATTCATTCTTCTTGATCC

3.5.2 RT - qPCR primer sequences

Table 7. List of RT - qPCR primers used in this study

Gene Name	Sequence (5'-3' direction)
DANCR.F	GCGCCACTATGTAGCGGGTT
DANCR.R	TCAATGGCTTGTGCCTGTAGTT
GAPDH.F	CTGGTAAAGTGGATATTGTTGCCAT
GAPDH.R	TGGAATCATATTGGAACATGTAAACC
IL-1a.F	AGTAGCAACCAACGGGAAGG

IL-1a.R	AAGGTGCTGACCTAGGCTTG
IL-1b.F	GCCATGGACAAGCTGAGGAA
IL-1b.R	TCGTTATCCCATGTGTCGAAGA
lincNMR-amp#1.F	CATGGGACAGCCCTCTGAAA
lincNMR-amp#1.R	CTGTTTGAGGTCCTGGACGG
lincNMR-amp#2.F	TGCTTTAATCCTGTCGTGGC
lincNMR-amp#2.R	CGGAAAGGCTTGGACGAAGT
lincNMR-amp#3.F	TTATGAGGACTGCACCACAGC
lincNMR-amp#3.R	GTTTGAGGTCCTGGACGGAA
MALAT1 1787 F	GAATTGCGTCATTTAAAGCCTAGTT
MALAT1 1871R	GTTTCATCCTACCACTCCCAATTAAT
NEAT1.F	GTCTTTCCATCCACTCACGTCT
NEAT1.R	GGACAACTAGATGCCGAGGTAG
PPIA.F	CTGCTGTCTTTGGGACCTTGT
PPIA.R	GTCAACCCCACCGTGTTCTT
RNU1-1.F	TTATCCATTGCACTCCGGATGT
RNU1-1.R	CCCCACTACCACAAATTATGCAG
RRM2.F	AGGACATTCAGCACTGGGAA
RRM2.R	TTCTTGGCTAAATCGCTCCA
SRSF4.F	TGCAGCTGGCAAGACCTAAA
SRSF4.R	TTTTTGCGTCCCTTGTGAGC
TK1.F	TGCCAAAGACACTCGCTACA
TK1.R	CGATGCCTATGACAGCCAC
TYMS.F	TTCTGGAAGGGTGTTTTGGA
TYMS.R	TGGCATCCCAGATTTTCACT
YBX1.F	AGGGTGCAGGAGAACAAGGT
YBX1.R	TCATTGCCGTCCTCTCTAGG

3.5.3 Sequences of 5’ and 3’ RACE primer

Table 8. List of primers used for 5’ and 3’ RACE experiments

RACE	GSP Name	Sequence (5'-3' direction)
5'RACE	5'RACE_GSP_001	ACGTTGCCACGACAGGATTAAAGC
3'RACE	3'RACE_GSP_e1	CGAGTGAGGACGACCTCTTCCTATATGC

3.5.4 Sequences of biotinylated DNA oligos

Table 9. Sequences of biotinylated DNA oligos used for *lincNMR* RAP-MS

Name	Bases	Modification	Sequence
*lincNMR*_2	90	/5Biosg/	/5Biosg/TGGGCGTGGGCGAAGCTGATCCCTCTAGGTCGGACTAAGGCAGAGCCAGATCCAAGAGGGAGAATCCAACTGTAAAAGGGATCTGGGGAA
*lincNMR*_3	90	/5Biosg/	/5Biosg/AAAGGGGAGAACTGTAGTTTTCAGAGTTCTAATGAACATCCCAATGGGCCTAAAAGGCTTCAATAAGAGATGAAAGGTTCCGGGTGAGAG
*lincNMR*_4	90	/5Biosg/	/5Biosg/TCTTGCCTTTCTGAATTCTGAAAAAAGAGTGGTATTGGAATCTCTTCTTACCGGAACCCAGGAGAGGGCGAGCTGTGGTGCAGTCCTCAT
*lincNMR*_5	90	/5Biosg/	/5Biosg/GGATTGTCGAAAAGGTGGCTCCCTTCAGACAGACCAAGCCCAATTCATGGCAGCGTTCCCAGCCCCAGTTTGAAGCTCAGTAAGGTGGTC
*lincNMR*_6	90	/5Biosg/	/5Biosg/ACGTTTATTCTGCTTTGGTTCTTCTTAATCTGACCTCTATAGACTTCGCCACGATCCAAGGTGTAATTCCAACAGGCAAAAGAAGTCTAA
*lincNMR*_7	90	/5Biosg/	/5Biosg/TCCTATCTCGTCCTTAATGTTCAAAACGCAGGGTATAGCAAAGCATATAGGAAGAGGTCGTCCTCACTCGTGAACTCAGCATCGGGTTCT
*lincNMR*_8	90	/5Biosg/	/5Biosg/TCAGAGGGCTGTCCCATGGGCTCACTCTGCAACCAGGTGGAAGTCAACGTTGCCACGACAGGATTAAAGCAAGAAGAAACATTATGGGCC
*lincNMR*_9	90	/5Biosg/	/5Biosg/TCTTCTTGTGATTGGATCTGTTTGAGGTCCTGGACGGAAAGGCTTGGACGAAGTCCTTGCAGACTCAGCATGGTTGTAAGCAGTATAA

			TT
*lincNMR*_10	90	/5Biosg/	/5Biosg/TTTTTCCACTTAACATGATTATTTTCCCAGTCATTTCATGTTC TTCAAAAACCCCGATGATAGGAATAATTTTCTCTTTCCTGAAATCTC

3.6 Biological material

3.6.1 Human cancer cell lines

Table 10. Cell line, origin, growth medium and biosafety level

Organ	Cell line	Description	Medium	Biosafety
Lung	A549	Human lung adenocarcinoma cell line	DMEM	1
Lung	NCI-H1299	Human NSCLC epithelial cell line	DMEM	1
Lung	NCI-H460	Human large cell lung cancer epithelial cells	DMEM	1
Liver	FLC-4	Human hepatocellular carcinoma cell line	RPMI-1640	1
Liver	Hep3B	Human hepatocellular carcinoma cell line	RPMI-1640	1
Liver	HepG2	Human hepatocellular carcinoma cell line	RPMI-1640	1
Liver	HLE	Human hepatocellular carcinoma cell line	RPMI-1640	1
Liver	HLF	Human hepatocellular carcinoma cell line	RPMI-1640	1
Liver	Huh6	Hepatoblastoma	RPMI-1640	1
Liver	Huh-7	Human hepatocellular carcinoma cell line	RPMI-1640	1
Liver	PLC	Human hepatocellular carcinoma cell line	RPMI-1640	2
Liver	SK-HEP1	Adenocarcinoma	RPMI-1640	1
Liver	SNU-182	Human hepatocellular carcinoma cell line	RPMI-1640	1
Liver	SNU-387	Human hepatocellular carcinoma cell line	RPMI-1640	1
Breast	MCF7	Human mammary ADC epithelial cell line	DMEM	1
Breast	KPL-1	Human mammary carcinoma cell line	DMEM	1
Breast	T47D	Human mammary Invasive ductal cancer	DMEM	1

3.6.2 Antibodies

Table 11. List of antibodies used in this study

Antibody Name	Host	Company	Catalogue No.	MW (kDa)	Dilution

anti-Flag-M2	Mouse	Sigma	1804	-	1:1000
anti-HA.11	Mouse	Covance	MMS-101P	-	1:1000
GAPDH	Mouse	Millipore	MAB374	37	1:20000
Goat Anti-Mouse	Goat	Abcam	ab6789	-	1:2500
Goat Anti-Rabbit	Goat	Abcam	ab6721	-	1:2500
RRM2	Mouse	Abcam	ab57653	30/45	1:1000
TK1	Rabbit	Abcam	ab76495	25	1:5000
TYMS	Rabbit	Abcam	ab168853	36	1:2000
Vinculin	Mouse	Santa Cruz	sc-25336	116	1:1000
YBX1	Mouse	Abcam	ab12148	36	1:1000

3.6.3 Plasmids

Table 12. List of plasmids used in this study

Plasmid	Source
pFRT-Flag-HA-ΔCmR-ΔccdB	From Sandeep Dukare
pFRT-Flag/HA-YBX1	Gene and clone repository DKFZ
pRL-TK	From Sven Diederichs
pRL-SV40	From Sven Diederichs
Y-Box-TATA-Luc	Gift from Prof. Birgit Schittek group

3.7 Softwares

Table 13. List of softwares used in this study

Software	Provider
Adobe Illustrator	Adobe
Flow Jo	FlowJo, LLC
GraphPad Prism 8	GraphPad Software, San Diego, USA
GSEA	Broad Institute, Cambridge, USA
Image J	NIH and the Laboratory for Optical and Computational Instrumentation, USA
Ingenuity	Qiagen, USA
MS Office	Microsoft
Perseus	Max Planck Institute of Biochemistry, Munich, Germany
StepOne v2.3	Applied Biosystems, Darmstadt, Germany

3.8 Online tools and databases used in this study

Table 14. List of web tools used in this study

Name
ENCODE – Accessed through tracks in the UCSC genome browser
KM Plotter – http://kmplot.com/analysis/
Panther Database – http://www.pantherdb.org/
PhyloCSF - Accessed through tracks in the UCSC genome browser
Primer-Blast – https://www.ncbi.nlm.nih.gov/tools/primer-blast/
Switchgear TSS – Accessed through tracks in the UCSC genome browser
TANRIC – https://ibl.mdanderson.org/tanric/_design/basic/index.html
UCSC Genome Browser – https://genome.ucsc.edu/

This page has been intentionally left blank

4. METHODS

Parts of the text and figures presented in this chapter are revised versions of the figures and text submitted for publication as an original research article:

Gandhi et al., *"lincNMR* regulates Nucleotide Metabolism via a YBX1 - RRM2 Axis in Cancer"
Nature Communications (manuscript under review)

Unless otherwise indicated, all commercially available reagents and kits were used according to manufacturer's instructions.

4.1 Human cancer cell lines

4.1.1 Growth and propagation of human cancer cell lines

Details on the cell lines, growth medium used in this study are provided in Table 10

All cell lines were cultured in a cell culture incubator at 37°C and 5 % CO_2 without the addition of any antibiotics. Liver cancer cell lines (HLE, HLF, FLC - 4 and SNU - 387) used in this study were a kind gift from PD Dr. Kai Breuhahn (Institute of Pathology, University Heidelberg, Heidelberg Germany). Lung (A549, NCI - H1299 and NCI - H460) and breast cancer cell lines (MCF - 7, KPL - 1 and T47D) were purchased from ATCC. Liver cancer cell lines were grown in RPMI - 1640 medium supplemented with 10 % FBS whereas lung and breast cancer cell lines were grown in DMEM (high glucose) and supplemented with 10 % FBS.

For the cell culture, 1 X PBS and respective culture medium were pre-warmed in a water bath at 37°C. Cells were washed once with 1 X PBS and incubated with 0.05 % trypsin at 37°C until cells were detached from the surface. Detachment time varied depending on the cell line used. Two volumes of respective growth medium was added to the plate and cells were pipetted to ensure complete mixing in order to inactivate the trypsin as well as to completely detach the cells from the surface. 10 µL of cell suspension was used to calculate cell number using the hemocytometer (Neubauer). After counting, required number of cells were diluted as per experimental requirement and either used for further downstream assays, further seeded and frozen.

4.1.2 Cryopreservation of cells lines

For long term storage of cell lines, growth medium was removed, cells were washed twice with 1 X PBS and trypsinized using 0.05% Trypsin-EDTA for 2 - 8 minutes depending on cell line used. Trypsin was deactivated using complete growth medium and cells in suspension were centrifuged at 200 *g* for 5 minutes to pellet the cells. Cell pellet was re - suspended in cryo - medium (10 % DMSO and 20 % FCS in complete growth medium) in cryo vials. Freezing container called Mr. Frosty was used to store the cryo vials to attain cooling rate of -1°C / min in - 80°C freezer. For long term storage, vials were transferred to the liquid nitrogen tank.

4.1.3 Thawing of cryo - preserved cells

To thaw cryo-preserved cells, respective complete growth medium was warmed to a temperature of 37°C in a water bath. 1 ml of warmed medium was added to the cryo vials and mixture was re-suspended in growth medium. Cells were centrifuged at 200 *g* for 5 minutes in order to remove freezing medium and then plated on a 10 cm dish.

4.1.4 Cell line authentication and mycoplasma test

As a quality control measure, all cell lines used in this study were periodically tested at a 3-month interval for mycoplasma contamination using a PCR based detection kit. Genomic DNA was isolated from the cell lines to be tested and sent for authentication by using cell authentication services from Multiplexion, Heidelberg, Germany [159].

4.2 Transfections

4.2.1 siPOOL transfections

siPOOL sequences used in this study are provided in Table 6

For RNAi mediated knockdowns, siPOOLs were used [160]. siPOOLs were reverse transfected onto the cells using Lipofectamine RNAiMAX as a transfection reagent in serum free RPMI-1640 medium to a final concentration of 10 nM.

4.2.2 Plasmid transfections

Details of plasmids used in this study are provided in Table 12

For plasmids transfections, required number of cells were seeded on day 1 into 6 well plates and transfected with plasmids on day 2. For all plasmid transfections in this study, TurboFect transfection reagent together with serum free medium opti-MEM was used. Two reaction mixtures were prepared, master mix 1 (DNA and opti-MEM) and master mix 2 (TurboFect and opti-MEM) in such a way that DNA: TurboFect ratio was in the range of 1:2-1:2.5 for all transfections. Both master mixes were combined and incubated at room temperature for 15 minutes. After the incubation, master mix was added dropwise on the cells. Cell plate was swirled to ensure proper mixing of reagents.

4.3 RNA isolation, reverse transcription and quantitative PCR

4.3.1 RNA isolation using TRIzol

Cells were prepared for RNA isolation by washing with pre-warmed 1 X PBS. 1 ml of TRIzol was added to the cells and shaken on a rotor for 5 minutes at room temperature to ensure complete denaturation of cells. Lysate was then transferred to fresh tubes and stored at – 20°C for up to a week until ready for RNA isolation. For isolating RNA, frozen TRIzol lysates were thawed at room temperature and 200 µL of chloroform was added to the tubes. Tubes were incubated for 2 - 3 minutes at room temperature after shaking for 30 s. Tubes were then further centrifuged at 10,000 g for 15 minutes at 4°C. Next, about 230 µl of aqueous phase was transferred into a new tube containing 500 µl of isopropanol. Tubes were mixed by inverting multiple times. Next, RNA was precipitated for at least 1 h at -20°C after subsequent centrifugation at 4°C at a speed of 12,000 *g.* Pelleted RNA was washed twice with 1 ml of 70 % ethanol and centrifuged at 8000 *g* for 5 minutes at 4°C. Supernatant was then carefully removed, pellet was partially air dried to ensure complete removal of ethanol and then re-suspended in pre-heated nuclease free water.

4.3.2 RNA isolation using kits

Isolation of RNA from RAP-MS and UV-RIP-qPCR samples was performed as per manufacturer's protocol using miRNeasy Mini kit.

4.3.3 DNase digestion of total RNA

DNase digestion was performed in a 50 µL reaction with up to 50 µg of RNA, 5 µL of 10X buffer (Roche), 1 µL of DNase I. This mix was incubated for 30 min at 37°C. After incubation, 150 µL of nuclease free water was added to the reaction. Further samples were shaken for 15 s after addition of 200 µL of Roti-

Aqua-P/C/I for RNA extraction and incubated for 2 minutes at room temperature. Next, samples were centrifuged for 2 minutes at a speed of 13,000 rpm. Upper phase was transferred into the new tubes containing 200 µL of chloroform. At this step, RNA was treated as per the RNA isolation procedure and upper aqueous phase was transferred in to new tube containing 1 µl of 10 µg/µl of glycogen (Carl Roth) and 19 µl of 3 M sodium acetate (pH5.2, Carl Roth). Next, 500 µl of ice cold ethanol was added to the tube and contents were mixed by inverting multiple times. Tubes were stored at -80°C for at least 2 h to precipitate RNA. After the incubation, tubes were centrifuged at 16,000 g minutes at 4°C and pellet washed twice with 70% ethanol. RNA pellet was re-suspended in pre warmed nuclease free water after complete removal of ethanol and stored at 80°C until further downstream applications.

4.3.4 DNase digestion of RNA isolated using kits

DNAse digestion was performed as per manufacturer's instruction using TURBO DNA *free* kit.

4.3.5 Reverse transcription

1 µg of RNA was mixed in a reaction with 2 µL of 10 mM dNTPs, 1 µL random hexamer primer to the total volume of 15 µL with ultra-pure water. Sample was mixed by vortexing and heated to 65°C for 5 minutes to denature RNA. Sample tubes were immediately transferred to ice where 4 µL of 5 X reverse transcriptase buffer and 1 µL of Revert Aid reverse transcriptase was added to the reaction. Samples were incubated using thermal cycler at room temperature for 10 min and later at 42°C for 1 h. Reaction was terminated by heating the sample to 70°C for 10 minutes.

4.3.6 qPCR primer design

All the primers used in this study were designed by Primer-Blast tool based on Primer3 algorithm. Following parameters were considered while designing: PCR product between of 70 – 150 bp, primer length of 20 – 27 bp and melting temperature in the range of 59 – 61°C. Primers were synthesized and delivered by Sigma-Aldrich.

4.3.7 qPCR

Sequences for primers used in this study are provided in Table 7

This method was used to determine the relative expression of the genes. cDNA was diluted to 1:40 with DNAse and RNAse free water and 4 µL of diluted cDNA was used in a qPCR reaction. RT - qPCR was performed using Power SYBR Green PCR Master Mix on Applied Biosystems StepOne Plus thermal cycler

with holding stage of 95°C for 10 min followed by a 40 cycles of 95°C for 15 sec and 60°C for 30 sec. Normalization of the obtained data was performed with PPIA, GAPDH and/or SRSF4 as internal reference controls. Data was analyzed using StepOne Software v2.3.

4.4 Protein isolation, quantitation, western blot

4.4.1 Protein lysate preparation

For preparing protein lysates, cells were washed with 1 X PBS to ensure complete removal of growth medium and the plates were transferred to ice. Cells were washed again with 2 ml of ice cold PBS and complete PBS was removed. Every use, RIPA buffer was freshly supplemented with protease and phosphatase inhibitor cocktail. 200 µL of RIPA buffer supplemented with 1 X Protease (Roche) and Phosphatase Inhibitors was added in each well and incubated on ice with intermittent mixing for 30 minutes. After incubation, cell lysate was collected from the well and centrifuged at 17000 g for 10 mins at 4°C. Next, supernatant was transferred to a new Eppendorf tube and protein quantification was performed using Pierce BCA Protein Assay Kit.

4.4.2 Bicinchoninic Acid (BCA) assay

For BCA assay, first a BSA standard curve was prepared from Bovine Serum Albumin (BSA) Fraction V in the range of 0 - 1.4 mg/ml in technical duplicates using the same aliquot of supplemented RIPA buffer. Depending on the experiment schematic in terms of number of cells used for cell lysis, samples were either undiluted or diluted up to 1: 50 in the same RIPA buffer in duplicates. 10 µl of each sample was transferred to a new tube and 200 µl of BCA reagent mixture in the ratio of 50: 1 for BCA: Copper (II) sulfate solutions was added. Samples were next incubated for 30 minutes at 37°C on a mixer. After incubation, 80 µl of sample was transferred to a cuvette and absorbance was measured at 550 nm using the BioPhotometer Plus.

4.4.3 Sodium Dodecyl Sulfate - Polyacrylamide Gel Electrophoresis (SDS-PAGE)

The recipe for buffers used is provided in Table 4.

In this study, sample concentration used for loading on to SDS-PAGE gel was 10 - 20 µg per sample. Required volume of samples were boiled for 10 mins at 95°C in 4 X laemmli buffer before loading onto 10 % gel. SDS mini gels were cast in-house using 4 % gel stacking layer. Gels were run at room temperature at up to 160 V using a power pack from Bio-Rad. 5 µl pre-stained PAGE ruler was used as a

size marker on each gel to assist in size analysis of the blotted proteins. SDS - PAGE was performed using Mini-Protean system.

4.4.4 Western Blot

After the electrophoresis, proteins were transferred to nitrocellulose membrane using transfer buffer (0.25 M Tris-base, 1.92 M Glycine, 1 % SDS with 20 % Methanol) at 120 V for 90 minutes. Membrane was blocked with 5% Milk in 1 X TBS-T (1 X TBS, 0.1 % Tween-20) for 30 minutes. Blots were incubated in 5 % skimmed milk solution containing the respective dilutions of primary antibody overnight at 4°C. Details on antibodies used and their respective dilutions is available in Table 11. After the overnight incubation, blots were washed 5 times with 1 X TBS-T to ensure complete removal of primary antibody solution. Blots were then incubated in respective secondary antibody for 1 h at room temperature at a concentration of 1: 2500. After incubation with secondary antibodies, membranes were washed 5 times with 1 X TBS-T to remove the unbound antibodies. Membranes were incubated in 1: 1 Super Signal West Pico Stable Peroxidase Solution and the Luminol Enhancer Solution for 5 min. After incubation, images were acquired for detection of specific bands using ChemoCam Imager and quantification of the signal was done using LabImage 1D software.

4.5 Plasmid isolation, purification and sequencing

4.5.1 Generation of plasmids in Gateway vector system

Respective gateway entry vectors were obtained from DKFZ plasmids and clone repository. LR reaction was performed with 50 - 150 ng of entry vector using LR Clonase II as per manufacturers instructions into the gateway destination vector pFRT-Flag/HA. Mach-1 cells were used for transformation. Mini Prep was performed using NucleoSpin® Plasmid kit. Midi Prep was done using PureLink™ HiPure Plasmid kit. Services from Eurofins genomics/ GATC were used for sequencing with CMV.for CGCAAATGGGCGGTAGGCGTG and BGH.rev TAGAAGGCACAGTCGAGG primers. Finally, cells were transfected with respective plasmid of interest and empty vector pFRT-Flag-HA-ΔCmR-ΔccdB as a control plasmid. Overexpression was confirmed by western blot using anti-Flag-M2 or anti-HA antibody (Table 11).

4.5.2 Genomic DNA isolation

GenElute Mammalian Genomic DNA Miniprep kit was used to isolate genomic DNA from cultured cells. From respective cells, $6*10^6$ were harvested and pelleted after centrifugation at 300 *g* for 5 minutes. Cell pellet was re-suspended in 200 µL of resuspension solution with 20 µL of RNAse A. Mix was incubated for 2 minutes at room temperature. 200 µL of cell lysis solution containing 20 µL of proteinase K was added to the mix and vortexed for 15 s vigorously. Sample was incubated at 70°C for 10 minutes. 500 µl of column preparation solution was used to equilibrate the columns and then centrifuged for 1 minutes at 12,000 *g*. 200 µl of ethanol was added to the lysate and vortexed to homogenize the solution. Next, the lysate was loaded onto the column and centrifuged for 1 minutes at 6500 *g*. Supernatant/ flow through was discarded and 500 µl of wash solution was added to the column and centrifuged for 1 minutes at 6500 *g*. The column was washed for the second time and centrifuged for 3 minutes at a maximum speed. Columns were then incubated for 5 minutes with 200 µl of elution buffer at room temperature. The DNA was eluted by centrifugation at 6500 *g* for 1 min.

4.5.3 Transformation of bacteria

Chemically competent E.coli (Mach 1) cells were used in this study. 50 µL of Mach 1 cells were incubated with approximately 1 µL of plasmid DNA. The sample was mixed gently by pipetting up and down using a sterile cut tip and incubated on ice for 15 minutes. The sample was then at incubated at 42°C for 40 s in a thermocycler for a heat-shock. Next, samples were immediately transferred to ice and 200 µL of LB media without antibiotics was added. 100 µl of reaction mix was then pipetted on to pre-warmed selective LB-plates after incubation at 900 rpm at 37°C for 45 min and distributed with the help of sterile glass balls/ spreader. Plates were then incubated overnight at 37°C and single clones were picked the next morning and inoculated into about 80 ml of LB medium with 100 µg / mL ampicillin for plasmid DNA preparation.

4.5.4 Plasmid DNA isolation

NucleoSpin plasmid kit was used to perform mini prep as per manufacturer's instruction. Sequences were confirmed using sanger sequencing services from Eurofins genomics/GATC Biotech. Nanodrop 2000 was used to check the DNA concentrations. Plasmids were stored at -20°C until further use.

4.6 Basic characterization of *lincNMR*

4.6.1 Subcellular fractionation

Recipes for buffers used for this protocol are provided in Table 4. All buffers used in this protocol were supplemented with RNase inhibitor cocktail SUPERase-In. Fraction specific controls were used to assess the quality of fractions obtained (chromatin fraction: *NEAT1*, *MALAT1*, nucleoplasmic fraction: *RNU-1*, cytoplasmic fraction: *DANCR*).Primer sequences are provided in Table 7.

Subcellular fractionation was performed in HLE cells to separate chromatin associated, nucleoplasmic and cytoplasmic fractions as per the previously described protocol [161]. HLE cells were grown on a 15-cm dishes and allowed to achieve 80 % - 90 % confluency. $10*10^6$ cells were harvested, pelleted and used for each replicate for a fractionation experiment. Pellets was carefully washed twice with 1 X ice cold PBS to ensure complete removal of growth medium. Cells were centrifuged at 500 x *g* and kept on ice in order to avoid any RNA degradation. Cell pellet was then re-suspended in 380 µl of hypotonic lysis buffer (HLB) and incubated for 10 mins on ice. The samples were vortexed to ensure complete mixing and then centrifuged at 4°C for 3 min at 1000 x *g*. The supernatant fraction = cytoplasmic fraction was transferred carefully to a fresh tube and mixed with 1 mL of RNA precipitation solution (RPS) and kept at -20°C for at least 1 h. The remaining cell pellet= nuclei were washed thrice with 1 mL of ice-cold HLB and centrifuged at 4°C for 2 mins at a speed of 500 x *g*. Next, 380 µl Modified Wuarin - Schibler buffer (MWS) was added to the pellet and carefully vortexed for 30 s and later incubated on ice for 5 min. Nuclei were incubated on ice for 10 min after vortexing for 30 s. Later, at 4°C sample was centrifuged for 3 min at 1000 x *g* and the supernatant = nucleoplasmic fraction was transferred to a fresh tube. 1 mL of RPS was then added and the fraction was stored for at least 1 h at -20°C. The remaining pellet, now chromatin fraction was carefully washed thrice using 1 mL of cold MWS to remove any leftover nucleoplasmic fraction and centrifuged at 4°C for 2 min at a speed of 500 x *g*. Sample was stored at 20°C after adding of 1 mL of TRIzol. The stored cytoplasmic and nucleoplasmic fractions were vortexed and centrifuged at a high speed of 18000 x *g* at 4°C for 15 min. The pellet was washed with ice-cold 70% ethanol after discarding the supernatant and centrifuged at 18000 x *g* at 4°C for 15 min. 1 mL of TRIzol was added to the pellets and stored at -20°C. Now as next steps, 10 µl 0.5 M EDTA was added, samples were mixed by vortexing and heated to 65°C until the pellet was completely dissolved. Samples were then cooled to room temperature and 200 µl of chloroform: isoamyl alcohol was added, samples were vortexed and immediately centrifuged at 18000 x *g* at RT for 10 min. The supernatant was then

transferred to a fresh tube and 1 volume of isopropanol was added and precipitated overnight at -20°C. After centrifugation at high speed of 18000 x *g* at 4°C for 5 min, the supernatant was discarded, and the now RNA was re-suspended in DNase, RNase free ultra-pure H2O. Nanodrop 2000 was used to measure the RNA concentration. DNase digestion of 5 µg of RNA was performed by adding 5 µL of 0.5 µL Ribolock, 10X DNase buffer, 0.5 µL DNAse for a total reaction volume of 50 µL with ultra-pure H_2O. Further steps, reverse transcription and quantitative real time polymerase chain reaction were performed as described in the section 4.3.

4.6.2 Rapid Amplification of cDNA ends (RACE)

The SMARTer RACE cDNA Amplification Kit was used to perform 5' and 3' RACE analysis according to the manufacturer's instructions. The gene-specific primers used are listed in Table 8.

Total RNA (DNAse I treated) from HLE cells was used for first strand cDNA synthesis. PCR reaction was performed in Bio-Rad DNA Engine PTC200 thermal cycler using Advantage 2 polymerase mix. Obtained PCR products were resolved on 1% agarose gel and visible bands were extracted using GeneJET Gel Extraction kit. Extracted bands were eluted in 30 µl of nuclease free water. Purified fragments were cloned into pCR2.1 TOPO TA vector backbone and Mach1 *E-coli* cells were transformed. Plasmids were isolated using Axyprep Plasmid Mini Prep Kit after picking the colonies the next day. Gene specific primers were used for sequencing using services from GATC Biotech.

4.7 Cellular function of *lincNMR*

4.7.1 Cell viability assay

CellTiter-Glo Luminescent Cell Viability Assay was performed 72 h after knockdown with the respective siPOOLs. At the time point for the assay, growth medium was removed from the cells using multi-channel pipette and 60 µL of 1:4 CellTiter-Glo reagent: 1X PBS was added to the cells. Plate was incubated for 15 minutes at room temperature in the dark using an orbital shaker. After the incubation, chemiluminescence was measure using luminometer.

4.7.2 Cell proliferation assay

Cell Proliferation Assay kit was used to assess the impact of knockdown on proliferative capacity of cells. For the assay, at respective time point, the BrdU reagent was added to the final concentration of 10 µM to each well and the cells were allowed to grow for 6 h. Next, the medium was removed and the plate

was further incubated for 30 minutes at room temperature after the addition of 200 µL of FixDenat solution. After the incubation, the FixDenat solution was removed and 100 µL of 1:100 dilution of BrdU antibody-POD solution was added and plate was incubated for 90 minutes on an orbital shaker in dark. Next, the cells were washed thrice with washing buffer at room temperature on a shaker for 5 minutes each. After washing steps, 100 µL of Luminol substrate was added and plate was incubated for 3 minutes. After the incubation, chemiluminescence was measure using luminometer.

4.7.3 Cell cycle analysis

72 h post treatment with siPOOLs, cells were trypsinized and fixed in 70 % Ethanol overnight at -20°C. Fixed cells were pelleted and washed with 1 X PBS. After washing step, cells were re-suspended in 1 X PBS containing 100 µg/ml RNAse A and incubated at 37°C for 30 minutes. Post RNAse treatment, cells were stained with 100 µg/ml Propidium Iodide (PI). 10000 cells were acquired on BD FACSCanto II Flow Cytometer and data analysis was performed using FlowJo v10 software.

4.7.4 Senescence associated β-GAL assay

Cell were reverse transfected with respective siPOOLs on a 6-well plates and 96 h post transfection SA-β-GAL activity was detected. Cells were washed with 1 X PBS and fixed at room temperature with 0.5% Glutaraldehyde for 20 mins. Cells were washed twice with 1 X PBS supplemented with 1 mM MgCl2 (pH 6.0) for 10 min on a rocker. 2 ml X-Gal staining solution (1X PBS containing 1 mM MgCl2, 41 mg potassium hexacyanoferrate (III), 52.5 mg potassium hexacyanoferrate (II) trihydrate, 1 mg / ml X-Gal (5-bromo-4-chloro-3-indolyl-beta-D-galacto-pyranoside), pH 6.0) was added and the dishes were sealed with parafilm and incubated overnight at 37°C. Next day, the cells were washed 3 X with distilled water and microscopy pictures were taken using 10x objective of a Zeiss Cell Observer microscope. For analysis, 100 cells were manually counted per condition in 3 independent experiments.

4.8 Molecular Function

4.8.1 Triple label SILAC-MS

- Generation of HLE cell lines with light (Lys0, Arg 0), medium (Lys4, Arg 6) and heavy (Lys8, Arg 10) metabolic labels

SILAC Protein Quantitation Kit RPMI 1640 was used to generate light and heavy labelled HLE cells. For generation of medium labelled cells 4, 4, 5, 5-D4 L-Lysine-2HCL (Fischer Scientific) and L-Arginine-HCL

13C6 (Life technologies) were individually purchased. Cells were grown in respective medium supplemented with 200 µg/ml of L-Proline for at least 8-10 passages in a humidified incubator at 37°C with 5 % CO2 for achieving > 99 % incorporation of each respective labels.

- Cell Culture, transfections, lysate preparation, protein quantification, LC-MS/MS

After confirmation of label incorporation, respective HLE cells were grown to 80% confluency. Cells were reverse transfected with respective siPOOLs targeting gene of interest. Lysates were harvested 48 h post transfection. Cells were lysed in 200 µL RIPA buffer supplemented with protease and phosphatase inhibitors. Additionally 0.1 % Benzonase was added to digest nucleic acids. After incubation on ice for 1 h, cell lysates were cleared by centrifuging at 15000 g, for 30 minutes at 4°C. 2-D Quant Kit was used to quantify proteins.

4.8.2 *In vivo* RNA Antisense Purification - Mass Spectrometry (*In vivo* RAP - MS)

This experiment was performed in collaboration with Lander Lab at Broad Institute based in Cambridge MA USA. Biotinylated DNA oligo's complementary to *lincNMR* sequence were ordered from IDT, sequences available in Table 9. 1 billion HLE cells were used per pulldown/condition per biological replicate. *In vivo* RAP-MS was performed as per the protocol described [162].

4.8.3 Crosslinking RNA Immunoprecipitation (UV - RIP)

- Cell seeding, transfection, UV crosslinking and harvesting of cell lysates

On day 1, $4x10^6$ HLE cells were seeded onto 15-cm dish. On day 2, 2 µg of respective constructs (Empty vector plasmid pFRT-Flag-HA-ΔCmR-ΔccdB and pFRT-Flag/HA-YBX1) were transfected using Turbofect transfection reagent with a forward transfection protocol. On day 4, cells were UV crosslinked at a wavelength of 254 nm using 8000 J energy settings and then lysed in high strength cell lysis buffer supplemented with inhibitors cocktail containing SUPERase-In, protease and phosphatase inhibitors. Lysate was passed through syringe to break up the pellet and DNAse digestion was performed as per manufacturer's instruction using Turbo DNA-*free* Kit. Protein quantification was done using BCA reagent and overexpression YBX1 was confirmed by probing with anti-HA antibody using western blot.

- Pulldown

1.5 µg of cell lysate was used to perform UV - RIP using anti-Flag magnetic beads and IP was confirmed by probing for anti-HA using western blot. For UV - RIP protocol, 150 µL of anti-Flag magnetic beads

were used per pulldown. Beads were prewashed 5 X using 1 X TBS and re-suspended in supplemented cell lysis buffer. 5% lysate was removed each for Input fraction and 150 µL of prewashed beads were added to cell lysate and incubated for 1 h at 4°C with rotation. After the incubation, beads were magnetically separated. 50 µL of flow through was saved to confirm depletion of YBX1 and remaining flow through was discarded. Beads were washed 2X first with low salt wash buffer and then with high salt wash buffer with rotation for 5 mins per wash. Beads were magnetically separated and re-suspended in 500 µL of RNAse free pure water. Beads were then separated into fractions of 20 % (for protein extraction) and 80 % (RNA isolation) to confirm the IP and *lincNMR* interaction respectively.

-Elution of RNA

RNA was eluted from the beads by reversal of UV crosslinking in high salt buffer combined with Proteinase K digestion. 160 µL of Proteinase K buffer and 40 µL of Proteinase K were added to the eluted beads and incubated with shaking at 37° C for 30 mins at 1000 rpm. 500 µL of Trizol was added, tube was vortexed for 10 seconds and stored at -20 C until ready for RNA isolation. RNA isolation, reverse transcription and qPCR was performed as described above in section 4.3.

-Elution of Proteins

Captured, washed beads were boiled with 1 X SDS Loading buffer at 95° C for 10 mins and western blot was performed with input and flow through samples to confirm the pulldown. 10 % IP was loaded onto 10 % SDS-PAGE gel.

4.8.4 dNTP measurement assay

This experiment was performed in collaboration with Prof. Kim Baek Lab at Emory University in Atlanta, GA USA. Cellular dNTPs were extracted from cells (HLE and FLC-4) transfected with respective siPOOLs 72 h post transfection as per previously published protocol [163]. The dried dNTPs were re-suspended to proper volumes of water and added to the HIV-1 RT mediated single dNTP incorporation reactions. The percent of primer extension were converted to the incorporated dNTP amounts and the determined dNTP amounts were normalized by 1 million cells for comparison. Further, data was normalized to negative control siPOOLs.

4.8.5 dNTP bathing assay

1250 cells were reverse transfected with respective siPOOLs in a clear bottom 96 well plate. Desired concentration of extracellular dNTPs were added to the cells 24 h later. Cell proliferation assay was performed at 96 h post siPOOL transfection to assess proliferation potential of the cells.

4.8.6 Luciferase reporter assay

HLE and FLC-4 cells were reverse transfected with 10 nM of control siPOOL and siPOOLs targeting *lincNMR* on day 1. Control pRL-TK / pRL-SV40 reporter constructs and Y-Box-TATA-Luc were co-transfected using a forward transfection protocol on day 2. Cell culture medium was changed on day 3. Luciferase reporter assay was performed using a Dual Luciferase Reporter Assay System kit on day 4 as per manufacturer's instruction and luminescence was measured on Spectra Max M5e.

4.8.7 Chick Chorioallantoic Membrane (CAM) Assay

Pathogen free, fertilized eggs were purchased from Valo Biomedia GmbH and incubated in an incubation oven with 60 % humidity at 37°C. On day 8, *lincNMR* was knocked down with 10 nM siPOOLs using a forward transfection protocol described before in HLE cells. On day 9, eggs were windowed with an electric drilling tool. On the same day, in parallel, $1x10^6$ of respective HLE cells were re-suspended in 10 µL growth media, mixed with 10 µL Matrigel and incubated for 10 min at 37°C and 5 % CO2. Cell-matrigel mix was seeded onto the CAM and window was further sealed for 5 days and incubated at 37°C with 60% humidity. Next days, eggs were observed and dead or injured embryos were excluded from further experiments. On day 6, Chicken embryos were euthanized by a quick decapitation and tumors were harvested from the CAM. Harvested tumors were processed, cleaned and collected in ice-cold 1 X PBS. Images of tumors from HLE cells transfected with negative control siPOOL and two independent siPOOLs targeting *lincNMR* were taken. Tumors were weighed on a micro-scale.

4.9 Statistical analysis, softwares, databases and online tools

4.9.1 T-TEST

For calculation of statistical significance, Microsoft Excel function TTEST was used. P-values were calculated using a two-tailed distribution with either hetero/homoscedasticity. All data are shown as mean ± standard error mean from at least three independent biological replicates. * = $P < 0.05$; ** = $P < 0.01$; *** = $P < 0.001$

4.9.2 Software, databases and online tools

LncRNA expression data for transcriptome-wide profiling was downloaded from TANRIC platform. Correlation plots were also obtained from TANRIC portal. Kaplan Meier survival plots were generated using KM plotter. UCSC genome browser interface was used to study genomic orientation, gene neighborhoods etc. Coding potential of LncRNA was determined using PhyloCSF and CPC tools. Primers were designed using Primer3 interface on NCBI. Proteomics data obtained from Triple label SILAC experiment was analyzed using Perseus and Ingenuity Pathway Analysis platform. Gene set enrichment analysis was performed using Broad Institute's GSEA platform. GraphPad Prism 8 and Adobe Illustrator were used to prepare figures. All the softwares and tools were used as per the usage guidelines provided. List of softwares, online databases, tools and resources used in this study is provided in Table No. 13 and Table No. 14.

5. RESULTS

Parts of the text and figures presented in this chapter are revised versions of the figures and text submitted for publication as an original research article:

Gandhi et al., *"lincNMR* regulates Nucleotide Metabolism via a YBX1 - RRM2 Axis in Cancer"
Nature Communications (manuscript under review)

5.1 Transcriptome-wide expression analysis of lncRNAs in liver cancer

In order to identify novel lncRNAs deregulated in liver cancer, I performed a transcriptome-wide expression profiling of lncRNAs using publicly available sequencing datasets from liver cancer patients. Upon further investigation of existing databases with lncRNA annotation, I chose to use the TANRIC database [164] where the patient dataset was derived from the TCGA data portal. The TANRIC dataset was chosen primarily due to the sample size, recent updates to the database and availability of associated clinical information. Next, expression data of liver cancer patients (tumor = 200 samples, normal = 50 samples) with 12727 lncRNAs annotations was downloaded and subjected to selection as per the outlined matrix (Fig. 1). As a first step, lncRNAs were selected primarily based on high expression and strength of induction in liver cancer compared to normal samples.

Out of 12727 annotated lncRNAs, 217 lncRNAs were strongly and significantly induced by at least 5-fold (median tumor / median normal) and selected for further analysis (List available as Table 15 in the appendix section). Out of 217 lncRNAs, 49 lncRNAs were further chosen based on their genomic orientation, gene neighborhoods, low content of repeats or pseudogenes, CAGE tags and clinical attributes like subtype differentiation. Primarily goal behind second selection was to filter out lncRNAs with repeats, reported pseudogenes and to select for cancer-relevant locus by examining genes up and downstream of reported transcription start site. Next, the expression of selected 49 lncRNAs was validated in nine liver cancer cell lines to further select the candidates and identify suitable cell line models for further experiments (List of 49 lncRNAs available as Table 16 in the appendix section). Candidates were ranked for their abundance based on raw CT values obtained from RT-qPCR (data available as Table 16 in the appendix section) and nine lncRNAs were selected based on their expression in cell lines of interest, novelty and non-coding potential for further RNAi-based cellular function and phenotypic analysis.

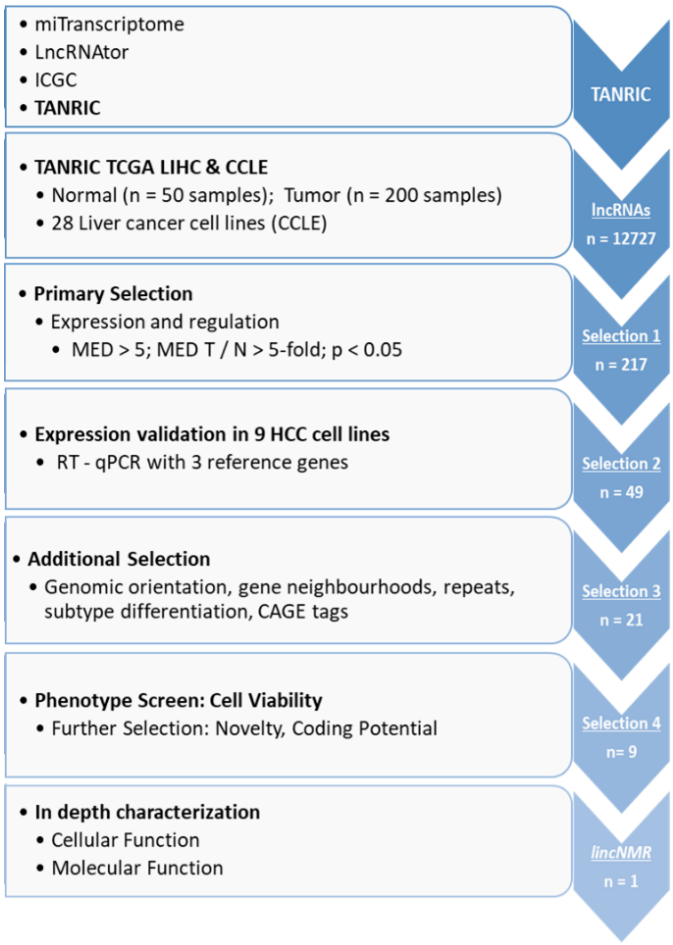

Figure 1: Schematic: Transcriptome-wide lncRNA profiling in liver cancer
Flow chart detailing selection steps performed for transcriptome-wide lncRNA profiling in RNA sequencing dataset (data derived from TANRIC data portal). Funnel-down approach was employed with indicated multiple parameters of selection to select *lincNMR* for further in-depth characterization from initial 12727 lncRNAs.

In order to circumvent off-target effects caused by single siRNAs, a more specific approach called siPOOLs was used. siPOOLs consist of a pool of 30 single siRNAs targeting one gene of interest and are used at much lower concentrations, thereby attenuating potential off-target effects conferred by individual siRNAs [160].

Next, the candidates were subjected to cellular function analysis using cell viability assay in HLE cells. Among the candidates screened, the uncharacterized transcript RP6-65G23.3 showed the strongest

decrease of cell viability in liver cancer cells where siPOOLs targeting *PLK1* [165] and *HULC* [166] were used as a positive control (Fig. 2a).

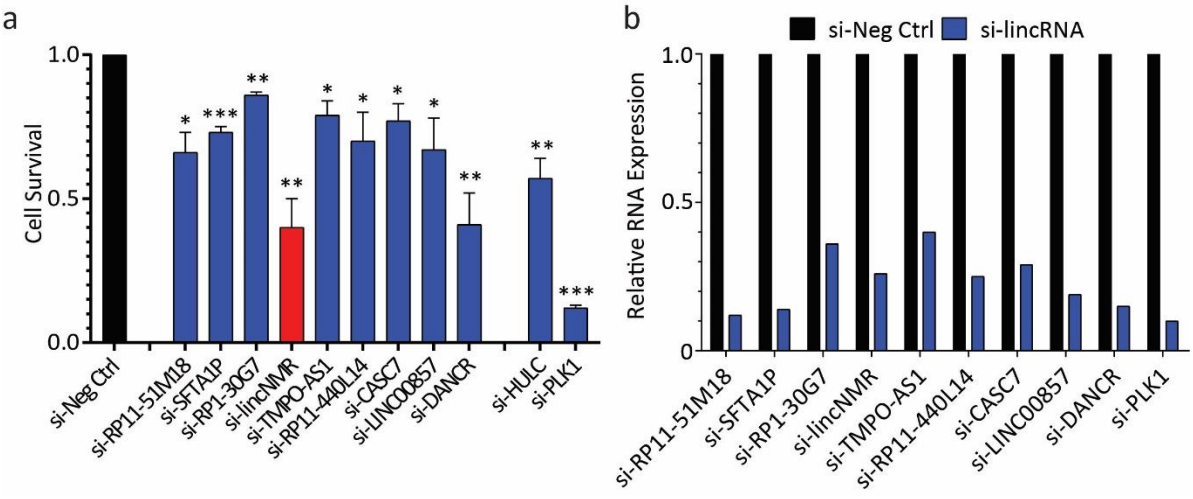

Figure 2: *lincNMR* emerged as a candidate with the strongest impact on cell viability
a. Cell viability screen to assess the impact of depletion of selected lncRNAs with 10 nM siPOOLs at 72 h in HLE cells (n=4). si-HULC and si-PLK1 were used as positive controls. Data represents mean and error bars represent SEM. Significance was calculated by unpaired, two-tailed t-test with *, $P < 0.05$; **, $P < 0.01$; ***, $P < 0.001$ **b**. Knockdown efficiency for selected siPOOLs targeting lncRNAs in HLE cells at 24 h post depletion (n=1). **a, b:** Data shown was normalized to negative control siPOOL.

The knockdown efficiency of siPOOLs (sequences available in Table 6) targeting nine lncRNAs was between 60 % – 90 % as determined by RT-qPCR (primer sequences available in Table 7) in HLE cells (Fig. 2b). For reasons described in further sections in this thesis, this transcript RP6-65G23.3 was named *lincNMR* (long intergenic non-coding RNA Nucleotide Metabolism Regulator).

5.2 Basic characterization of *lincNMR*

LincNMR is a lncRNA transcribed from a bidirectional promoter in a head-to-head orientation with MAP3K9 on chromosome 14. Since the *lincNMR* transcript had never been studied before, I first performed Rapid Amplification of cDNA ends (RACE) experiment to define its gene boundaries. By using 5‘RACE, I identified a new transcription start site (TSS) upstream of the current GENCODE annotation (Fig. 3a). This finding is supported by RNA-Pol II ChIP and switchgear TSS datasets corroborating the extended transcript identified in our 5'-RACE (Fig. 3b). I further performed 3'-RACE and not only confirmed the previously annotated 3'-end of *lincNMR*, but also identified a second, less abundant isoform of *lincNMR* including an additional internal exon (Fig. 3c). Both isoforms have been deposited into Genbank with the accession numbers MK652436 and MK652437. 5’- and 3’-RACE results are supported by ENCODE / Cold Spring Harbor long RNA - Seq tracks from the ENCODE consortium [167] (Fig. 3a, b, c).

5.2.1 *lincNMR* is a long non-coding RNA

Next, I analyzed the coding potential of *lincNMR* using coding potential scores from widely used online tools phyloCSF [168] (Fig. 3d) and the Coding Potential Calculator [169] (Fig. 4a) and found both algorithms to classify *lincNMR* as a non-coding transcript.

Figure 3: Basic characterization of *lincNMR*

a. *lincNMR* genomic orientation from UCSC genome browser derived from GENCODE gene annotation tracks. Black bar depicts the blat sequence search representing 5' RACE data. Additionally, subcellular fraction-specific HepG2 RNA-Seq data from ENCODE/CSHL tracks confirming the further upstream transcription start site of the *lincNMR* transcript and predominant cytoplasmic localization of *lincNMR*. **b.** UCSC genome browser tracks depicting data from Switchgear transcription start site (TSS) annotation supporting longer *lincNMR* exon with another TSS. Also shown is a grey bar depicting RNA Pol II binding site from Transcription factor binding site ChiP-Seq data set from ENCODE/HAIB supporting the new TSS. **c.** *lincNMR* genomic orientation from UCSC genome browser derived from comprehensive gene annotation set GENCODE tracks. Black bar depicts the blat sequence search representing 3' RACE data. Two different gene specific primers (GSP) were used for 3'RACE, 3RACE_GSP.e1 and 3RACE_GSP.e2. **d.** PhyloCSF tracks indicate the lack of coding potential of *lincNMR* in all three translation frames.

5.2.2 *lincNMR* is a predominantly cytoplasmic lncRNA

Since subcellular localization maybe linked to the biological function of non-coding RNAs [32, 170], I further performed subcellular fractionation with fraction-specific controls *NEAT1* (chromatin fraction), *RNU-1* (nucleoplasmic fraction) and *DANCR* (cytoplasmic fraction). *lincNMR* localized predominantly 60 % - 70 % to the cytoplasmic fraction, but also showed considerable presence in the nucleoplasmic fraction (Fig. 4b).

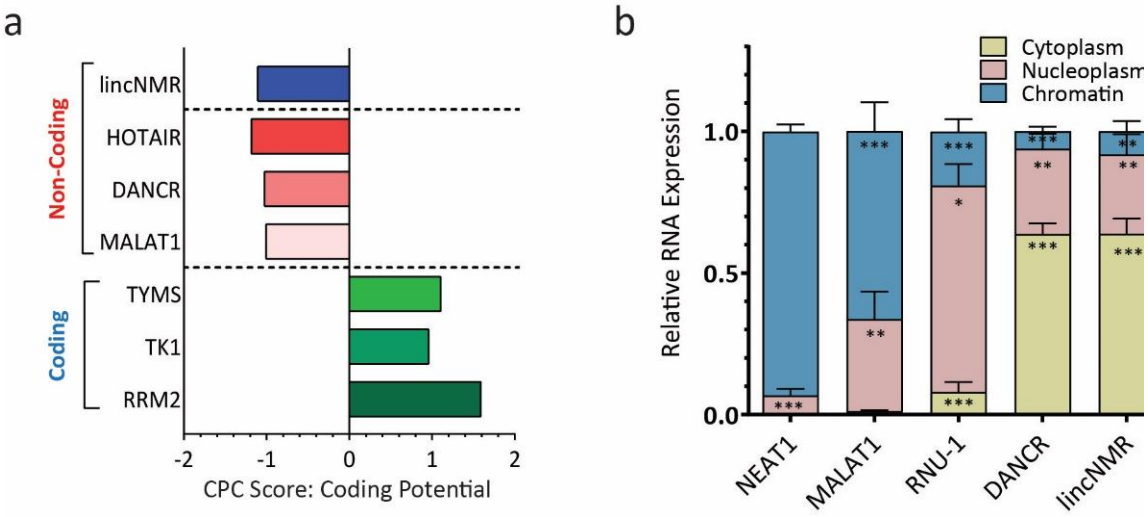

Figure 4: *lincNMR* is non-coding and predominantly cytoplasmic
a. Coding Potential Calculator: Bar graph representing coding potential scores for a set of coding (*RRM2*, *TK1* and *TYMS*) and non-coding (*lincNMR*, *HOTAIR*, *DANCR* and *MALAT1*) genes where positive scores indicate a gene coding for proteins and negative scores confirm the non-coding potential of lncRNAs **b.** Subcellular fractionation of HLE cells and subsequent RT-qPCR confirms the cytoplasmic and partially nucleoplasmic localization of *lincNMR*. Fraction-specific controls are included to ensure fraction quality (**Chromatin**: *NEAT1*, *MALAT1*; **Nucleoplasm**: *RNU1*; **Cytoplasm**: *DANCR*). Data represent mean and error bars represent SEM (n=4). Significance was calculated by unpaired, two-tailed t-test with *, $P < 0.05$; **, $P < 0.01$; ***, $P < 0.001$.

5.3 Cellular function of *lincNMR*

5.3.1 Depletion of *lincNMR* invokes a strong proliferation defect in multiple cancer cell lines

To elucidate the cellular function of *lincNMR*, I silenced *lincNMR* using two independent siPOOLs for additional specificity and to exclude any off-target effects observed with single siRNAs [160] in multiple cancer cell lines.

Since *lincNMR* knockdown decreased cell viability in liver cancer cells (Fig. 2a), I investigated whether depletion of *lincNMR* would impact cancer cell proliferation using a BrdU incorporation assay. *lincNMR* silencing with two independent siPOOLs resulted in 30 % - 80 % decrease in cell proliferation in four liver cancer cell lines (HLE, HLF, SNU-387 and FLC-4) (Fig. 5a).

Additionally, depletion of *lincNMR* also invoked a proliferation defect in three breast (MCF-7, KPL-1 and T47D) (Fig. 5b) and three lung (A549, NCI-H460 and NCI-H1299) cancer cell lines (Fig. 5c) suggesting a broader function of *lincNMR* in cancer.

As a quality control to ensure the functioning of siPOOLs, I also tested the knockdown efficiency of both siPOOLs targeting *lincNMR*. Both siPOOLs silenced *lincNMR* expression efficiently in multiple liver (Fig. 5d), breast (Fig. 5e) and lung (Fig. 5f) cancer cell lines with an efficiency of 85 % - 98 %.

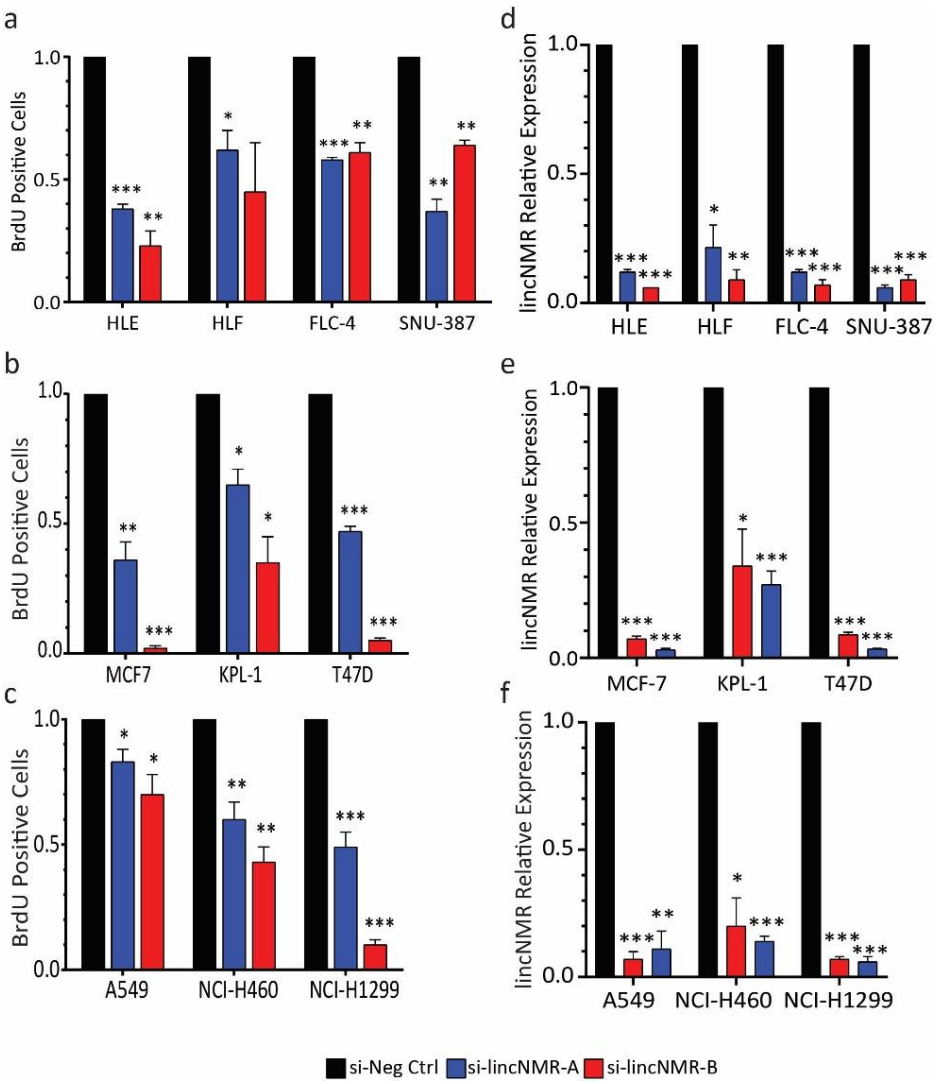

Figure 5: Depletion of *lincNMR* invokes a proliferation defect in multiple cancer cell lines
a. Depletion of *lincNMR* with 10 nM of two independent siPOOLs invokes a strong proliferation defect in four liver cancer cell lines (HLE, HLF, FLC-4 and SNU-387) 72 h post transfection (n=3) **b.** Depletion of *lincNMR* with 10 nM siPOOLs invokes a proliferation decrease in multiple breast cancer cell lines (MCF7, KPL-1 and T47D) 72 h post transfection (n=3) **c.** Depletion of *lincNMR* with 10 nM siPOOLs invokes a proliferation decrease in multiple lung cancer cell lines (A549, NCI-H460 and NCI-H1299) 72 h post transfection (n=3). **d.** *LincNMR* knockdown with 10 nM of two independent siPOOLs (si-*lincNMR*-A and si-*lincNMR*-B) leads to 80 % – 94 % silencing at 24 h post knockdown in multiple liver cancer cell lines (HLE, HLF, FLC4, and SNU-387) **e.** *LincNMR* knockdown with 10 nM of two independent siPOOLs (si-*lincNMR*-A and si-*lincNMR*-B) leads to 75 % – 99 % silencing at 72 h post knockdown in multiple breast cancer cell lines (MCF-7, KPL-1, and T47D) **f.** *LincNMR* knockdown with 10 nM of two independent siPOOLs (si-*lincNMR*-A and si-*lincNMR*-B) leads to 80 % – 93 % silencing of *lincNMR* at 72 h post knockdown in multiple lung cancer cell lines (A549, NCI-H460 and NCI-H1299). **a – f:** Data represents mean and error bars represent SEM (n=4). Significance was calculated by unpaired, two-tailed t-test with *, $P < 0.05$; **, $P < 0.01$; ***, $P < 0.001$. Data shown was normalized to

negative control siPOOL.

5.3.2 Silencing of *lincNMR* causes a cell cycle arrest in G0/G1 phase of cell cycle

After investigating the effect of *lincNMR* depletion on cell proliferation, cell cycle analysis was performed using flow cytometry and where I found an increase in the number of *lincNMR* depleted cells in the G0/G1 phase of the cell cycle in multiple cancer cell lines (Fig. 6 a, b, c).

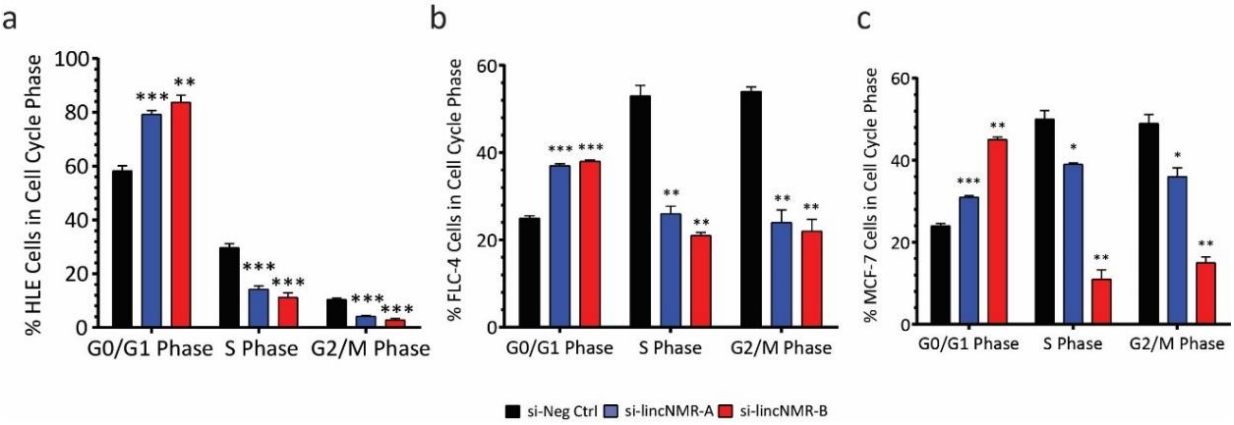

Figure 6: Silencing of *lincNMR* caused a cell cycle arrest in G0/G1 phase
a. Silencing of *lincNMR* with 10 nM siPOOLs induces cell cycle arrest in G0/G1 phase as shown by flow cytometry 72 h post transfection in HLE (n=3). **b.** Silencing of *lincNMR* with 10 nM siPOOLs induces cell cycle arrest in G0/G1 phase at 72 h post transfection in FLC-4 (n=3) **c.** Silencing of *lincNMR* with 10 nM siPOOLs induces cell cycle arrest in G0/G1 phase at 72 h post transfection in MCF-7 (n=3). **a – c:** Analysis was performed using FlowJo v10. Data represents mean and error bars represent SEM (n=4). Significance was calculated by unpaired, two-tailed t-test with *, P < 0.05; **, P < 0.01; ***, P < 0.001. Data shown was normalized to negative control siPOOL.

5.3.3 Loss of *lincNMR* triggers an induction of senescence in multiple cancer cell lines

The arrest of cells in the G0/G1 phase prompted me to evaluate whether there was an induction of senescence in *lincNMR* depleted cells. Indeed, depletion of *lincNMR* triggered an induction of senescence in multiple liver cancer cell lines with two independent siPOOLs as evident by β-GAL-positive blue cells in SA-β-GAL assay (Fig. 7a, b). The induction of senescence was supported by the increased expression of the pro-inflammatory cytokines IL-1a and IL-1b, which have been known to be the *bona fide* markers of senescence-associated secretary phenotype (SASP) (Fig. 7c).

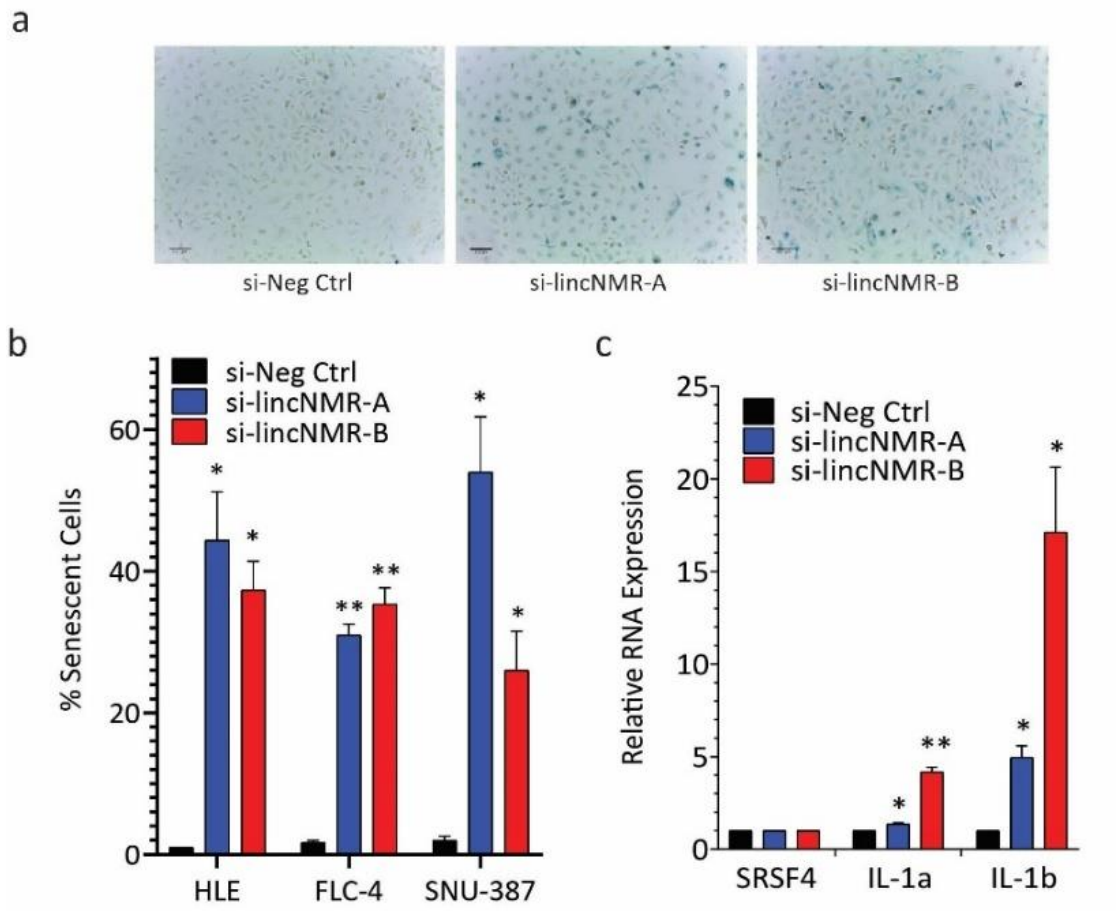

Figure 7: Loss of *lincNMR* triggers an induction of senescence and SASP

a. Representative microscopic images showing increased β-Gal activity indicating senescent cells in HLE, 96 h post *lincNMR* knockdown with 10 nM siPOOLs **b.** Bar graph representing the percent β-Gal-positive cells in multiple liver cancer cell lines after *lincNMR* depletion **c.** Induction of senescence associated secretary phenotype (SASP) markers IL-1a and IL-1b determined by RT-qPCR at 72 h after *lincNMR* knockdown in HLE with 10 nM siPOOLs (n=3); **b, c:** Data represents mean and error bars represent SEM. Significance was calculated by unpaired, two-tailed t-test with *, $P < 0.05$; **, $P < 0.01$; ***, $P < 0.001$. Data shown was normalized to negative control siPOOL

5.4 Molecular function of *lincNMR*

5.4.1 RAP-MS to identify direct protein binding partners *of lincNMR*

I performed an *in vivo* RNA Antisense Purification (RAP-MS) in order to identify protein interaction partners and gain insight into the molecular function of *lincNMR* [162, 171] in collaboration with the lab of Eric Lander at the Broad Institute in Cambridge, MA, USA, where I spent two weeks to learn this important technique. I used biotinylated DNA oligos (sequences available in Table 9) complementary to the sequence of *lincNMR* to pulldown *lincNMR* and associated direct protein binding partners (schematic Fig. 8a).

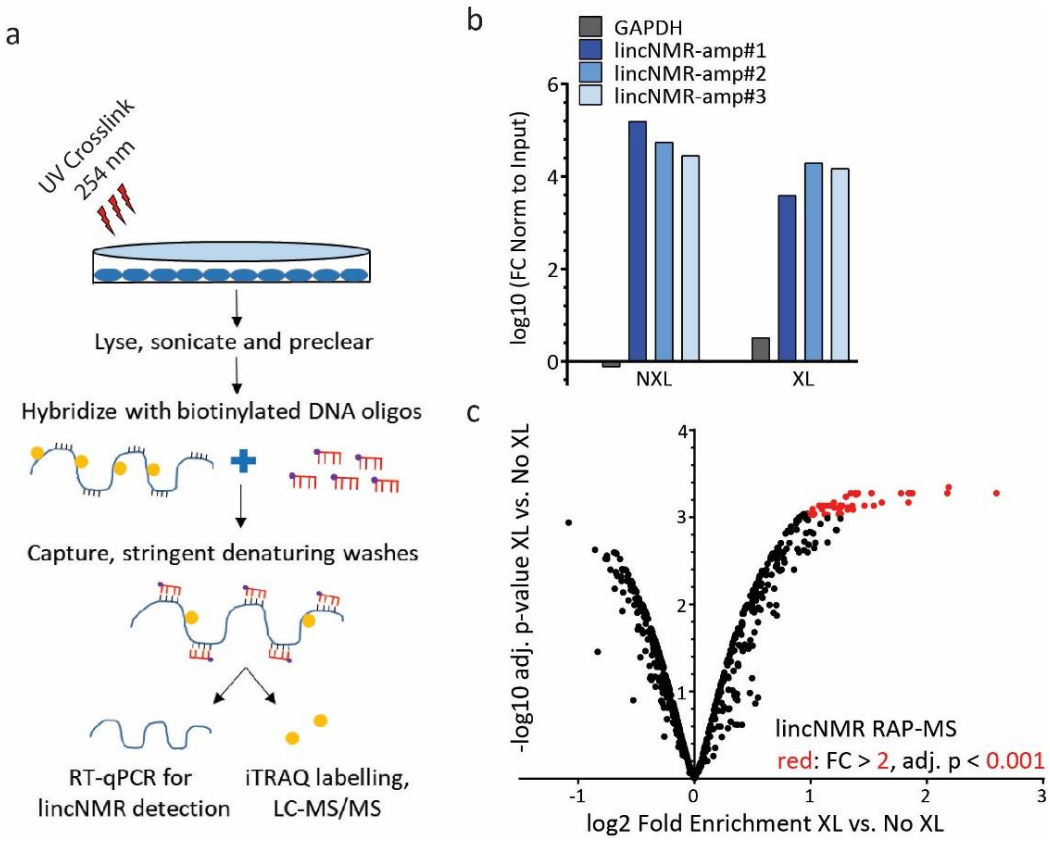

Figure 8: Schematic: *LincNMR in vivo* RNA Antisense Purification (RAP-MS)
a. Schematic of *lincNMR* RAP-MS, used to identify direct protein interaction partner **b.** *lincNMR* RAP-MS pulldown efficiency: data represent log10 fold change normalized to reference gene *PPIA* and input in HLE with three different *lincNMR* amplicons and *GAPDH* as additional negative control (n=2) **c.** Volcano plot depicting total proteins (n = 701) identified by *lincNMR* RAP-MS. 48 candidates highlighted in red were selected for fold enrichment and significance: (FC > 2) and adjusted p-value of enrichment (P < 0.001)

Pulldown efficiency of *lincNMR* was confirmed by RT-qPCR with three different *lincNMR* amplicons where PPIA and GAPDH mRNAs were used as negative controls (Fig. 8b). Mass spectrometry of *lincNMR* RAP-MS from crosslinked compared to non-crosslinked lysates identified 701 proteins in total (Fig. 8c) with 48 proteins enriched at least two fold with strong significance of adjusted p-value < 0.001 (List available as Table 17).

5.4.2 *lincNMR* directly binds to YBX1 protein, which regulates cell survival

To further select relevant *lincNMR* binding partners linked to HCC, I analyzed their correlation to survival in HCC using a web-based tool called KM Plotter, based on patient dataset from the TCGA liver cancer cohort (Fig. 9a).

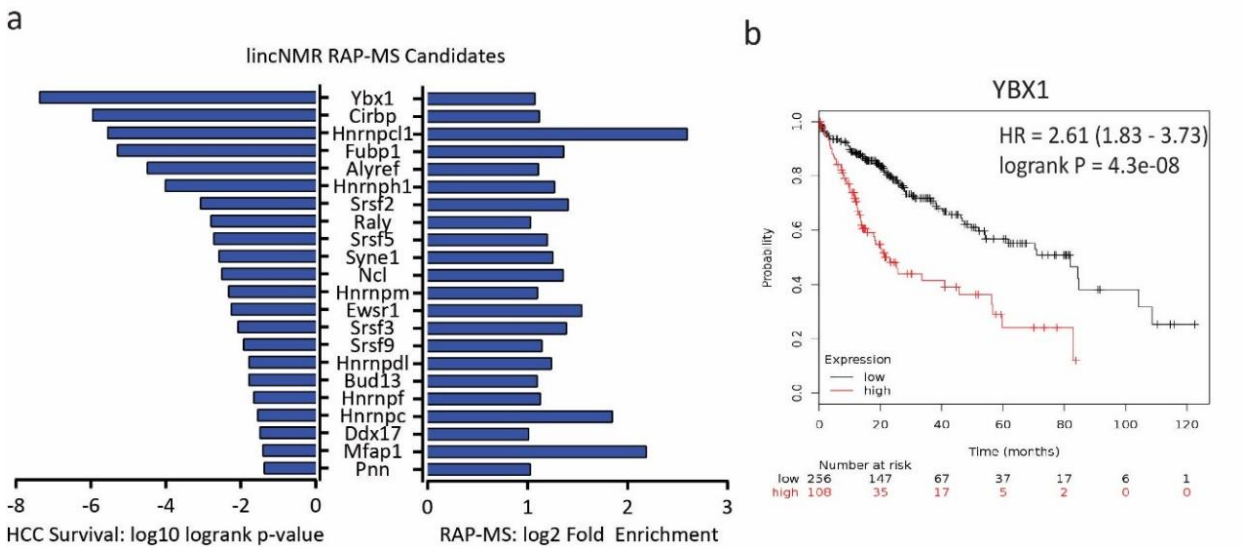

Figure 9: YBX1 has a strongest association with survival in liver cancer patients
a. Interaction partners identified by *lincNMR* RAP-MS are selected for fold enrichment in crosslinked over non-crosslinked samples (FC > 2), adjusted p-value of enrichment (P < 0.001), and sorted for logrank p-value in liver cancer survival (based on TCGA data) **b.** Kaplan-Meier plot correlating high YBX1 expression to poor survival in liver cancer patients (TCGA survival data accessed through web-based tool KM Plotter)

Upon ranking, the candidates using logrank survival p-value, 22 candidates were found to be significantly associated with the overall survival of liver cancer patients (highlighted in bold in Table 18). Moreover, YBX1 emerged as a direct binding partner with strongest significant correlation to survival in liver cancer (Fig. 9a, b). Additionally, to further support *lincNMR* - YBX1 interaction, I also searched for predicted RBP binding sites in the *lincNMR* transcript using RBPmap [172] and found three YBX1 and two SRSF3 sites (p < 0.001) consolidating the results obtained from the RAP-MS experiment.

5.4.3 Validation of *lincNMR* - YBX1 interaction using UV - RIP

In order to further validate *lincNMR* - YBX1 interaction identified by RAP - MS, I performed crosslinking RNA Immuno-precipitation (UV – RIP) in HLE cells. After immunoprecipitation of Flag-HA tagged YBX1 (Fig. 10a), *lincNMR* was found to be significantly enriched in the YBX1 pulldown as compared to the negative control (Fig. 10b) thus confirming the direct interaction between the *lincNMR* transcript and YBX1 protein.

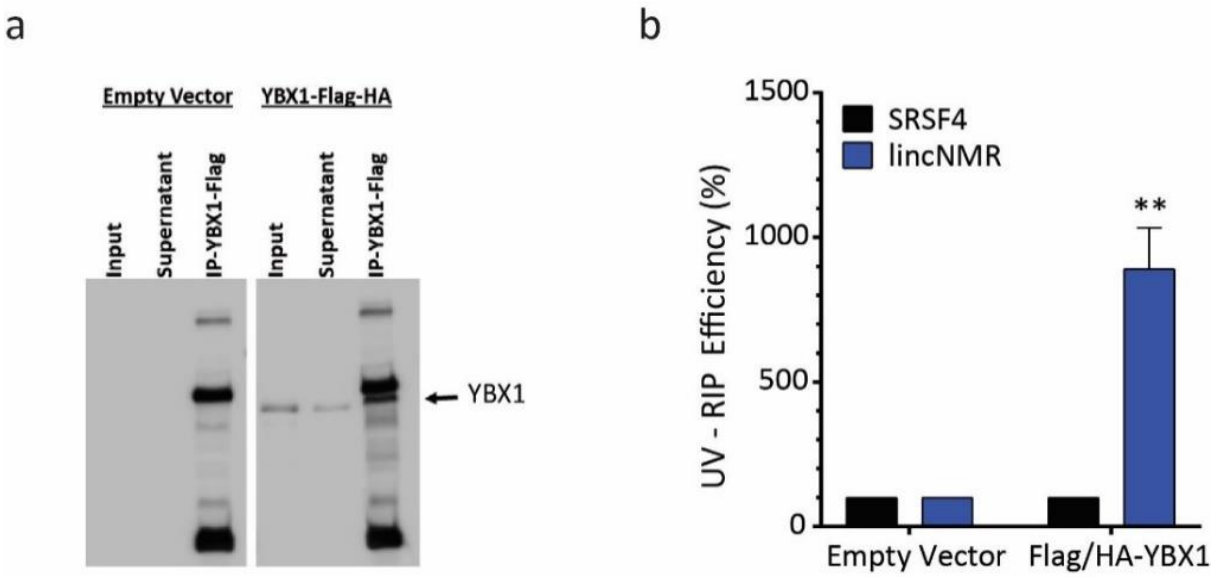

Figure 10: Direct interaction between *lincNMR* - YBX1 validated by UV – RIP
a. Representative western blot for YBX1 UV – RIP validating YBX1 pulldown using anti-HA antibody in HLE cells. Input, supernatant and IP fractions are loaded onto 10% SDS-PAGE gel **b.** Determination of RNA pulldown efficiency in UV - RIP by RT-qPCR validating the interaction between YBX1 and *lincNMR* in HLE cells (n = 4). Data represents mean and error bars represent SEM. Significance was calculated by unpaired, two-tailed t-test with *, $P < 0.05$; **, $P < 0.01$; ***, $P < 0.001$. Data shown is normalized to SRSF4 as negative control gene and to control vector.

5.4.4 Silencing of YBX1 mimics the phenotype induced by *lincNMR* depletion

Depletion of YBX1 also impaired the cell proliferation by 50% (Fig. 11a), resembling the effect of *lincNMR* knockdown. I also found significant positive correlation between *lincNMR* and *YBX1* mRNA in HCC patient samples (Fig. 11b). Additionally, *lincNMR* levels were found to be decreased by 49 % after YBX1 silencing (Fig. 11c); vice versa we found that YBX1 protein levels were only marginally decreased by about 20% when *lincNMR* was silenced by two independent siPOOLs (Fig. 11d, e).

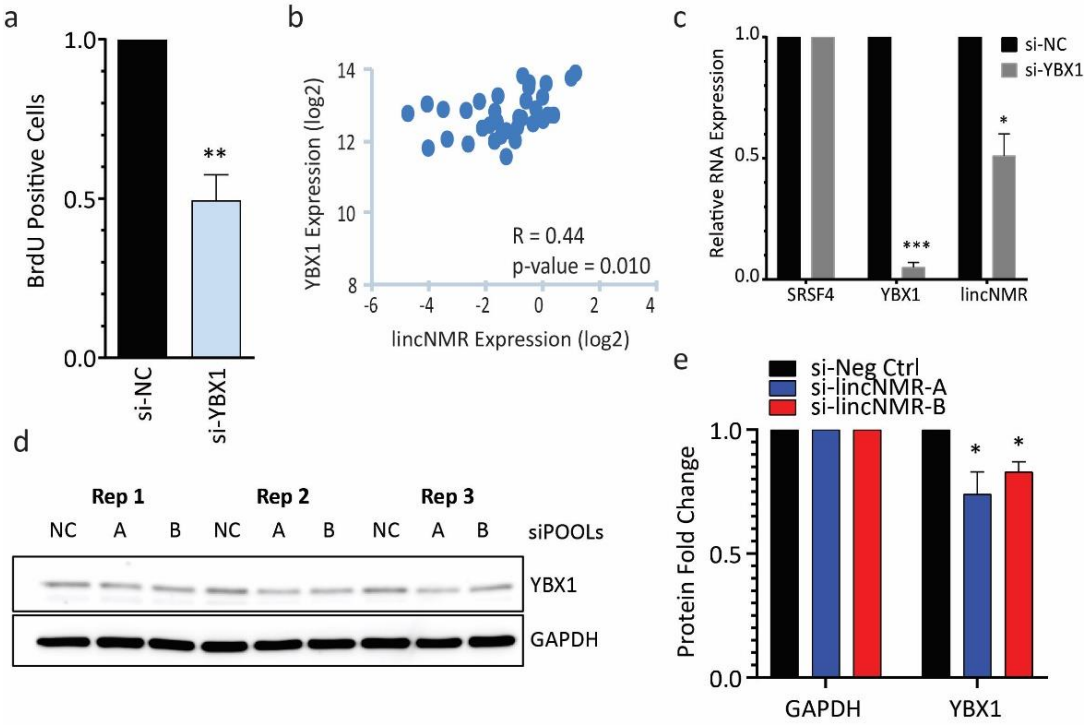

Figure 11: Depletion of YBX1 mimics phenotype induced by *lincNMR* depletion
a. Silencing of YBX1 with 10 nM siPOOL imparts a proliferative disadvantage to HLE cells determined at 72 h post transfection. Data shown is normalized to negative control siPOOL (n = 3). **b.** *LincNMR* expression levels significantly correlate with *YBX1* mRNA with a correlation coefficient of R = 0.44 in hepatocellular carcinoma patients (data derived from TCGA through TANRIC platform) [164] **c.** Depletion of YBX1 using 10 nM siPOOLs in HLE cells is effective and leads to downregulation of *lincNMR* expression at 72 h in HLE cells. *LincNMR* and *YBX1* RNA were measured by RT-qPCR and the data was normalized to SRSF4 and negative control siPOOL. **d.** Western blot image of YBX1 expression upon *lincNMR* depletion in HLE using 10 nM YBX1 siPOOLs (n = 3) **e.** Depletion of *lincNMR* using 10 nM siPOOLs in HLE cells leads to marginal, but significant downregulation of YBX1 protein at 72 h. Protein fold change was calculated by normalizing the YBX1 signal to loading control GAPDH and negative control siPOOL. **a, c, e:** Data represent mean and error bars represent SEM. Significance was calculated by unpaired, two-tailed t-test with *, $P < 0.05$; **, $P < 0.01$; ***, $P < 0.001$.

5.4.5 *LincNMR* directly binds to YBX1 and regulates its transactivational activity

The direct interaction of *lincNMR* and YBX1 protein prompted us to assess whether there was change in activity of YBX1 upon *lincNMR* depletion. Dual luciferase assay was performed where *lincNMR* depleted cells were transfected with control or YBX1 reporter plasmids together with renilla luciferase reporter construct for in-experiment normalization. Depletion of *lincNMR* significantly decreased the YBX1 activity in two independent liver cancer cell lines HLE and FLC - 4 (Fig. 12).

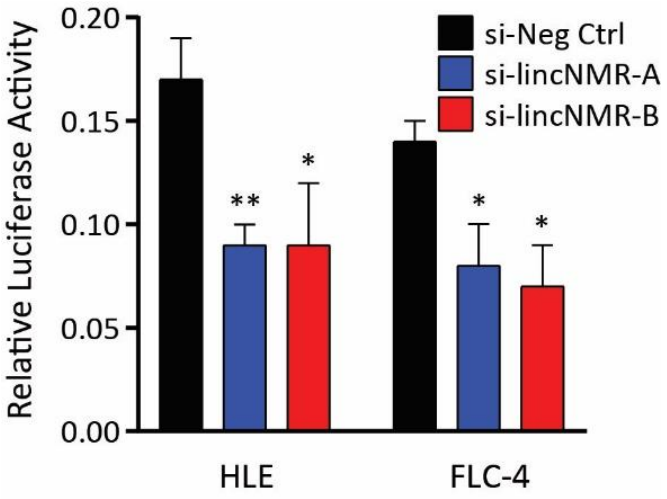

Figure 12: *LincNMR* regulated the transactivation activity of YBX1 in liver
Dual Luciferase assay for the transactivational activity of YBX1 unravels the inhibition of YBX1 by *lincNMR* silencing. Data shown is the ratio of YBX1-dependent Firefly luciferase activity divided by Renilla luciferase used for standardization after depletion of *lincNMR* with 10 nM siPOOLs in HLE and FLC-4 cells (n = 3).

Taken together, this data concludes that *lincNMR* directly interacts with and regulates YBX1 (section 5.4.1 – 5.4.3), YBX1 mimics the impact of *lincNMR* on cell proliferation and the regulation of *lincNMR* by YBX1 generates a feedforward loop leading to the correlation of expression in liver cancer (section 5.4.5).

5.4.6 Total cellular proteome after *lincNMR* depletion using triple-label SILAC approach

To investigate the impact of *lincNMR* depletion on the cellular proteome and identify the target genes, I optimized and established a triple-label stable isotope labelling by amino acids in cell culture (SILAC) approach in the lab (Fig. 13a). SILAC ratios were used for analysis comparing lysates from cells treated with siPOOLs targeting *lincNMR* to cells treated withthe negative control siPOOL (si-*lincNMR*-A / si-Neg Ctrl = M/L and si-*lincNMR*-B/si-Neg Ctrl = H/L). A correlation analysis depicted by multi-scatter plot served as a quality control for the complete dataset: a significant correlation was observed across three biological replicates (individual correlation coefficients displayed on the plot) and in between both siPOOLs targeting *lincNMR* with an average correlation coefficient of R = 0.74 (Fig. 13b).

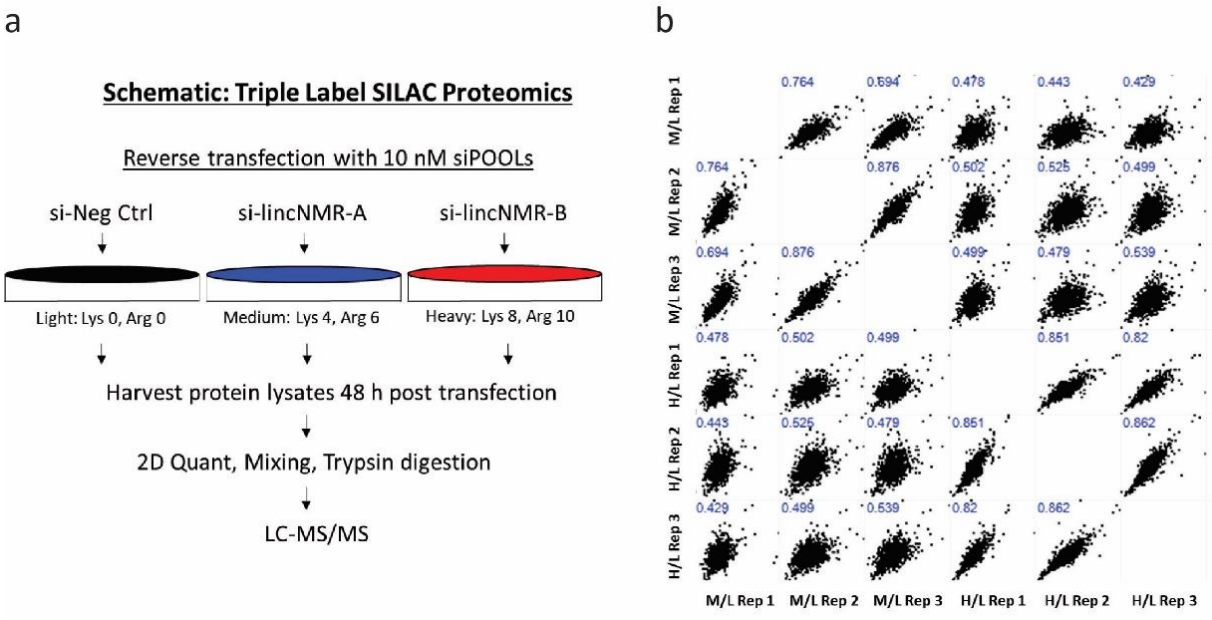

Figure 13: Schematic overview and reproducibility of triple-label SILAC experiment
a. Schematic of triple-label SILAC-MS experiment to identify proteins deregulated upon *lincNMR* loss. **b.** Multi-scatter plot depicting all deregulated proteins identified within and across three biological replicates using two independent siPOOLs (si-*lincNMR*-A = Medium (M), si-*lincNMR*-B = Heavy (H), vs. control siPOOL = Light (L)) in triple-label SILAC-MS. HLE cell lysates were harvested at 48 h after depletion of *lincNMR* with 10 nM siPOOLs (n = 3). Data represents fold change normalized to negative control siPOOLs. A total of 2088 proteins were identified across biological replicates and only candidates deregulated with both siPOOLs were selected for further analysis. Pearson correlation coefficient is displayed on the multi-scatter plot.

Further, stringent analysis with a significance filter of adjusted p-value < 0.001 led to the identification of 242 candidates deregulated by both *lincNMR*-targeting siPOOLs. Panther overrepresentation analysis was performed using Fisher test with Bonferroni correction on these selected 242 candidates. This revealed a significant enrichment of key reactome pathway terms - G1/S transition, cell cycle checkpoints, and metabolism of RNA etc. corroborating the phenotype observed after *lincNMR* depletion (Fig. 14).

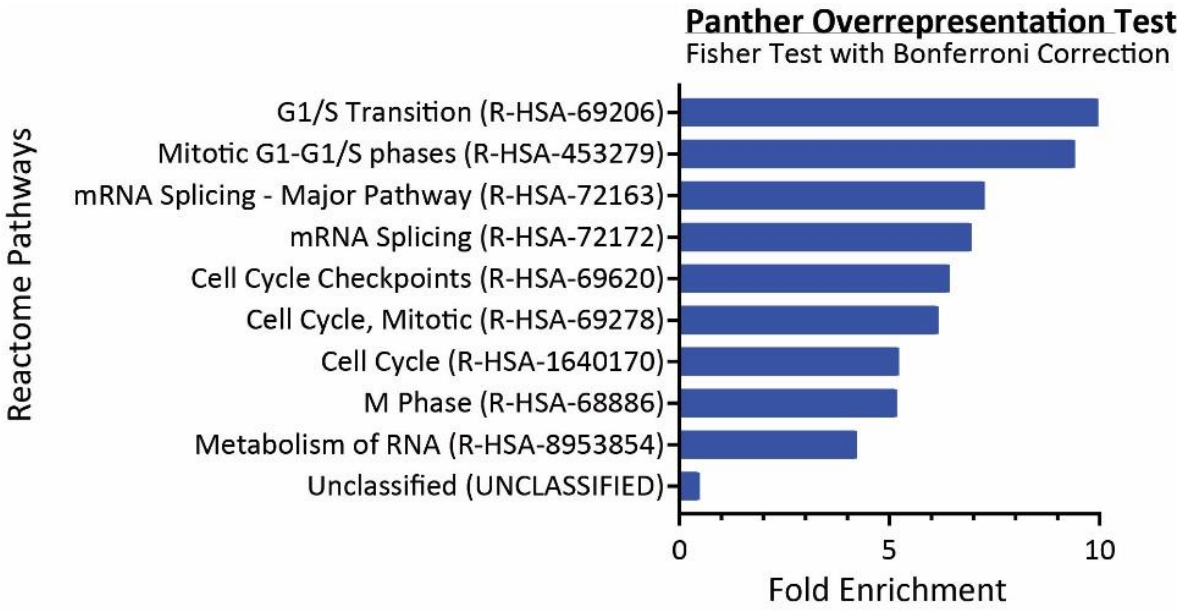

Figure 14: Panther overrepresentation analysis reveals enrichment of key cell cycle terms
Panther overrepresentation test: Fisher test was performed on 242 deregulated candidates (P < 0.001) with Bonferroni correction on a dataset obtained from triple-label SILAC-MS experiment after depletion of *lincNMR* in HLE cells. Depicted is the fold enrichment of key terms associated with these deregulated hits from SILAC-MS.

5.4.7 Loss of *lincNMR* causes downregulation of key enzymes in nucleotide metabolism

Upon further in-depth analysis of strongly deregulated candidates after *lincNMR* depletion, I identified RRM2 (si-*lincNMR*-A = - 68%, si-*lincNMR*-B = - 67%), TK1 (si-*lincNMR*-A = - 52%, si-*lincNMR*-B = - 58%) and TYMS (si-*lincNMR*-A = - 43%, si-*lincNMR*-B = - 57%) as strongly downregulated proteins among other key enzymes implicated in nucleotide metabolism pathways (Fig. 15a). This decrease of RRM2, TK1 and TYMS proteins after *lincNMR* depletion was validated by western blotting in HLE cells (Fig. 15b) in good accordance with the independent triple-label SILAC-MS approach (Fig. 15c). Additionally, a decrease of RRM2, TK1 and TYMS mRNA was also observed after *lincNMR* depletion with both siPOOLs (Fig. 15d).

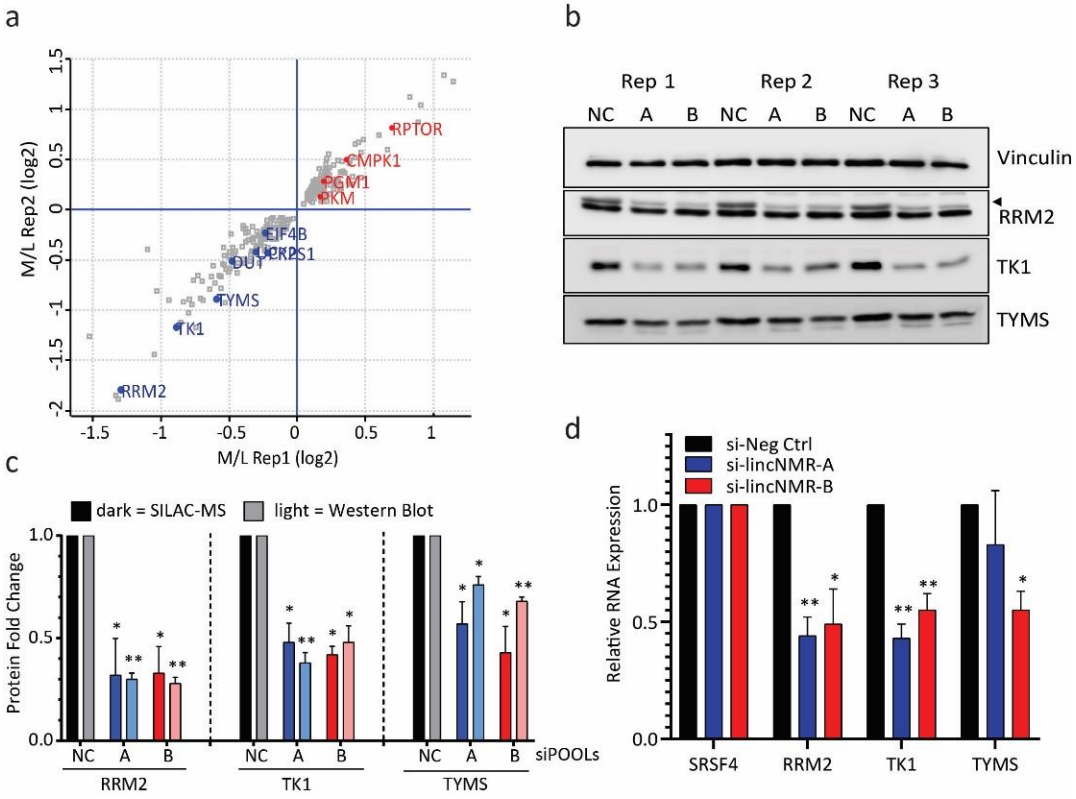

Figure 15: Loss of *lincNMR* causes depletion of enzymes regulating nucleotide metabolism

a. Triple-label SILAC-MS: Scatter Plot shows deregulated proteins 48 h after *lincNMR* knockdown with 10 nM siPOOLs in HLE cells. Data represents log2 fold change normalized to negative control siPOOL from two independent replicates. Highlighted proteins represent key deregulated players in purine and pyrimidine metabolism according to KEGG pathway annotations. Color key: red = upregulated proteins; blue = downregulated proteins **b.** Western blot validation of SILAC-MS data depicting downregulation of RRM2, TK1 and TYMS proteins in HLE cells 72 h after *lincNMR* knockdown with 10 nM siPOOLs (n=3). Vinculin was used as a loading control **c.** Quantitative comparison of SILAC-MS and western blot results confirming consistent downregulation of RRM2, TK1 and TYMS (n=3). log2 fold change was calculated and normalized to negative control siPOOL **d.** Depletion of *lincNMR* with two independent siPOOLs (si-*lincNMR*-A and si-*lincNMR*-B) leads to downregulation of *RRM2*, *TK1* and *TYMS* mRNAs in HLE cells at 72 h after *lincNMR* knockdown with 10 nM siPOOLs (n=3). **c – d:** Data represents mean and error bars represent SEM. Significance was calculated by unpaired, two-tailed t-test with *, $P < 0.05$; **, $P < 0.01$; ***, $P < 0.001$.

5.4.8 Silencing of RRM2, TK1 and TYMS also mimics the phenotype induced by *lincNMR* loss

To investigate the impact of depletion of *lincNMR* target genes on cellular function, I silenced RRM2, TK1 and TYMS using siPOOLs with a knockdown efficiency in the range of 90 % - 98 % in HLE cells (Fig. 16a) and interestingly observed a strong induction of proliferation defect upon the loss of RRM2, TK1 and TYMS thus mimicking the phenotype observed after *lincNMR* depletion (Fig. 16b).

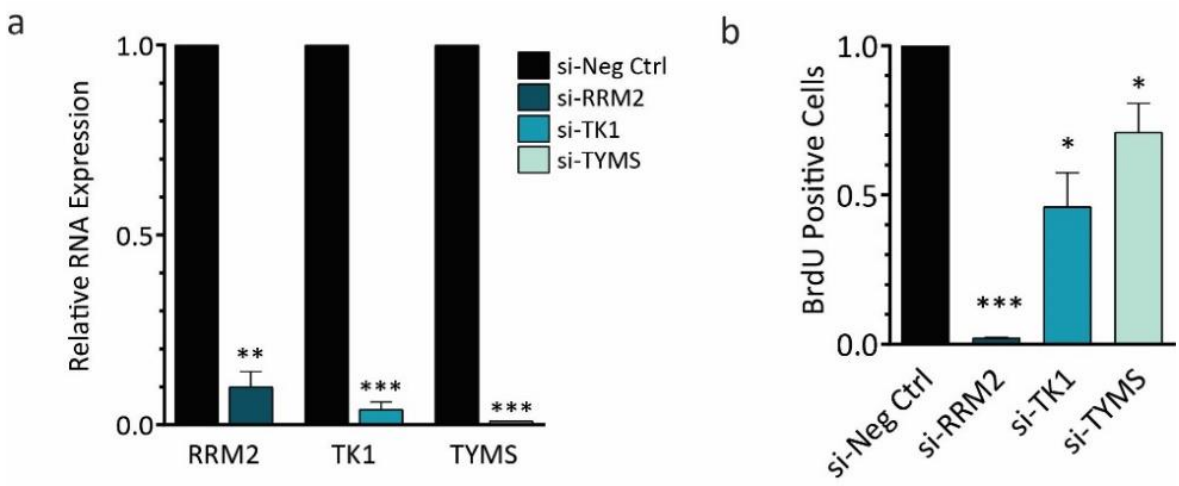

Figure 16: Depletion of *RRM2*, *TK1* and *TYMS* mimicks the phenotype induced by *lincNMR* loss
a. RT-qPCR data showing knockdown efficiency of RRM2, TK1 and TYMS in HLE with 10 nM respective siPOOLs at 72 h post knockdown (n =3). Data was normalized to reference gene SRSF4 and negative control siPOOL **b.** Depletion of RRM2, TK1 and TYMS invokes a strong proliferation defect 72 h after knockdown using 10 nM RRM2, TK1 or TYMS targeting siPOOLs in HLE cells in at least 3 biological replicates. **a, b:** Data represents mean and error bars represent SEM. Significance was calculated by unpaired, two-tailed t-test with *, $P < 0.05$; **, $P < 0.01$; ***, $P < 0.001$. Data shown is normalized to negative control siPOOL.

5.4.9 *LincNMR* and YBX1 share common target genes regulating nucleotide metabolism

Since we identified *lincNMR* as a regulator of the transcription factor YBX1 activity, I tested whether YBX1 depletion would also affect RRM2, TK1 and TYMS expression levels. Indeed, upon the loss of YBX1, we observed a significant decrease of RRM2, TK1 and TYMS protein levels (Fig. 17a, b) establishing the *lincNMR* - YBX1 - RRM2 / TK1 / TYMS axis in liver cancer.

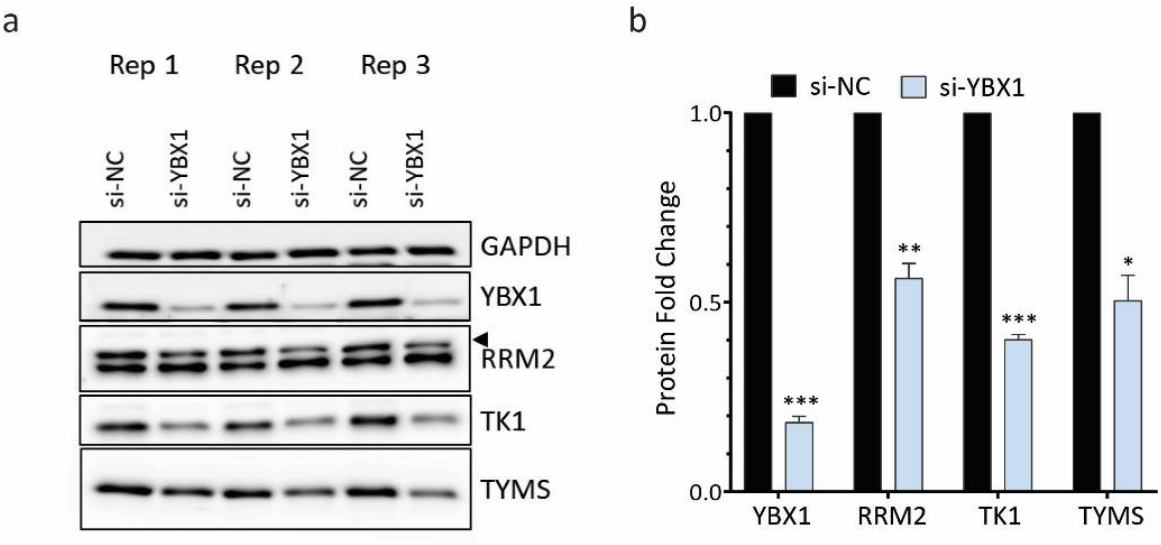

Figure 17: Loss of YBX1 also regulates *lincNMR* target genes RRM2, TK1 and TYMS
a. YBX1 silencing inhibits the expression of RRM2, TK1 and TYMS at 72 h post transfection with 10 nM siPOOL in HLE cells as documented by western blotting. GAPDH was used as a loading control **b.** Quantification of western blot from (a): protein fold change was calculated by normalizing the RRM2, TK1 and TYMS signal to loading control GAPDH and to negative control siPOOL (n=3). Data represents mean and error bars represent SEM. Significance was calculated by unpaired, two-tailed t-test with *, $P < 0.05$; **, $P < 0.01$; ***, $P < 0.001$.

5.4.10 *LincNMR* target genes are regulated and associated with poor survival in liver cancer

Next, I analyzed the clinical significance for *lincNMR* target genes and found *RRM2*, *TK1* and *TYMS* to be strongly and significantly induced by about ten-, six- and four-fold respectively in liver cancer patient datasets from TCGA data portal compared to normal tissue (Fig. 18a, b, c).

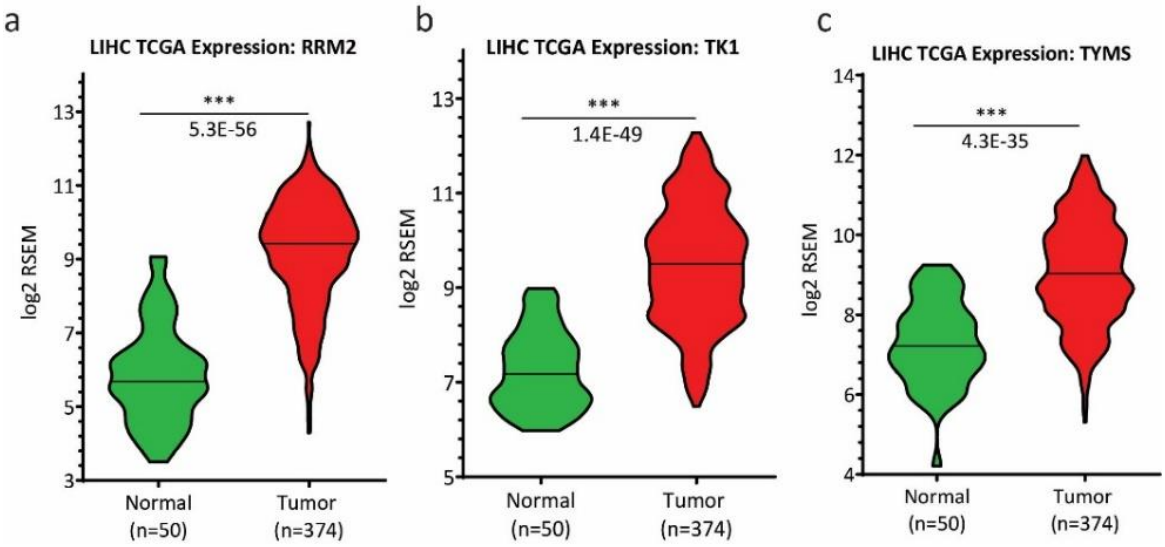

Figure 18: *RRM2*, *TK1* and *TYMS* are expressed and regulated in liver cancer
a. *RRM2* is expressed and regulated in liver cancer (N=normal, T=tumor; data obtained from TCGA data portal). LIHC=Hepatocellular Carcinoma (N=50, T=374) **b.** *TK1* is expressed and regulated in liver cancer (N=normal, T=tumor; data obtained from TCGA data portal). LIHC=Hepatocellular Carcinoma (N=50, T=374) **c.** *TYMS* is expressed and regulated in liver cancer (N=normal, T=tumor; data obtained from TCGA data portal). LIHC=Hepatocellular Carcinoma (N=50, T=374) **a – c:** Data is represented as log2 RSEM. Significance was calculated by unpaired, two-tailed t-test with *, $P < 0.05$; **, $P < 0.01$; ***, $P < 0.001$.

Furthermore, all three *lincNMR* target genes, *RRM2*, *TK1* and *TYMS* were also significantly associated with poor survival in liver cancer patient datasets (Fig. 19a, b, c).

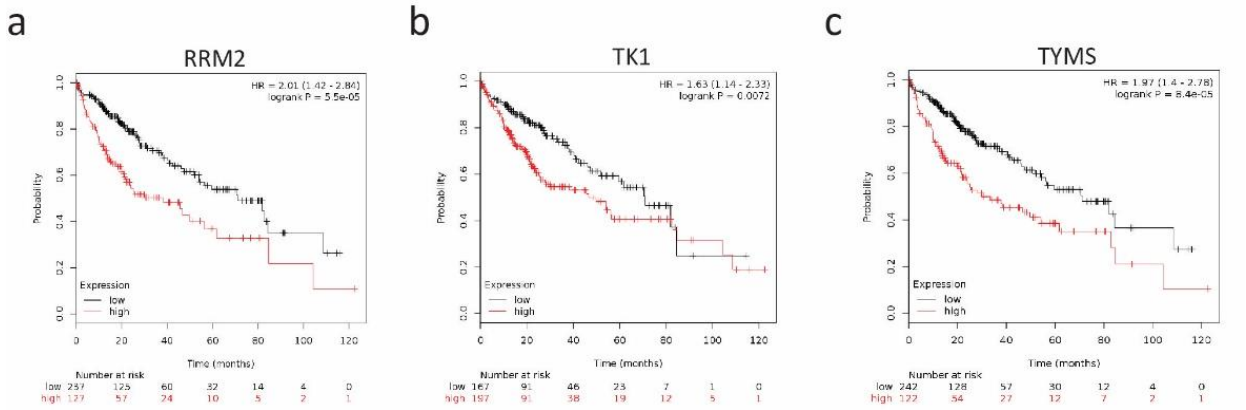

Figure 19: Impact of *lincNMR* target genes on survival in liver cancer
a. Kaplan-Meier plots of liver cancer patients stratified by RRM2 expression levels **b.** Kaplan-Meier plots of liver cancer patients stratified by TK1 expression levels **c.** Kaplan-Meier plots of liver cancer patients stratified by TYMS expression levels

Moreover, the *lincNMR* expression level significantly and positively correlated with *RRM2*, *TK1* and *TYMS* mRNA in liver cancer patient samples (Fig. 20a, b, c) further corroborating the strong link between *lincNMR*, these three regulators of nucleotide metabolism and liver cancer.

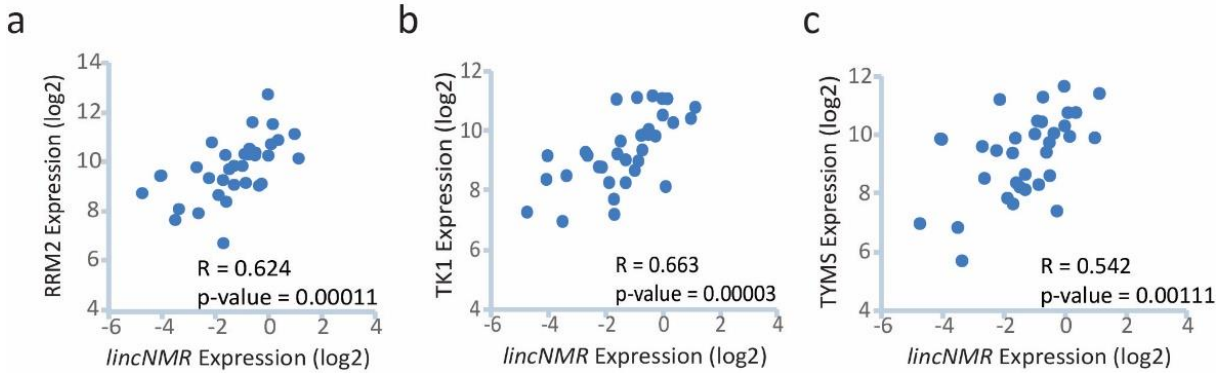

Figure 20: Correlation of expression between *lincNMR* and its targets in liver cancer patients
a. Correlation plot: *lincNMR* expression correlates with RRM2 mRNA expression in liver cancer patients **b.** Correlation plot: *lincNMR* expression correlates with TK1 mRNA expression in liver cancer patients
c. Correlation plot: *lincNMR* expression correlates with TYMS mRNA expression in liver cancer patients

5.4.11 Depletion of *lincNMR* leads to reduced dNTP levels in liver cancer

Since dNTP-synthesizing enzymes were downregulated by the knockdown of *lincNMR*, I further investigated whether the levels of dNTPs were also accordingly affected. Interestingly, all four dNTPs - dATP, dCTP, dGTP and dTTP - were significantly downregulated after *lincNMR* depletion in two independent cell liver cancer lines HLE (Fig. 21a) and FLC-4 (Fig. 21b) solidifying the role of *lincNMR* in regulation of nucleotide metabolism.

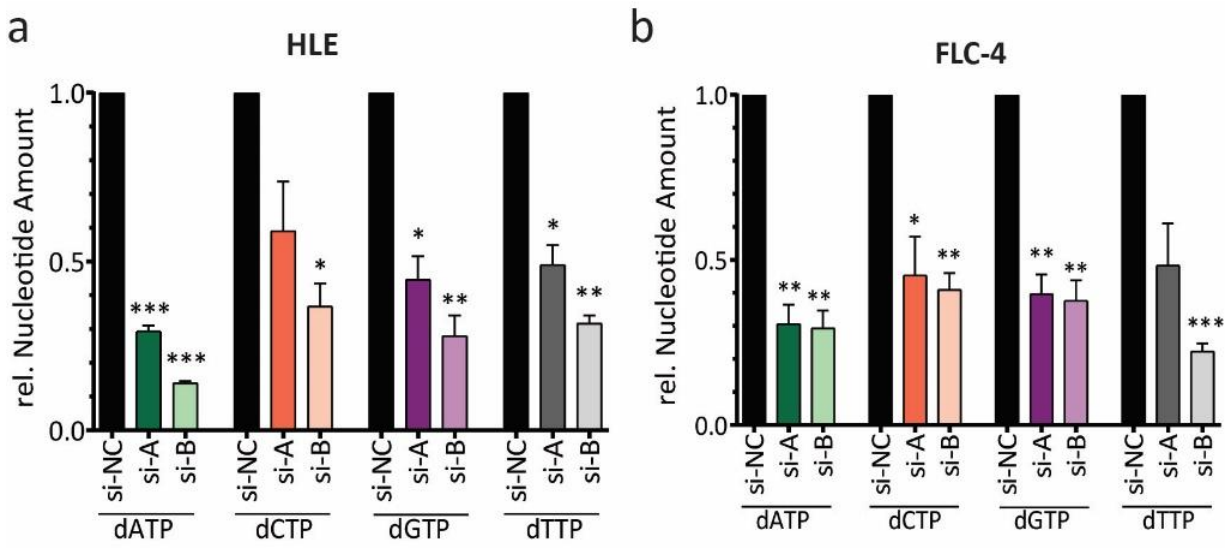

Figure 21: Depletion of *lincNMR* leads to reduced dNTP levels
a. Quantification of dNTP levels uncovers that the depletion of *lincNMR* with 10 nM siPOOLs leads to strong downregulation of dATP, dCTP, dGTP and dTTP in HLE cells **b.** Quantification of dNTP levels uncovers that the depletion of *lincNMR* with 10 nM siPOOLs leads to strong downregulation of dATP, dCTP, dGTP and dTTP in FLC-4 cells. **a - b**: Data represents mean and error bars represent SEM (n = 3). Significance was calculated by unpaired, two-tailed t-test with *, $P < 0.05$; **, $P < 0.01$; ***, $P < 0.001$. Data shown is normalized to negative control siPOOL.

5.4.12 Extracellular supply of dNTPs rescues the phenotype induced by depletion of *lincNMR*

Interestingly, supplying exogenous dNTPs by bathing the *lincNMR* depleted cells rescued the impact of *lincNMR* knockdown on cell proliferation (Fig. 22a, b). This effect was found to be dose-dependent and statistically significant illustrating the essential role of nucleotide metabolism in the pro-proliferative function of *lincNMR*.

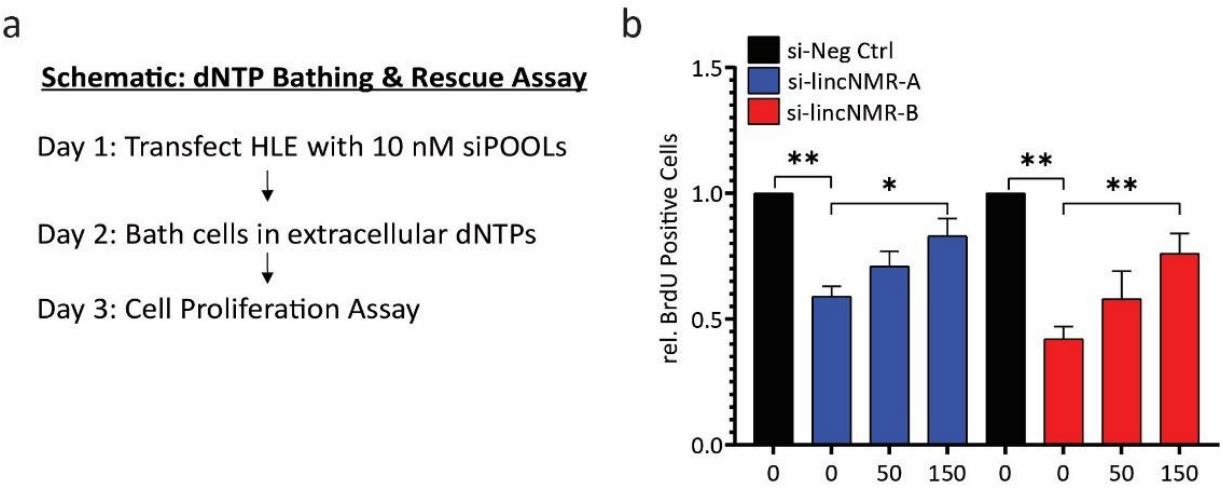

Figure 22: Exogenous supply of dNTPs rescues the phenotype induced by *lincNMR* loss
a. Schematic outline of dNTP bathing & rescue assay **b.** Supplying dNTPs rescues dose-dependently the proliferation decrease caused by *lincNMR* silencing determined by a BrdU incorporation assay. HLE cells were reverse transfected with 10 nM of the respective siPOOLs and bathed in increasing concentrations (0 µM to 150 µM) of extracellular pools of dNTPs 24 h post *lincNMR* depletion (n = 4). Data shown represents the results of the cell proliferation assay normalized to negative control siPOOL with the respective dNTP concentration. Data represents mean and error bars represent SEM. Significance was calculated by unpaired, two-tailed t-test with *, $P < 0.05$; **, $P < 0.01$; ***, $P < 0.001$. Data shown is normalized to negative control siPOOL

In summary, the regulation, association with survival and correlation of expression between *lincNMR*, YBX1, RRM2, TK1 and TYMS links them to liver cancer and to each other, respectively. *LincNMR* affects cell viability, proliferation, senescence and tumor growth *in vivo* and the interactors and targets mimic its phenotypes. At the molecular level, these data suggest a model in which the lncRNA *lincNMR* binds to YBX1, increases its activity resulting in the upregulation of the enzymes RRM2, TK1 and TYMS, which in turn govern an increase in nucleotide metabolism which can rescue the effect of *lincNMR* depletion.

5.5 Potential clinical significance of *lincNMR* in cancer

5.5.1 *lincNMR* is induced and regulated in multiple cancer entities

In line with the impact of *lincNMR* knockdown in cell lines from different tumor entities, *lincNMR* was also found to be significantly induced between tumor and normal tissues across multiple cancer types including breast invasive carcinoma, lung adenocarcinoma, lung squamous cell carcinoma, bladder urothelial carcinoma and cervical squamous cell carcinoma (Fig. 23) suggesting broader cancer-wide significance.

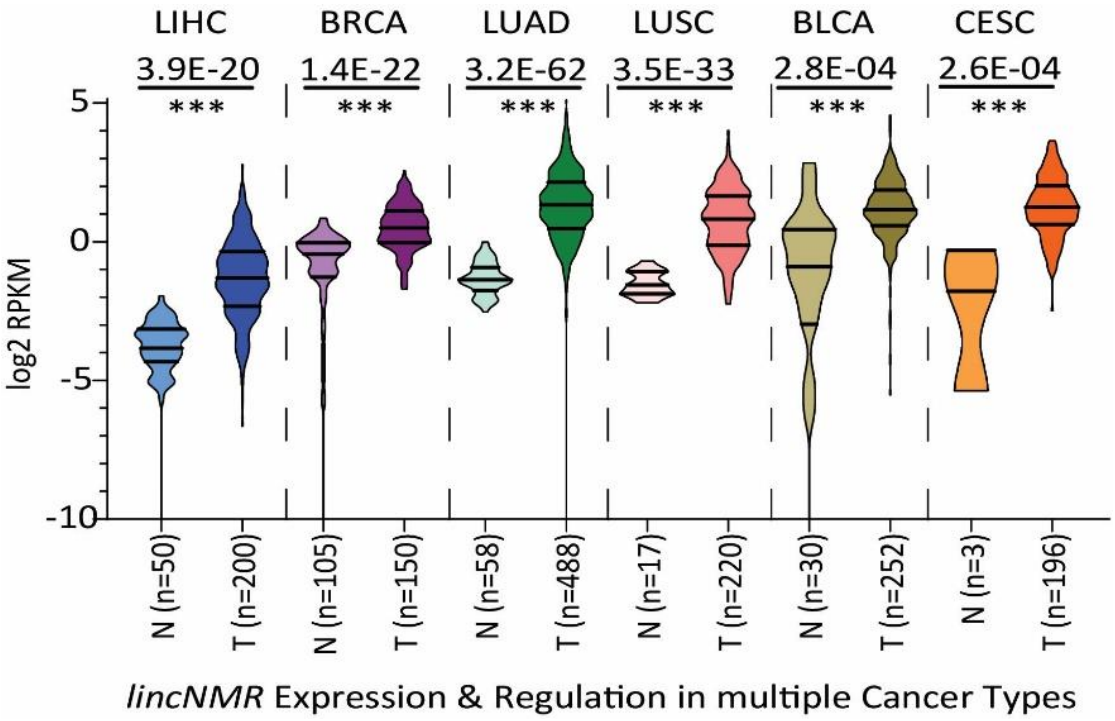

Figure 23: *lincNMR* is induced in multiple cancer entities
LincNMR is expressed and regulated in multiple cancer types (N=normal, T=tumor; data obtained from TCGA data portal). LIHC = Hepatocellular Carcinoma (N=50, T=200), BRCA = Breast Cancer (N=105, T=150), LUAD = Lung Adenocarcinoma (N=58, T=488), LUSC = Lung Squamous Cell Carcinoma (N=17, T=220), BLCA = Bladder Cancer (N=30, T=252), CESC = Cervical Serous Carcinoma (N=3, T=196). Data is represented as log2 RPKM.

5.5.2 *lincNMR* is also expressed in multiple human cancer cell lines

Additionally, to test whether *lincNMR* transcript was also expressed in other human cancer cell lines of diverse origins, I performed RT-qPCR in a panel of 73 different human cancer cell lines and found both isoforms of *lincNMR* to be expressed (Fig. 24) suggesting the relevance of *lincNMR* in multiple cancer types.

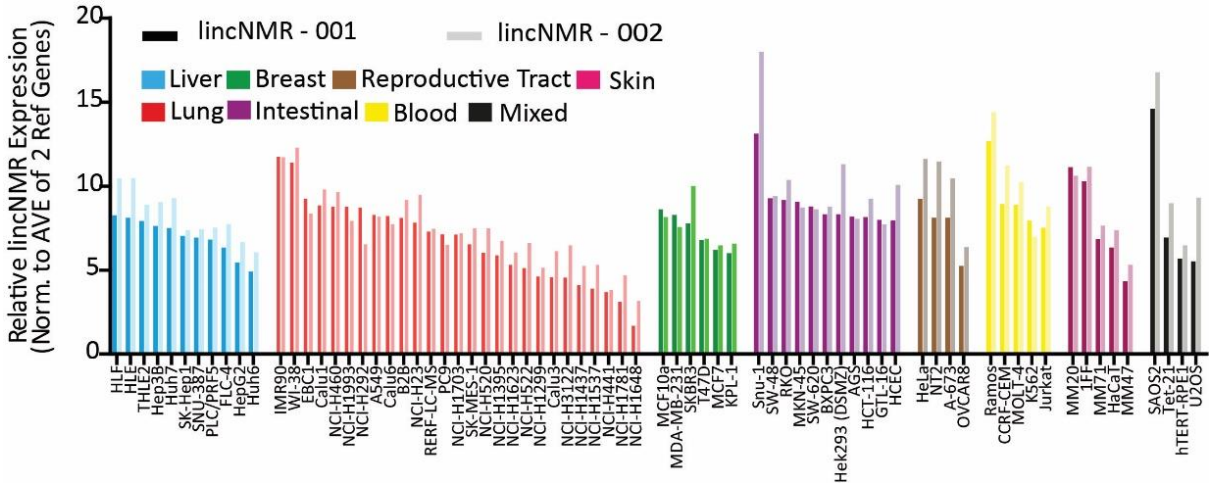

Figure 24: *lincNMR* is also expressed in multiple human cancer cell lines
RT-qPCR data in a panel of 73 human cancer cell lines (except IMR90, WI38, B2B, MCF10a, 1°FF, RPE1 = non-cancerous) showing expression of the two *lincNMR* isoforms (*lincNMR*-amp#1, *lincNMR*-amp#2) across multiple cancer types (liver, lung, breast, skin, intestinal, reproductive tract, blood etc.). Expression data shown is normalized to an average of two reference genes SRSF4 and PPIA.

5.5.3 *lincNMR* induced knockdown and growth inhibitory phenotype is stable until 168 h

Prior to performing *in vivo* xenograft experiments, I first confirmed the presence of siPOOL-induced *lincNMR* knockdown over an extended time period by checking for the knockdown efficiency and the presence of the growth-inhibitory phenotype. The siPOOL induced knockdown (Fig. 24a) and phenotype (Fig. 24b) upon *lincNMR* depletion were persistent until 168 h / day 7 after transfection fitting for the duration of the CAM assay.

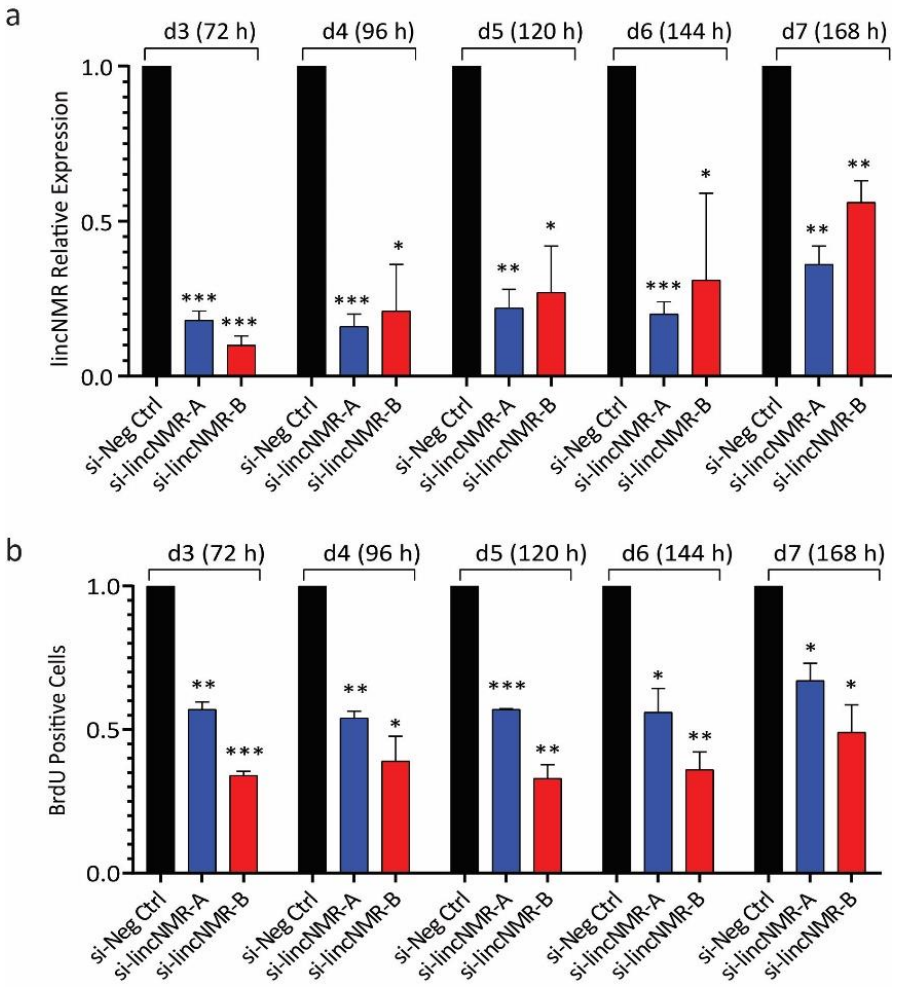

Figure 25: *lincNMR*-induced phenotype using siPOOLs is stable until day 7 after transfection
a. Time course of knockdown efficiency determined by RT-qPCR to verify stable knockdown of *lincNMR* until seven days after transfection with 10 nM siPOOLs in HLE cells. **b.** Time course of BrdU incorporation assays in HLE cells showing induction and maintenance of proliferation defect up to 168 h / day 7 post *lincNMR* knockdown with 10 nM siPOOLs. **a, b**: Data is normalized to negative control siPOOL. Data represent mean and error bars represent SEM (n=3). Significance was calculated by unpaired, two-tailed t-test with *, $P < 0.05$; **, $P < 0.01$; ***, $P < 0.001$.

5.5.4 Depletion of *lincNMR* leads to decreased tumor size and growth *in vivo*

To test the impact of *lincNMR* depletion on tumor size and growth *in vivo*, I performed xenograft experiments using the Chicken Chorioallantoic Membrane (CAM) model considering the ethical responsibility and aiming to replace, reduce or refine (3R) the use of animal models for research purposes. After seeding *lincNMR*-silenced or control-treated cells onto the CAM, tumors were harvested, measured and weighed. Tumors derived from *lincNMR*-depleted cells were significantly smaller in size as compared to the tumors derived from the control group (Fig. 26a). The tumor weight was also significantly reduced in *lincNMR*-depleted tumors in comparison to the control group (Fig. 26b).

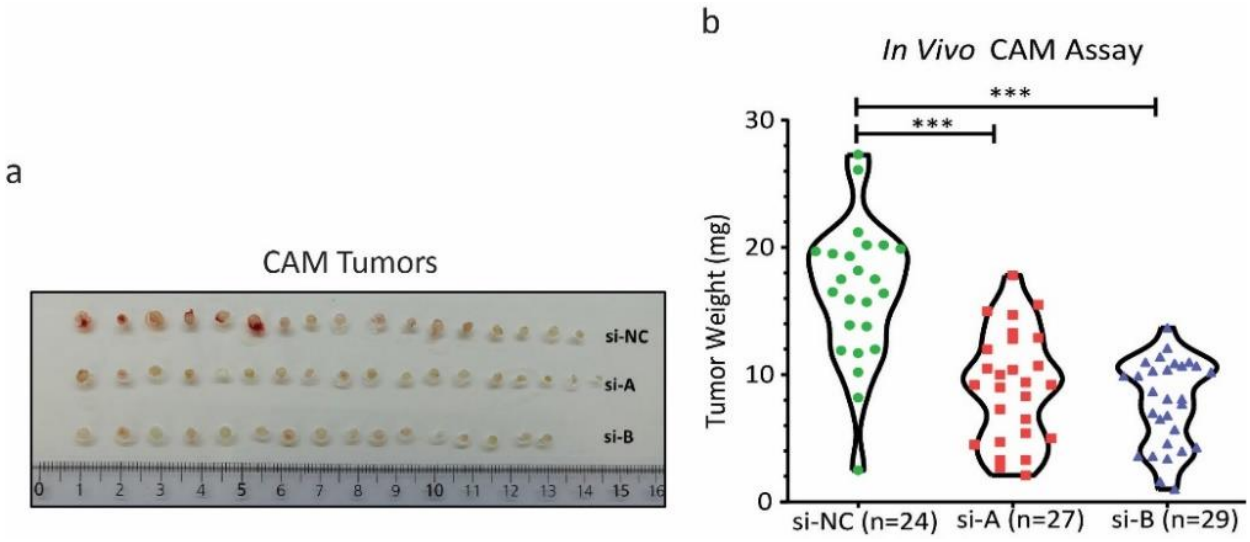

Figure 26: Loss of *lincNMR* leads to decreased tumor weight and size in vivo
a. Chick Chorioallantoic Membrane (CAM) assay: Picture showing tumors harvested from the CAM formed from HLE cells transfected with *lincNMR*-targeting or control siPOOLs. Tumors were harvested on day six. *LincNMR*-depleted cells gave rise to smaller tumors. (Number of chick embryos used in total: si-negative control=24, si-*lincNMR*-A=27, si-*lincNMR*-B=29)
b. Quantification of tumors harvested from CAM assay: show decreased tumor weight in *lincNMR*-depleted tumors compared to the control group. Significance was calculated by unpaired, two-tailed t-test with *, $P < 0.05$; **, $P < 0.01$; ***, $P < 0.001$.

6. DISCUSSION

Parts of the text and figures presented in this chapter are revised versions of the figures and text submitted for publication as an original research article:

Gandhi et al., *"lincNMR* regulates Nucleotide Metabolism via a YBX1 - RRM2 Axis in Cancer"
Nature Communications (manuscript under review)

This is the first study to investigate and unveil the molecular mechanism of *lincNMR* in cancer and also the first report linking the involvement of lncRNA in regulation of cell proliferation through nucleotide metabolism pathways.

Primary aim of my PhD project was to identify strongly deregulated novel lncRNAs in liver cancer and to further perform in-depth characterization of its cellular and molecular function. First, to identify strongly deregulated novel lncRNA candidates, a transcriptome-wide expression profiling was performed using publicly available RNA-sequencing dataset. LncRNA expression data was downloaded from the TANRIC database [164], derived from publicly available patient data from TCGA data portal. Out of 12727 lncRNA annotations, first selection of lncRNAs was made based on their high expression and strong regulation in liver cancer. Primary selection lead to the identification of 217 lncRNAs, where some of the well-studied lncRNAs such as *MALAT1*, *HULC*, *NORAD*, *ANRIL, CRNDE, LINC00857, TMPO-AS1, DANCR, ZFAS1* were found among the top deregulated candidates along with novel lncRNA transcripts, validating the rationale for primary selection. Second selection was made based on individually analyzing the attributes - novelty, coding potential, cancer-related gene neighborhood, presence of independent transcription start site etc. Second selection was made to ensure that only independently transcribed lncRNAs were selected for further steps by analyzing human promoterome dataset and also transcription start sites from Switchgear [173] . This led to the identification of 49 lncRNAs comprising of novel as well as well-studied lncRNAs. Well studied lncRNAs were included to be used as a positive control for further analysis. Expression analysis was performed on selected 49 lncRNAs using RT-qPCR in nine liver cancer cell line models of interest. Only HCC cell lines were chosen for further expression analysis to assist in identification of relevant and essentially disease specific transcripts. Expression analysis of selected lncRNAs led to the identification of nine well-expressed lncRNAs to be further probed for cellular function.

For cellular function analysis, RNAi based approach was used considering the predominant cytoplasmic localization of the lncRNAs in order achieve optimum knockdown efficiency. To circumvent off-target effects often displayed while using higher concentrations of single siRNAs, a pool of 30 single siRNAs called siPOOLs was used in much lower concentrations to target the gene of interest [160]. siRNA sequences in negative control siPOOL had no complementarity with human genome thus acting as an ideal negative control in further experiments. siPOOLs targeting *HULC* and *PLK1* were used a positive controls pools for added confidence due to their documented impact on cell viability. Cell viability screen led to the identification of novel lncRNA transcript *RP6-65G23.3*, now named *lincNMR* for reasons discussed further below in the text. *LincNMR* was selected as a novel lncRNA candidate due to the strength of the phenotype for in-depth cellular and molecular function analysis.

Since lncRNA *lincNMR* was a novel, so far uncharacterized transcript, basic characterization steps were performed to investigate its coding potential, subcellular localization and gene boundaries. Coding potential of *lincNMR* was analyzed using two tools, namely CPC and PhyloCSF. CPC analyzes putative open reading frames and assigns a score called CPC score to the transcript, where negative score corresponds to non-coding transcript and positive score indicates protein coding potential. A score from PhyloCSF algorithm determines whether alignment of multi-species nucleotide sequence is likely to represent protein-coding region. *LincNMR* was found to be a non-coding RNA using both the algorithms. Recently, there have been reports of micro-peptides being coded by non-coding transcripts [174, 175], ribosome profiling data was also analyzed for *lincNMR* locus through UCSC genome browser tracks to ensure the absence of often reported smaller open reading frames. Next, RACE experiments were performed in order to define the gene boundaries of *lincNMR* and to obtain a complete transcript sequence. 5' RACE data revealed a new transcription start site with a longer 1^{st} exon in the abundant *lincNMR* isoform, supported by independent CAGE tags and switchgear transcription start site dataset. Further, 3' RACE data revealed a presence of a novel second exon in the less abundant *lincNMR* isoform however since all further experiments were performed using only the highly abundant isoform, the presence of new exon in less abundant isoform was duly noted and no further characterization experiments were performed. Next, subcellular fractionation experiments revealed a predominant cytoplasmic localization of the *lincNMR* transcript. Thus the basic characterization experiments confirmed *lincNMR* to be non-coding, predominantly cytoplasmic and independently transcribed lncRNA.

Since the cell viability screen measured the metabolic activity of the *lincNMR* depleted cells, the reduced ATP content could either come from the reduced cell numbers or reduced metabolic activity. Considering the role of liver cells in ATP intensive gluconeogenesis and glycogenolysis pathways [176], the cell proliferation assay was performed to further investigate and characterize the cellular function of *lincNMR*. For additional specificity, a second siPOOL with 30 unique siRNAs targeting *lincNMR* was ordered and used in all further experiments. The knockdown efficiency of second siPOOL was also found to be >95 %. Depletion of *lincNMR* with two independent siPOOLs invoked a strong proliferation defect in multiple HCC cell lines. Observation of deregulated cell proliferation in multiple cell lines after *lincNMR* silencing also confirmed the effects to be *lincNMR*-mediated and not cell line dependent. Further, cell cycle analysis after *lincNMR* loss revealed a cell cycle arrest in G0/G1 phase of the cell cycle in multiple cancer cell lines confirming the role of *lincNMR* in regulating cancer cell proliferation.

Since induction of cell cycle arrest could also mean cells slipping to senescent state, β - Gal activity in *lincNMR* depleted cells was measured. And indeed, increased β - Gal activity was found in multiple HCC cell lines confirming the induction of senescence after *lincNMR* loss. Since RNAi mediated depletion of *lincNMR* is transient in nature and not every cell is guaranteed to receive siPOOLs irrespective of excellent knockdown efficiency of >90 %, further experimental approach could involve using CRISPR approach to generate *lincNMR*-knockout cell lines and to selective sort for senescent cells for further investigations, however given the strong induction of proliferation defect upon *lincNMR* loss, this approach could prove challenging in terms of remaining cell numbers for further investigations.

Further, in order to gain a functional insight into the role of *lincNMR*, RNA Antisense Purification followed by MS was performed and YBX1 protein was identified as a direct binding partner of *lincNMR*. YBX1 is a transcription factor and has been reported several times to play diverse functional roles in cancer progression upon its binding to lncRNAs [177-180]. YBX1 has also been reported to drive tumorigenicity and invasiveness of melanoma cells and its high expression was correlated with negative prognosis in primary melanoma patients [181]. YBX1 expression was also shown to correlate with poor outcome in breast cancer patients [182]. Accordingly, in our dataset, YBX1 expression was found to correlate with poor overall survival in liver cancer patients. And an additional positive and significant correlation was also observed between *lincNMR* and *YBX1* mRNA levels in liver cancer patient samples supporting the relevance of *lincNMR*-YBX1 interaction in cancer.

Further, to understand the proteome-wide impact and to identify *lincNMR* regulated candidate proteins, triple-label SILAC-MS was performed. Triple label SILAC-MS assisted in circumventing technical

variability and sensitivity issues normally posed in mass spectrometry experiment, especially for detecting smaller differences. Usage of light, medium and heavy label for metabolic labelling allowed for each cell line to be respectively transfected with either negative control siPOOL, or two different *lincNMR*-targeting siPOOLs whereas the mass variations in different labels allowed for sample specific quantification of respective proteins in the individual sample. Ratios of *lincNMR*-targeting siPOOL/ negative control siPOOL were used for further quantification and pathway enrichment analysis.

Triple label SILAC - MS data revealed that silencing of *lincNMR* caused a strong depletion of key dNTP synthesizing enzymes RRM2 (Ribonucleotide Reductase subunit 2), TK1 (Thymidine Kinase) and TYMS (Thymidylate Synthetase). These enzymes have been reported to play key roles in the biosynthesis of dNTP pools in nucleotide metabolism pathways. Both *de novo* and salvage pathways lead to the synthesis of ribonucleotides where, the enzyme ribonucleotide reductase (RNR) performs a key reduction of ribonucleotides to deoxy-ribonucleotides [125, 139], a rate limiting step in nucleotide biosynthesis. The enzyme RNR consists of tetrameric complex with two large catalytic subunits of RRM1 and two regulatory subunits of RRM2, where RRM2 has been shown to regulate dNTP biosynthesis during S-phase of the cell cycle [183]. TK1 has been shown to be essential for synthesizing dTMP, a first step in synthesis of dTTP whereas TYMS is known to catalyze the conversion of dUMP to dTMP, thus both aiding in maintaining the dTMP levels in cells.

Since the balanced levels of dNTP pools are known to be critical for DNA replication, DNA repair of both nuclear and mitochondrial DNA and maintenance of genomic integrity [184], synthesis of nucleotides is carefully regulated during cell proliferation. Disturbances in nucleotide pools have been linked to wide spectrum of diseases like immunodeficiency [185, 186], aging [127, 187], kidney diseases [188, 189], mitochondrial pathologies [190, 191] including in cancer [192-195]. In line with the observations from literature, along with strong depletion of RRM2, TK1 and TYMS silencing of *lincNMR* also triggered induction of senescence in multiple liver cancer cell lines, in great concordance with multiple reports linking the imbalances in levels of RRM2, TK1 and TYMS with induction of senescence in cancer cells [130, 196, 197].

Consequently, all four dNTPs were also found to be depleted upon *lincNMR* loss in multiple liver cancer cell lines, consolidating the role of *lincNMR* in the regulation of nucleotide metabolism axis. Findings from this study are complemented with the previous reports where all four dNTPs were also found to be significantly decreased during OIS [130, 198, 199]. Importantly, bathing the cells in exogenous dNTP pools dose-dependently could also rescue the proliferation defect phenotype caused by *lincNMR*

knockdown in two liver cancer cell lines, which is in good accordance with previous studies stating that increasing dNTP levels by RRM2 overexpression or exogenous nucleoside supply overcomes aberrant DNA replication, DNA damage and senescence induced by oncogenic RAS or BRAF [198, 199]. It has also been reported that ectopic co-expression of TYMS and RRM2 suppresses OIS in normal human fibroblasts [198, 200]. Additionally, TYMS and RRM2 were reported to be suppressed in c-MYC-depleted melanoma cells undergoing OIS and that this senescent effect could be rescued by overexpression of TYMS and RRM2 or by addition of deoxyribonucleosides [196]. Since multiple triggers for induction of senescence have been reported based on the involved pathways, next step for this project could benefit from the experiments involving induction of senescence in cells using different approaches such as DNA damage inducing drug treatment, using hydrogen peroxide and overexpression of RAS and then to quantify the expression of *lincNMR*.

To stress on the significance of this axis, these dNTP synthesizing enzymes were additionally also found to be strongly and significantly induced in our liver cancer patient datasets. Further stratification of RRM2, TK1 and TYMS using expression identified their association with poor overall survival and their correlation with *lincNMR* levels in liver cancer patients.

Importantly, after silencing of *lincNMR* binding partner - YBX1, cells also mimicked the phenotype induced after *lincNMR* depletion in decreasing cell proliferation and also the RRM2, TK1 and TYMS levels. To further functionally understand the significance of *lincNMR*-YBX1 binding, *lincNMR* was also found to regulate the transactivational activity of YBX1 as identified by reporter assays – thus documenting a novel role for the *lincNMR*-YBX1 axis in regulation of nucleotide metabolism in cancer.

Notably, depletion of *lincNMR* not only reduced proliferation in liver cancer but also impaired proliferation in multiple breast and lung cancer cell lines. Additionally, upon analysis of *lincNMR* expression in patient derived datasets of multiple cancer types, *lincNMR* was found to be significantly induced and regulated also in lung, breast, bladder and cervical cancer making it a broadly relevant oncogenic lncRNA. Further to validate the effects observed in cell line models and to elucidate the effect of *lincNMR* loss on tumor growth *in vivo*, xenograft experiments were performed using the CAM model. CAM model design allowed for *in vitro* and highly efficient knockdown of *lincNMR* in HLE cells, before being seeded *in vivo* onto the CAM membrane. *LincNMR*-depleted tumors harvested from the CAM membrane were found to be significantly smaller in size and weight, confirming its role in reduction of tumor size and growth *in vivo* and also implicating it as a promising target in cancer treatment.

Considering issues with cell lines bearing distinct genomic and transcriptomic profiles due to prolonged cultures, further experiments into preclinical models could be performed using patient-derived xenografts or patient-derived organoids to further enrich and solidify the current understanding of the role of *lincNMR* in tumor growth *in vivo*. Patient-derived xenografts provide for valuable tool to evaluate tumor growth rate or assess the therapeutic response of lncRNA targeting in vivo. Some examples where patient derived xenografts have been used include lncRNA *HOTAIR* [48, 201] and lncRNA *SAMMSON* [202]. *Malat1* and *MaTARs* have also been depleted in mouse mammary tumor-derived organoids using ASO based approach to study branching morphogenesis [203, 204].

Targeting nucleotide metabolism has already been identified as a promising therapeutic strategy in cancer where the first chemotherapeutics used were cytotoxic nucleoside analogs and nucleobases like thiopurines and fluoropyrimidines [205]. These cytotoxic nucleoside analogs have similar structure as nucleosides and function via interfering in biosynthesis of DNA/RNA [206]. Gemcitabine was the first nucleoside analog clinically approved and still continues to be a frontline therapy against pancreatic, bladder and lung cancer [207] but unfortunately resistance to Gemcitabine was common through increase in dNTP biosynthesis or mechanism involving transport of nucleosides [208]. Ribonucleotide reductase (RNR) inhibitors were approved for treatment of cancer to target nucleotide metabolism axis [130]. Clofarabine, a purine analog targeting nucleic acid biosynthesis and ribonucleotide reductase was the second approved drug targeting refractory pediatric leukemia [209, 210]. A combination therapy with Gemcitabine, Clofarabine and Carboplatin has also been shown to significantly improve progression-free survival of patients with platinum-sensitive recurrent ovarian cancer [211]. Another successful chemotherapeutic agent methotrexate has also been reported to function via reducing the substrates for purine and pyrimidine biosynthesis [206, 212]. RNR inhibitor, Hydroxyurea (HU), has also shown promise and has been approved for use in the treatment of AML, CML and glioblastomas [213-215].

Several approaches have been reported to target lncRNAs for therapeutic purposes. For example, cytoplasmic lncRNAs could be targeted by siRNAs for argonaute mediated degradation whereas nuclear transcripts could be targeted using antisense oligo mediated degradation via an RNase H-dependent mechanism. Additional reported strategies to target lncRNAs include catalytic degradation using ribozymes or deoxy-ribozymes, aptamers, small molecule inhibitors, RNA destabilizing elements and synthetic lncRNA mimics [216-219]. The use of AntagoNAT for use in therapeutics has been investigated to regulate expression of sense mRNA [220]. Since depletion of *lincNMR* caused strong downregulation

of key enzymes in nucleotide metabolism pathways, targeting *lincNMR* could further be exploited for its use in cancer-wide therapeutic avenues.

Interestingly, nucleotide metabolism pathways have also been linked to metabolism-related disorders such as diabetes, obesity and insulin resistance circling around mTOR signaling cascade [221-223]. mTOR signaling pathway has been shown not only to promote glucose uptake and protein and lipid biosynthesis but also to regulate nucleotide biosynthesis and uptake of nucleosides through transporters [224-226]. Additionally pyrimidine metabolism has been linked to fatty liver, which predisposes liver to HCC where a link has also been shown to be established between obesity and non-alcoholic fatty liver disease [227, 228]. To this direction, a phosphoproteomics screen (screen data shown and discussed in the next chapter as: future directions for a follow up study) after the loss of *lincNMR* revealed a strong induction of UBE2O phosphorylation. UBE2O is a hybrid E2/E3 ligase shown to mediate monoubiquitination of target proteins [229, 230] and to negatively regulate TRAF6-mediated NF-kappa-B activation independently of its E2 activity [231]. UBE2O has also been reported to act as a positive regulator of BMP7 signaling mediated by SMAD6 in adipogenesis [229]. Additionally, UBE2O has been shown to regulate cytoplasmic retention of BAP1 by mediating its monoubiquitination [230]. Thus this dataset provides for an interesting starting point for a follow up study to further investigate the role of *lincNMR* in regulation of phosphorylation of E2/E3 ligase UBE2O.

Taken together, this study identified a novel lncRNA *lincNMR* and reported a first lncRNA regulating nucleotide metabolism pathways. This study showed that, the lncRNA *lincNMR* and RNA binding protein YBX1 formed a complex and regulated cancer cell proliferation through modulation of key dNTP synthesizing enzymes RRM2, TK1 and TYMS. Moreover, *lincNMR* regulation of nucleotide metabolism could be supported by the decrease in all four dNTP levels post *lincNMR* silencing and the rescue of *lincNMR* mediated phenotype by bathing the cells in exogenous pools of dNTPs. In-depth analysis of *lincNMR*-YBX1 interaction revealed the functional role of *lincNMR* in regulating transactivational activity of the transcription factor YBX1. Together with the direct functional interaction, this study showed a common set of regulated target genes between *lincNMR* and YBX1, further consolidating the relevance of this binding in nucleotide metabolism axis.

In summary, this study showed that loss of *lincNMR* lead to impaired cell proliferation, induction of a G0/G1 phase cell cycle arrest, deregulation of nucleotide metabolism and eventual induction of senescence in multiple human cancer cell lines. Thus identifying a novel tumor-promoting lncRNA - *lincNMR* - and unveiling its functional role along YBX1 - RRM2 / TK1 / TYMS axis in regulating nucleotide

metabolism and governing the cancer cell fate between proliferation and senescence. Importantly and in addition to unveiling the functional role of *lincNMR,* this study also discusses the avenues highlighting the potential of *lincNMR* as a potential therapeutic target in cancer.

This page has been intentionally left blank

7. FURTHER EXPERIMENTAL DIRECTIONS FOR THIS PROJECT

In this study, I report the role of the novel lncRNA *lincNMR* in the regulation of nucleotide metabolism through *lincNMR*-YBX1-RRM2-TK1-TYMS axis as discussed in details in the previous chapter (Chapter 6. Discussion). Involvement of kinases in the regulation of nucleotide metabolism pathways is well documented, so in order to gain a deeper understanding of the role of *lincNMR* in the regulation of nucleotide metabolism, I also performed a phosho-proteomics screen using the triple-label SILAC approach - a methodology which I initially established in the lab (in collaboration with DKFZ Proteomics core facility). The methodology and schematic of the experiment is based on the initially described triple-label SILAC experiment to analyze the total cellular proteome after *lincNMR* depletion (described in details in the sections 4.8.1 and 5.4.6).

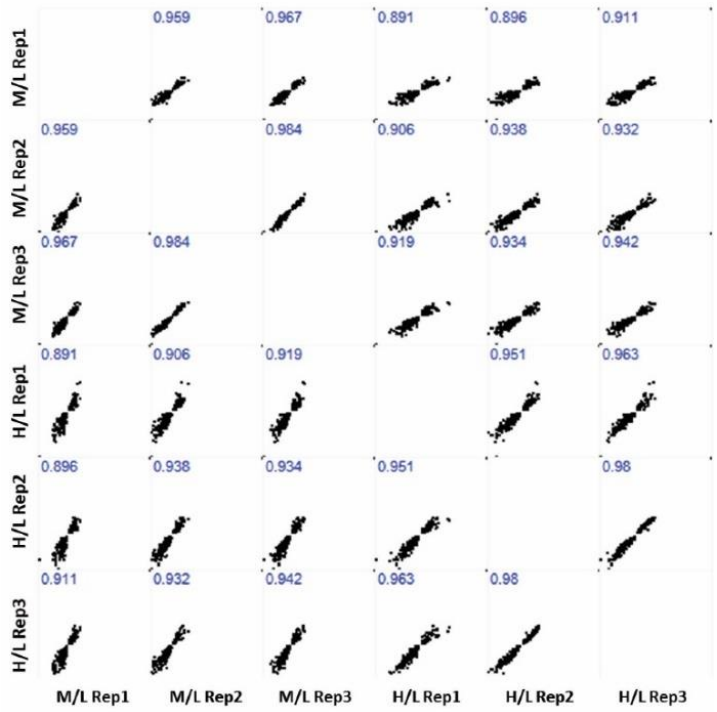

Figure 27: Multiscatter plot for phosphoproteomics dataset as a quality control reproducibility
Multi-scatter plot depicting deregulated phosphorylation of proteins identified across three biological replicates using two independent siPOOLs (si-*lincNMR*-A = Medium (M), si-*lincNMR*-B = Heavy (H), vs. control siPOOL = Light (L)) in triple-label SILAC-MS. HLE cell lysates were harvested 48 h after depletion of *lincNMR* with 10 nM siPOOLs (n = 3). Data represents fold change normalized to negative control siPOOLs. Proteins identified across biological replicates and only with phosphorylation deregulated with both siPOOLs were selected for further analysis. Pearson correlation coefficient is displayed on the multi-scatter plot.

The experiment was performed in three biological replicates and a significant correlation was observed across replicates and both the siPOOLs (Fig. 27) with an average person correlation coefficient of R = 0.938.

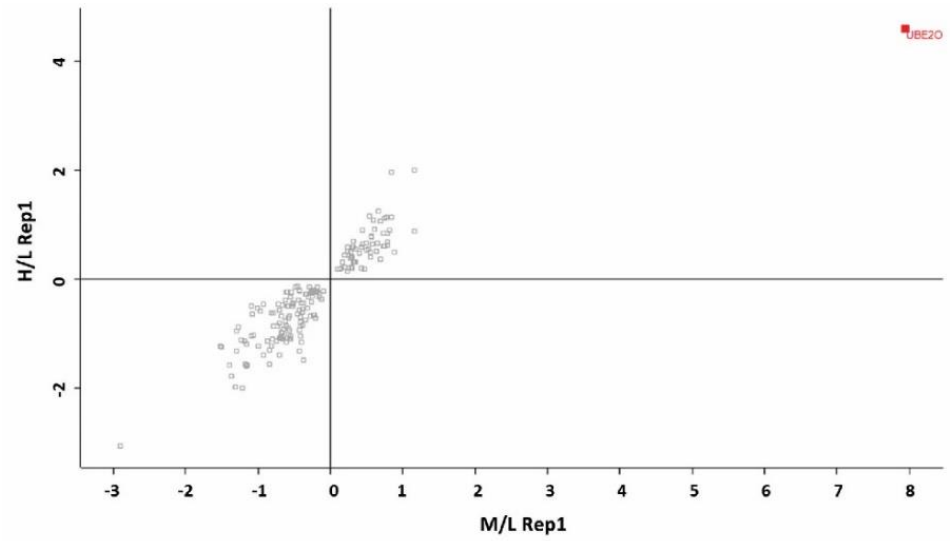

Figure 28: Depletion of *lincNMR* leads to strong induction of UBE2O phosphorylation
Scatter plot representing 222 candidates ($p < 0.001$) and correlation between log2 ratios of M/L (siPOOL-A / siPOOL Neg Ctrl) and H/L (siPOOL-B / siPOOL Neg Ctrl) where phosphorylation of UBE2O is strongly induced at 48 h after depletion of *lincNMR* in HLE with 10 nM of respective siPOOLs.

Further, the analysis of deregulated phospho-proteome upon *lincNMR* depletion led to a significant strong induction of phosphorylation of UBE2O in the dataset (Fig. 28) at Ser-401. UBE2O has been implicated in an oncogenic role and tumor initiation [232, 233]. This phosphorylation Ser-401 has not been characterized in terms of its activating / inactivating role of UBE2O before and thus offers a promising start for the next follow-up study to investigate the role of *lincNMR* in regulation of UBE2O activity.

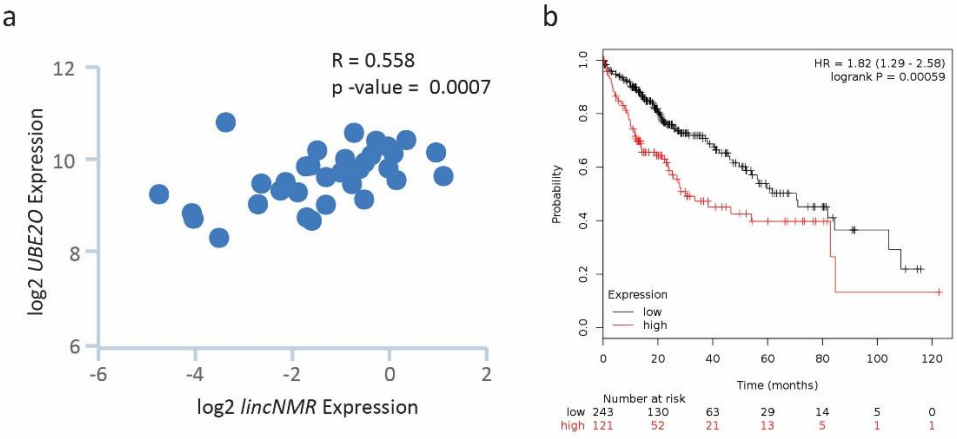

Figure 29: *lincNMR* levels correlates with *UBE2O* where UBE2O expression is linked to survival in liver cancer patients

a. Correlation plot: *UBE2O* mRNA levels significantly correlates with *lincNMR* with a correlation coefficient of 0.558 in liver cancer patients. Log2 values plotted **b.** Kaplan-Meier plot of liver cancer patients stratified by *UBE2O* expression level.

Moreover a significant correlation between *UBE2O* mRNA and *lincNMR* expression was observed in liver cancer patients (Fig. 29a). Furthermore, I also found *UBE2O* expression levels to significantly correlate with poor survival in liver cancer patient datasets (Fig. 29b). From these observations, we could propose that this dataset makes for a promising start for a follow up study.

This page has been intentionally left blank

8. ACKNOWLEDGEMENTS

First of all, I would like to thank Prof. Dr. Sven Diederichs for providing me the opportunity to work in his lab. I would like to express my gratitude for his constant support, encouragement and most importantly constructive criticism and close supervision. I am particularly grateful to him for giving me the opportunity to participate in relevant scientific meetings and pursue scientific collaborations during my time in the lab as a doctoral student. Next, I would like to thank Prof. Dr. Peter Angel and Prof. Dr. Gunter Meister for their support as members of my thesis advisory committee. I would also like to thank Prof. Dr. Georg Stoecklin and Dr. Julien Béthune for agreeing to be examiners on my defense examination committee.

I would also like to thanks PD Dr. Kai Breuhahn and Prof. Dr. Peter Schirmacher for providing laboratory facilities during my time in pathology. I would also like to thank Maria, Lisi, Geli, Sarah, Caro, Michaela and Eva for being so co-operative and making my time at the Institute of Pathology so much fun.

I would like to thank all B150 members for their inputs and suggestions during lab meetings. I would particularly like to thank Maria Polycarpou-Schwarz not only for scientific discussions but also for being an amazing soul and mentor that she is. A huge thank you to Matthias Gross for his technical help and endless fun activities. A big thanks to Tabea Nimz, even though for short time together, but making those weeks absolutely amazing. Additionally, I would like to thank my scientific collaborators Dr. Monika Langlotz (Flow Cytometry Facility at ZMBH), Dr. Martina Schnoelzer and Dr. Uwe Warnken (DKFZ Proteomics facility), Prof. Baek Kim and Jessica Holler (Emory University, Atlanta USA), Prof. Dr. Heike Allgayer, Dr. Nitin Patil and Dr. Jeorg Leupold (CBTM, Mannheim) and finally Dr. Mathias Munschauer, Monica Schenone, Christina Hartigan and Prof. Eric Lander (RAP-MS experiments).

On a personal front, I am grateful to amazing friends I made here in Heidelberg – Maria, Lisi, Kate, Caro, Kevin, Chaitali, Malwina, Ayca, Anna and I thank them for being my home away from home. I want to thank my family for being my “Rock of Gibraltar” and believing in me and supporting me unconditionally.

Special thanks to my first mentor, Prof. Dr. Vedang Murthy – I owe not only my drive and motivation towards cancer research to the time I spent working at ACTREC, but also a thing or two about life.

Finally, my husband Ajay - cannot thank him enough. He literally moved across the ocean for me when the going got tough. He encouraged, consoled, entertained and supported me throughout the last years. I feel blessed and lucky to call him mine.

This page has been intentionally left blank

9. APPENDIX

9.1.1 LncRNA expression data from liver cancer patient dataset from TANRIC

Table 15. LncRNA expression data of 217 lncRNAs with FC > 5 and p-value < 0.001

Gene Id	MED Normal	MED Tumor	MED Normal/MED Tumor	TTEST
ENSG00000272872.1	0.00	0.14	369.71	3.44E-14
ENSG00000267759.1	0.00	0.04	79.50	1.70E-09
ENSG00000259717.1	0.00	0.02	69.79	6.10E-05
ENSG00000204832.5	0.01	0.65	61.77	3.72E-21
ENSG00000267783.1	0.00	0.14	52.62	5.97E-07
ENSG00000236519.1	0.00	0.03	44.19	1.09E-19
ENSG00000224189.2	0.00	0.13	34.11	4.09E-09
ENSG00000272137.1	0.00	0.02	33.62	1.04E-02
ENSG00000228651.1	0.01	0.40	33.01	1.17E-14
ENSG00000258667.1	0.00	0.01	32.08	7.50E-04
ENSG00000237152.2	0.00	0.01	31.95	2.06E-09
ENSG00000261039.1	0.00	0.03	28.86	3.92E-08
ENSG00000271963.1	0.00	0.10	28.10	7.27E-08
ENSG00000232712.2	0.00	0.00	27.72	7.98E-09
ENSG00000240498.2	0.00	0.09	24.64	8.22E-22
ENSG00000262952.1	0.00	0.01	24.43	1.55E-05
ENSG00000226330.1	0.01	0.23	24.19	1.27E-22
ENSG00000266957.1	0.00	0.04	22.60	1.23E-03
ENSG00000215424.5	0.00	0.02	21.59	7.45E-15
ENSG00000240710.1	0.00	0.02	21.58	6.12E-11
ENSG00000253979.1	0.00	0.04	20.75	5.98E-04
ENSG00000243230.1	0.01	0.15	19.84	5.00E-22
ENSG00000245694.4	0.04	0.81	18.77	8.71E-24
ENSG00000272068.1	0.01	0.20	17.88	3.29E-09
ENSG00000215394.4	0.00	0.07	17.82	1.69E-17
ENSG00000236643.1	0.00	0.04	17.27	1.76E-18
ENSG00000237978.1	0.00	0.08	16.83	6.08E-13
ENSG00000225210.5	0.04	0.70	16.02	2.96E-22
ENSG00000205500.4	0.00	0.00	15.26	2.14E-02
ENSG00000273091.1	0.00	0.03	15.16	1.80E-07
ENSG00000206195.6	0.02	0.29	14.96	7.93E-25
ENSG00000245812.2	0.01	0.09	14.53	1.49E-04
ENSG00000237596.2	0.00	0.05	14.23	9.69E-05
ENSG00000231081.1	0.00	0.03	13.96	4.45E-09
ENSG00000235586.1	0.00	0.03	13.70	3.01E-03
ENSG00000254233.1	0.01	0.12	12.97	4.79E-09

ENSG00000273257.1	0.00	0.06	12.89	8.32E-09
ENSG00000270145.1	0.01	0.10	12.63	1.85E-21
ENSG00000265542.1	0.00	0.01	12.58	1.66E-03
ENSG00000270068.1	0.00	0.03	12.57	5.71E-10
ENSG00000244306.5	0.02	0.22	12.41	7.82E-24
ENSG00000271538.1	0.00	0.02	11.96	2.16E-07
ENSG00000262482.1	0.01	0.07	11.96	2.65E-15
ENSG00000230970.2	0.00	0.01	11.84	1.10E-03
ENSG00000273424.1	0.01	0.08	11.41	3.09E-16
ENSG00000228294.2	0.02	0.24	11.34	1.25E-16
ENSG00000266976.1	0.01	0.09	10.90	2.50E-05
ENSG00000228079.1	0.00	0.01	10.85	3.87E-04
ENSG00000231439.3	0.00	0.02	10.81	4.92E-08
ENSG00000260425.1	0.02	0.22	10.75	1.10E-17
ENSG00000272097.1	0.00	0.05	10.51	4.30E-27
ENSG00000265692.1	0.00	0.04	10.50	2.14E-23
ENSG00000236434.2	0.00	0.01	10.43	2.40E-02
ENSG00000259322.1	0.01	0.09	10.26	2.24E-08
ENSG00000270933.1	0.09	0.91	10.24	2.58E-26
ENSG00000224034.1	0.01	0.09	10.15	3.50E-14
ENSG00000249816.2	0.00	0.00	10.14	1.02E-02
ENSG00000264769.1	0.01	0.08	10.11	1.91E-05
ENSG00000226686.3	0.00	0.04	9.98	3.56E-15
ENSG00000262332.1	0.00	0.03	9.89	6.07E-10
ENSG00000259887.1	0.00	0.05	9.88	2.28E-19
ENSG00000273293.1	0.02	0.15	9.69	3.51E-19
ENSG00000261008.2	0.00	0.02	9.62	9.73E-18
ENSG00000228350.1	0.01	0.14	9.59	2.34E-20
ENSG00000273002.1	0.00	0.04	9.56	2.16E-15
ENSG00000228952.1	0.01	0.06	9.54	4.44E-07
ENSG00000248265.1	0.00	0.02	9.52	6.02E-07
ENSG00000267366.1	0.00	0.03	9.43	9.10E-05
ENSG00000263412.1	0.01	0.11	9.37	9.00E-17
ENSG00000225953.2	0.00	0.04	9.33	2.00E-20
ENSG00000256128.1	0.01	0.06	8.96	5.88E-09
ENSG00000253339.1	0.02	0.20	8.93	4.49E-11
ENSG00000235612.1	0.00	0.01	8.85	2.97E-02
ENSG00000268095.1	0.01	0.06	8.83	1.03E-06
ENSG00000228430.4	0.00	0.01	8.70	1.22E-10
ENSG00000246334.2	0.00	0.03	8.55	3.02E-15
ENSG00000264188.1	0.01	0.04	8.51	5.95E-07
ENSG00000244227.1	0.00	0.02	8.49	4.49E-04
ENSG00000238260.1	0.01	0.11	8.44	2.56E-23

ENSG00000253302.1	0.00	0.04	8.43	1.76E-15
ENSG00000238261.5	0.01	0.07	8.21	2.49E-18
ENSG00000269560.1	0.01	0.05	8.17	1.40E-10
ENSG00000229178.1	0.01	0.08	8.16	8.69E-13
ENSG00000256897.1	0.00	0.03	8.12	5.64E-10
ENSG00000258735.1	0.00	0.01	7.99	7.76E-09
ENSG00000234245.2	0.02	0.13	7.98	1.58E-06
ENSG00000226674.4	0.01	0.04	7.95	4.94E-14
ENSG00000264548.1	0.00	0.04	7.91	1.65E-21
ENSG00000253864.1	0.00	0.00	7.85	2.25E-02
ENSG00000245614.2	0.01	0.06	7.84	2.43E-24
ENSG00000250696.1	0.04	0.33	7.80	3.69E-18
ENSG00000271888.1	0.02	0.19	7.74	9.77E-19
ENSG00000259087.1	0.00	0.02	7.67	1.34E-06
ENSG00000229832.1	0.00	0.03	7.63	2.51E-10
ENSG00000260589.1	0.00	0.04	7.61	4.43E-23
ENSG00000240350.1	0.02	0.16	7.59	6.22E-21
ENSG00000227036.2	0.02	0.11	7.58	5.49E-10
ENSG00000265688.1	0.08	0.58	7.53	4.86E-13
ENSG00000182366.5	0.00	0.01	7.50	2.23E-05
ENSG00000255689.1	0.02	0.14	7.47	1.87E-11
ENSG00000230880.2	0.02	0.16	7.47	1.25E-20
ENSG00000270557.1	0.02	0.14	7.42	1.07E-27
ENSG00000270562.1	0.00	0.02	7.41	1.53E-14
ENSG00000236751.1	0.02	0.18	7.40	5.00E-14
ENSG00000259349.1	0.01	0.06	7.40	4.47E-25
ENSG00000262412.1	0.01	0.06	7.34	7.13E-13
ENSG00000273162.1	0.01	0.07	7.31	3.96E-16
ENSG00000242798.1	0.02	0.13	7.27	1.73E-22
ENSG00000273230.1	0.04	0.28	7.25	7.95E-25
ENSG00000226673.1	0.00	0.03	7.20	1.77E-07
ENSG00000255741.1	0.00	0.03	7.13	3.92E-05
ENSG00000196421.3	0.01	0.10	7.13	2.40E-08
ENSG00000233791.1	0.00	0.03	7.06	4.70E-10
ENSG00000163364.5	0.01	0.10	7.04	2.99E-04
ENSG00000272993.1	0.23	1.62	7.02	5.98E-30
ENSG00000258725.1	0.00	0.03	7.01	2.36E-20
ENSG00000226206.1	0.00	0.01	7.00	2.44E-03
ENSG00000267715.1	0.01	0.06	6.96	1.11E-11
ENSG00000261019.1	0.01	0.04	6.94	9.78E-19
ENSG00000253616.1	0.02	0.13	6.90	3.13E-14
ENSG00000272792.1	0.05	0.33	6.89	4.55E-28
ENSG00000270195.1	0.03	0.24	6.88	8.63E-13

ENSG00000271762.1	0.02	0.13	6.81	3.04E-09
ENSG00000227076.1	0.00	0.02	6.78	9.95E-06
ENSG00000232677.2	0.07	0.49	6.77	3.19E-15
ENSG00000234380.1	0.04	0.27	6.74	3.02E-12
ENSG00000257596.1	0.02	0.17	6.74	9.55E-19
ENSG00000227589.1	0.00	0.03	6.73	5.51E-06
ENSG00000234869.1	0.01	0.04	6.73	1.27E-13
ENSG00000267804.1	0.12	0.78	6.71	9.34E-28
ENSG00000271151.1	0.01	0.09	6.71	6.11E-22
ENSG00000225518.2	0.06	0.40	6.69	1.20E-24
ENSG00000259755.1	0.00	0.01	6.68	8.83E-05
ENSG00000273445.1	0.03	0.22	6.63	1.44E-04
ENSG00000243224.1	0.01	0.07	6.60	3.66E-22
ENSG00000223907.1	0.00	0.03	6.58	4.90E-09
ENSG00000272468.1	0.03	0.21	6.57	9.20E-11
ENSG00000237686.2	0.02	0.12	6.57	3.14E-06
ENSG00000249395.2	0.02	0.13	6.54	9.92E-14
ENSG00000250337.1	0.03	0.21	6.53	2.27E-13
ENSG00000272205.1	0.02	0.15	6.53	4.46E-17
ENSG00000228763.1	0.00	0.03	6.53	1.63E-05
ENSG00000255050.1	0.01	0.10	6.53	6.25E-08
ENSG00000272377.1	0.02	0.11	6.51	8.91E-19
ENSG00000237253.1	0.01	0.08	6.50	7.37E-18
ENSG00000271032.1	0.02	0.11	6.45	1.49E-08
ENSG00000261840.1	0.03	0.20	6.44	3.18E-14
ENSG00000236022.2	0.00	0.03	6.43	4.73E-04
ENSG00000249856.1	0.00	0.03	6.43	1.48E-18
ENSG00000232725.1	0.00	0.03	6.38	2.68E-15
ENSG00000203849.6	0.02	0.11	6.35	1.96E-13
ENSG00000231106.2	0.02	0.10	6.33	1.10E-03
ENSG00000224805.2	0.13	0.80	6.29	1.43E-21
ENSG00000236947.1	0.04	0.24	6.27	1.34E-19
ENSG00000273249.1	0.01	0.06	6.24	3.38E-11
ENSG00000266602.1	0.01	0.05	6.21	9.22E-10
ENSG00000272211.1	0.00	0.01	6.20	2.17E-05
ENSG00000261716.1	0.15	0.95	6.19	2.35E-28
ENSG00000272953.1	0.05	0.29	6.16	4.65E-30
ENSG00000223855.1	0.01	0.07	6.10	4.45E-10
ENSG00000258077.2	0.00	0.01	6.04	1.76E-08
ENSG00000271781.1	0.07	0.44	6.01	1.00E-06
ENSG00000251556.1	0.01	0.03	6.00	1.59E-06
ENSG00000234142.1	0.00	0.02	6.00	9.67E-11
ENSG00000250432.1	0.01	0.04	5.98	2.49E-05

ENSG00000236449.1	0.00	0.01	5.92	6.01E-09
ENSG00000172965.10	0.22	1.31	5.90	6.70E-30
ENSG00000260942.1	0.03	0.16	5.90	6.24E-35
ENSG00000272716.1	0.02	0.13	5.89	2.23E-19
ENSG00000255794.2	0.00	0.01	5.88	3.16E-07
ENSG00000260051.1	0.04	0.22	5.84	5.25E-17
ENSG00000228022.1	0.01	0.05	5.84	2.42E-06
ENSG00000254812.1	0.01	0.05	5.83	3.77E-14
ENSG00000272810.1	0.02	0.10	5.82	4.06E-02
ENSG00000259515.1	0.01	0.03	5.81	5.59E-05
ENSG00000255142.1	0.06	0.37	5.77	6.19E-17
ENSG00000224358.1	0.01	0.06	5.75	1.18E-16
ENSG00000271914.1	0.02	0.11	5.75	2.00E-14
ENSG00000232306.1	0.01	0.08	5.73	8.54E-14
ENSG00000260988.1	0.00	0.01	5.72	1.01E-10
ENSG00000228554.1	0.00	0.01	5.70	2.15E-06
ENSG00000222041.6	0.78	4.43	5.66	9.31E-22
ENSG00000256164.1	0.01	0.03	5.63	1.21E-03
ENSG00000266236.1	0.01	0.05	5.63	3.09E-11
ENSG00000249859.3	0.06	0.35	5.62	4.15E-20
ENSG00000239523.1	0.07	0.37	5.60	4.44E-26
ENSG00000260423.1	0.01	0.03	5.60	7.81E-11
ENSG00000225278.3	0.00	0.01	5.59	1.94E-05
ENSG00000259153.1	**0.07**	**0.40**	**5.57**	**3.89E-20**
ENSG00000271993.1	0.02	0.09	5.54	1.73E-22
ENSG00000260285.1	0.02	0.11	5.51	1.59E-11
ENSG00000267583.1	0.02	0.12	5.50	1.44E-17
ENSG00000203279.3	0.03	0.19	5.50	1.21E-17
ENSG00000250107.1	0.00	0.01	5.50	6.90E-04
ENSG00000233154.1	0.00	0.03	5.50	5.63E-16
ENSG00000261342.1	0.02	0.08	5.40	1.35E-08
ENSG00000261713.2	0.00	0.01	5.38	1.85E-05
ENSG00000271778.1	0.01	0.07	5.35	5.34E-19
ENSG00000232874.1	0.03	0.18	5.34	7.51E-19
ENSG00000236743.1	0.01	0.04	5.33	6.28E-08
ENSG00000262410.1	0.05	0.25	5.31	1.72E-23
ENSG00000251003.3	0.02	0.13	5.30	9.41E-15
ENSG00000235319.1	0.01	0.04	5.26	4.30E-15
ENSG00000271327.1	0.02	0.13	5.24	2.54E-20
ENSG00000232909.1	0.01	0.03	5.17	1.43E-15
ENSG00000260367.1	0.02	0.11	5.16	8.47E-17
ENSG00000226179.1	0.05	0.28	5.16	3.44E-19
ENSG00000272301.1	0.03	0.16	5.16	1.92E-09

ENSG00000260495.1	0.00	0.02	5.15	2.08E-24
ENSG00000237424.1	0.16	0.85	5.13	3.75E-23
ENSG00000270019.1	0.00	0.01	5.13	3.10E-10
ENSG00000262877.3	0.09	0.49	5.12	4.28E-07
ENSG00000253264.1	0.00	0.01	5.11	1.41E-06
ENSG00000253819.1	0.13	0.67	5.06	1.90E-13
ENSG00000227256.1	0.01	0.05	5.05	2.98E-17
ENSG00000260046.1	0.00	0.02	5.05	2.56E-15
ENSG00000267197.1	0.02	0.09	5.01	3.86E-24

9.1.2 List of 49 lncRNAs screened for expression in 9 liver cancer cell lines

Table 16: RT-qPCR expression data for 49 lncRNAs in multiple HCC cell lines

Gene ID	Gene Symbol	HLE	HLF	FLC-4	SNU-387	PLC/PRF15	Huh6	Huh7	SK-Hep1	HepG2	AVERAGE
ENSG00000262477.1	AC021224	18.134	18.282	16.743	17.130	18.783	17.268	20.288	18.187	18.482	18.144
ENSG00000232527.3	RP11-14N7.2	21.430	20.758	16.302	16.150	19.228	17.781	20.925	20.609	18.323	19.056
ENSG00000177410.8	ZFAS1	20.236	19.852	17.975	17.960	19.022	18.654	21.295	19.308	19.700	19.333
ENSG00000226950.2	**DANCR**	**21.553**	**20.647**	**18.726**	**19.983**	**19.434**	**18.624**	**19.709**	**20.569**	**19.930**	**19.908**
ENSG00000232388.2	linc00493	21.763	20.910	19.673	19.479	19.378	18.933	22.313	19.990	20.348	20.310
ENSG00000259758.1	**CASC7**	**22.588**	**22.651**	**21.004**	**21.175**	**22.440**	**20.594**	**22.719**	**21.812**	**21.616**	**21.844**
ENSG00000244306.5	CTD-2314B22	22.205	22.881	20.572	20.871	22.202	22.252	24.461	21.757	21.864	22.118
ENSG00000206195.6	AP000525	22.162	22.742	20.539	20.817	22.689	22.238	24.440	21.763	21.921	22.146
ENSG00000228294.2	BMS1P17	22.891	22.377	21.876	21.956	21.474	22.449	23.865	22.232	22.021	22.349
ENSG00000212978.5	AC016747	22.614	22.527	21.672	21.300	21.865	21.938	24.425	22.348	23.312	22.445
ENSG00000225210.5	AL589743	22.526	22.903	21.863	21.417	21.510	22.653	25.317	22.204	21.955	22.483
ENSG00000233137.2	RP11-220I1.1	23.530	23.388	21.921	21.539	21.502	22.281	22.373	23.202	22.786	22.503
ENSG00000188206.5	HNRNPU-AS1	24.581	23.571	22.205	22.317	22.169	22.467	22.733	22.900	22.794	22.860
ENSG00000272872.1	LL22NC03-N14H11	23.328	23.179	23.184	22.668	21.768	23.752	26.443	22.319	22.697	23.260
ENSG00000257167.2	**TMPO-AS1**	**23.157**	**22.820**	**23.239**	**22.834**	**22.930**	**23.268**	**24.624**	**23.166**	**23.971**	**23.334**
ENSG00000237523.1	**LINC00857**	**22.659**	**22.802**	**23.316**	**22.533**	**22.196**	**21.895**	**24.020**	**23.507**	**27.360**	**23.365**
ENSG00000215394.4	BMS1P18	23.573	23.579	23.026	22.850	22.696	23.446	24.920	23.276	23.286	23.406
ENSG00000225733.1	FGD5-AS1	24.356	23.921	22.597	22.304	23.192	22.835	24.613	24.249	23.815	23.542
ENSG00000215424.5	MCM3AP-AS1	24.805	24.832	23.630	24.313	23.770	24.253	23.943	23.938	24.811	24.255
ENSG00000236751.1	**RP1-30G7**	**23.609**	**23.757**	**23.494**	**24.713**	**23.283**	**24.460**	**27.743**	**23.877**	**24.200**	**24.348**
ENSG00000259153.1	**RP6-65G23.3 (lincNMR)**	**26.296**	**25.805**	**22.226**	**23.010**	**24.205**	**22.668**	**25.671**	**23.724**	**25.593**	**24.355**
ENSG00000255135.3	RP11-111M22	26.256	25.581	23.915	22.272	23.989	23.491	25.617	25.372	24.993	24.609
ENSG00000236519.1	AL773604	25.984	26.001	25.306	25.449	24.751	25.316	26.418	25.955	25.684	25.652
ENSG00000271762.1	LUCAT1	25.471	25.339	25.553	24.028	25.485	25.441	27.976	26.779	26.208	25.809
ENSG00000272761.1	RP11-572C15	25.539	26.551	25.289	23.138	28.205	28.563	26.896	22.209	28.919	26.145
ENSG00000243224.1	RP5-1157M23	26.846	26.893	26.533	26.541	24.355	25.937	27.338	26.599	25.924	26.329
ENSG00000245694.4	CRNDE	24.886	26.919	23.743	23.897	23.557	25.551	26.290	25.774	36.471	26.343
ENSG00000267296.2	CEBPA-AS1	28.867	31.729	24.946	28.528	24.189	23.002	24.528	27.501	23.995	26.365
ENSG00000204832.5	ST8SIA6-AS1	23.544	23.496	22.360	29.599	22.733	21.929	24.640	33.339	36.251	26.432
ENSG00000238045.5	AC009133	26.145	25.904	25.435	25.217	27.886	29.471	28.484	27.310	26.785	26.960
ENSG00000272097.1	RP11-421M1	26.965	26.669	27.471	25.726	26.300	27.661	28.196	26.716	27.478	27.020
ENSG00000249592.1	**RP11-440L14**	**26.551**	**26.895**	**27.182**	**26.919**	**24.267**	**27.856**	**27.545**	**28.752**	**28.179**	**27.127**
ENSG00000270145.1	CTD-2267D19	27.520	28.518	26.353	25.780	27.212	26.171	29.307	26.679	28.138	27.298
ENSG00000253877.1	linc01608	21.464	22.469	20.719	32.854	21.296	34.345	20.348	40.000	33.373	27.430
ENSG00000262482.1	LA16c-321D4	27.621	27.647	27.253	26.527	26.974	27.431	28.684	27.549	28.236	27.547
ENSG00000273424.1	CTA-223H9	28.619	27.930	26.774	27.148	26.930	27.196	27.722	28.642	28.375	27.704
ENSG00000253898.1	**RP11-51M18**	**29.415**	**24.503**	**21.625**	**24.784**	**20.689**	**28.577**	**20.722**	**40.000**	**40.000**	**27.813**
ENSG00000225383.2	**SFTA1P**	**21.914**	**21.898**	**20.385**	**25.478**	**40.000**	**32.985**	**35.435**	**20.905**	**34.157**	**28.129**
ENSG00000226330.1	ST8SIA6-AS1	34.923	38.028	22.823	23.769	25.310	24.945	28.202	32.575	25.492	28.452
ENSG00000285219.1	HULC	32.682	32.746	29.166	31.971	27.930	23.517	21.753	31.904	24.420	28.454
ENSG00000236643.1	RP11-175D17	31.130	29.930	27.895	28.082	27.809	27.417	27.646	29.693	27.875	28.609
ENSG00000243230.1	RP11-286H14	28.930	33.480	40.000	29.641	25.920	25.433	26.158	26.457	25.734	29.084
ENSG00000270933.1	CTD-2227E11	31.274	30.912	29.861	31.213	26.636	25.772	27.951	30.806	27.825	29.139
ENSG00000240498.2	ANRIL	24.644	24.531	24.189	40.000	25.446	30.580	25.941	40.000	33.529	29.873
ENSG00000273356.1	RP11-804H8	31.330	30.933	29.868	27.487	30.218	31.710	30.614	29.011	30.019	30.132
ENSG00000237978.1	RP11-385J1	40.000	35.877	24.603	28.930	33.224	24.271	24.804	30.318	31.899	30.436
ENSG00000240710.1	RP11-430C7	30.323	30.669	32.276	28.124	33.842	29.444	29.590	29.940	31.621	30.648
ENSG00000260032.1	NORAD	32.916	31.536	31.306	30.262	32.088	30.580	32.306	33.116	30.728	31.649
ENSG00000224034.1	RP11-445P17	35.753	39.813	31.602	26.673	30.392	30.938	31.302	33.323	31.631	32.381

9.1.3 Genbank submission of *lincNMR* sequences

Genbank accession numbers: *lincNMR-001* = MK652436 and *lincNMR-002* = MK652437

Table 17: Sequences of *lincNMR* 5' and 3' RACE Clones submitted to Genbank

>*lincNMR*-001 [organism=Homo sapiens] lincRNA Nucleotide Metabolism Regulator (*lincNMR*), transcript variant 1 GAGCCTTCATTCAAACTAAAAGGCTGGAAGGGAGGCAGCTGCCTTTGTTTGCCATGGATGGGTAGGGGCTGCACT GAGCAGCACCGGTGTTCTTCATCCGGCTGCACCCCCAACAGAGCTCTTTCTTCCCCAGATCCCTTTTACAGTTGGAT TCTCCCTCTTGGATCTGGCTCTGCCTTAGTCCGACCTAGAGGGATCAGCTTCGCCCACGCCCACTCTCACCCGGAAC CTTTCATCTCTTATTGAAGCCTTTTAGGCCCATTGGGATGTTCATTAGAACTCTGAAAACTACAGTTCTCCCCTTTAT GAGGACTGCACCACAGCTCGCCCTCTCCTGGGTTCCGGTAAGAAGAGATTCCAATACCACTCTTTTTTCAGAATTCA GAAAGGCAAGAGACCACCTTACTGAGCTTCAAACTGGGGCTGGGAACGCTGCCATGAATTGGGCTTGGTCTGTCT GAAGGGAGCCACCTTTTCGACAATCCTTAGACTTCTTTTGCCTGTTGGAATTACACCTTGGATCGTGGCGAAGTCTA TAGAGGTCAGATTAAGAAGAACCAAAGCAGAATAAACGTAGAACCCGATGCTGAGTTCACGAGTGAGGACGACC TCTTCCTATATGCTTTGCTATACCCTGCGTTTTGAACATTAAGGACGAGATAGGAGGCCCATAATGTTTCTTCTTGCT TTAATCCTGTCGTggCAACGTTGACTTCCACCTGGTTGCAGAGTGAGCCCATGGGACAGCCCTCTGAAATTATACTG CTTACAACCATGCTGAGTCTGCAAGGACTTCGTCCAAGCCTTTCCGTCCAGGACCTCAAACAGATCCAATCACAAG AAGAGAGATTTCAGGAAAGAGAAAATTATTCCTATCATCGGGGTTTTTGAAGAACATGAAATGACTGGGAAAATA ATCATGTTAAGTGGAAAAAAAAAAGAAATCTATCTGTTGTAATTTTCAAATAATTTTTAAATAAATTTGAAAAATTA AGAGAACTATATATATAA
>*lincNMR*-002 [organism=Homo sapiens] lincRNA Nucleotide Metabolism Regulator (*lincNMR*), transcript variant 2 GAGCCTTCATTCAAACTAAAAGGCTGGAAGGGAGGCAGCTGCCTTTGTTTGCCATGGATGGGTAGGGGCTGCACT GAGCAGCACCGGTGTTCTTCATCCGGCTGCACCCCCAACAGAGCTCTTTCTTCCCCAGATCCCTTTTACAGTTGGAT TCTCCCTCTTGGATCTGGCTCTGCCTTAGTCCGACCTAGAGGGATCAGCTTCGCCCACGCCCACTCTCACCCGGAAC CTTTCATCTCTTATTGAAGCCTTTTAGGCCCATTGGGATGTTCATTAGAACTCTGAAAACTACAGTTCTCCCCTTTAT GAGGACTGCACCACAGCTCGCCCTCTCCTGGGTTCCGGTAAGAAGAGATTCCAATACCACTCTTTTTTCAGAATTCA GAAAGGCAAGAGACCACCTTACTGAGCTTCAAACTGGGGCTGGGAACGCTGCCATGAATTGGGCTTGGTCTGTCT GAAGGGAGCCACCTTTTCGACAATCCTTAGACTTCTTTTGCCTGTTGGAATTACACCTTGGATCGTGGCGAAGTCTA TAGAGGTCAGATTAAGAAGAACCAAAGCAGAATAAACGTAGAACCCGATGCTGAGTTCACGAGTGAGGACGACC TCTTCCTATATGCTTTGCTATACCCTGCGTTTTGAACATTAAGGACGAGATAGGAGGCCCATAATGTTTCTTCTTGCT TTAATCCTGTCGTggCAACGTTGACTTCCAAAACAAGGTCTCACTGTGTCACCCAGGCTGGAGAGCAGTGGCACGA TCATAGCTCACTGATCACATGGCAGCCTCAAACTCCTGGACTCAGTGGGTCCTCCTGCCTCAGCATCCTGAGTAGCT GGGACTACAGCCTGGTTGCAGAGTGAGCCCATGGGACAGCCCTCTGAAATTATACTGCTTACAACCATGCTGAGT CTGCAAGGACTTCGTCCAAGCCTTTCCGTCCAGGACCTCAAACAGATCCAATCACAAGAAGAGAGATTTCAGGAAA GAGAAAATTATTCCTATCATCGGGGTTTTTGAAGAACATGAAATGACTGGGAAAATAATCATGTTAAGTGGAAAA AAAAAAGAAATCTATCTGTTGTAATTTTCAAATAATTTTTAAATAAATTTGAAAAATTAAGAGAACTATATATATAA

9.1.4 List of candidates identified in *lincNMR* RAP-MS

Table 18: List of candidates from *lincNMR* RAP-MS

Gene Symbol	log2 FC XL vs. no XL	adj. p-value XL vs. no XL -log10	Survival HCC logRank-test p-value
Ybx1	**1.076**	**3.13392**	**4.30E-08**
Cirbp	**1.121**	**3.03594**	**1.10E-06**
Hnrnpcl1	**2.599**	**3.27773**	**2.80E-06**
Fubp1	**1.364**	**3.09009**	**5.10E-06**
Alyref	**1.111**	**3.13392**	**3.20E-05**
Hnrnph1	**1.272**	**3.13392**	**9.60E-05**
Srsf2	**1.408**	**3.27773**	**8.40E-04**
Raly	**1.031**	**3.04348**	**1.60E-03**
Srsf5	**1.199**	**3.17046**	**1.90E-03**
Syne1	**1.256**	**3.13611**	**2.60E-03**
Ncl	**1.359**	**3.13392**	**3.10E-03**
Hnrnpm	**1.100**	**3.11930**	**4.70E-03**
Ewsr1	**1.544**	**3.13392**	**5.50E-03**
Srsf3	**1.391**	**3.26192**	**8.40E-03**
Srsf9	**1.145**	**3.02806**	**1.18E-02**
Bud13	**1.098**	**3.09448**	**1.65E-02**
Hnrnpdl	**1.241**	**3.03717**	**1.65E-02**
Hnrnpf	**1.131**	**3.13392**	**2.20E-02**
Hnrnpc	**1.852**	**3.27773**	**2.80E-02**
Ddx17	**1.013**	**3.02811**	**3.24E-02**
Mfap1	**2.189**	**3.34698**	**3.90E-02**
Pnn	**1.029**	**3.03594**	**4.23E-02**
Elavl1	1.379	3.27773	5.30E-02
Syncrip	1.073	3.13392	7.80E-02
Hnrnpa2b1	1.843	3.27773	9.40E-02
U2af1	1.464	3.13392	9.50E-02
Hnrnpk	1.524	3.27773	1.00E-01
Srsf7	1.305	3.23707	1.00E-01
Rnps1	1.017	3.09448	1.08E-01
Hnrnpab	1.264	3.11930	1.23E-01
Thrap3	1.109	3.13392	1.30E-01
Znf326	1.245	3.09795	1.32E-01
Ybx3	1.076	3.13392	1.73E-01
Taf15	1.877	3.27773	1.80E-01
Hnrnpa0	1.018	3.02811	1.94E-01
Pabpn1	1.322	3.11372	1.94E-01
Zc3h18	1.261	3.04348	2.63E-01
Fus	1.612	3.17046	3.00E-01

Srsf6	1.779	3.27773	3.50E-01
Hnrnpa1	1.345	3.27773	3.50E-01
Rbm3	1.165	3.13392	3.60E-01
Khsrp	1.204	3.11372	4.51E-01
Srsf4	2.177	3.27773	5.10E-01

9.1.5 Proteome after *lincNMR* depletion

Table 19: List of deregulated proteins post *lincNMR* loss (p < 0.001, data = *log2* ratios)

UniProt Names	M/L Rep1	M/L Rep2	M/L Rep3	H/L Rep1	H/L Rep2	H/L Rep3	AVE H/L & M/L
SPDLY_HUMAN	-1.048	-1.446	-1.625	-2.133	-2.201	-2.424	-1.813
CCNB1_HUMAN	-1.335	-1.846	-1.533	-1.839	-2.066	-2.227	-1.808
RIR2_HUMAN	-1.295	-1.795	-1.860	-1.331	-1.694	-1.739	-1.619
TOP2A_HUMAN	-1.315	-1.885	-1.762	-1.198	-1.379	-1.343	-1.480
SHCBP_HUMAN	-0.854	-1.127	-1.489	-1.541	-1.655	-1.664	-1.388
ANLN_HUMAN	-0.837	-0.918	-1.290	-1.323	-1.441	-1.510	-1.220
KIF11_HUMAN	-0.798	-1.030	-1.069	-1.214	-1.455	-1.489	-1.176
KITH_HUMAN	-0.884	-1.167	-1.157	-1.167	-1.301	-1.260	-1.156
KI20A_HUMAN	-0.689	-0.902	-1.148	-1.287	-1.337	-1.284	-1.108
KI67_HUMAN	-1.525	-1.261	-1.072	-0.855	-1.027	-0.890	-1.105
UBE2C_HUMAN	-0.710	-0.884	-1.372	-1.024	-1.256	-1.235	-1.080
CDK2_HUMAN	-0.531	-0.926	-1.077	-1.229	-1.161	-1.289	-1.036
PAI1_HUMAN	-0.742	-1.173	-1.108	-0.841	-1.304	-1.032	-1.033
TYMS_HUMAN	-0.593	-0.890	-0.931	-0.971	-1.335	-1.366	-1.014
FGF2_HUMAN	-0.945	-0.904	-0.743	-0.896	-1.046	-1.096	-0.938
RIF1_HUMAN	-0.774	-0.946	-0.771	-0.957	-0.920	-0.973	-0.890
TPM1_HUMAN	-1.030	-0.812	-0.728	-0.900	-0.955	-0.817	-0.874
IMA1_HUMAN	-0.559	-0.781	-0.860	-0.949	-0.969	-0.946	-0.844
CKS1_HUMAN	-0.559	-0.663	-0.623	-1.058	-0.976	-1.047	-0.821
KIF4A_HUMAN	-0.440	-0.633	-0.658	-1.043	-1.000	-1.063	-0.806
CD123_HUMAN	-0.603	-0.732	-0.631	-0.682	-0.891	-1.077	-0.769
TGFI1_HUMAN	-1.099	-0.392	-0.785	-0.621	-0.564	-0.795	-0.709
FANCI_HUMAN	-0.533	-0.544	-0.553	-0.927	-0.866	-0.716	-0.690
AN32E_HUMAN	-0.789	-0.887	-0.816	-0.541	-0.513	-0.482	-0.671
CCD86_HUMAN	-0.521	-0.591	-0.892	-0.300	-0.792	-0.856	-0.659
NAA40_HUMAN	-0.731	-0.659	-0.793	-0.619	-0.461	-0.655	-0.653
DYR_HUMAN	-0.458	-0.441	-0.563	-0.782	-0.723	-0.924	-0.648
DNMT1_HUMAN	-0.696	-0.713	-0.568	-0.665	-0.610	-0.558	-0.635
APC7_HUMAN	-0.630	-0.667	-0.669	-0.920	-0.510	-0.388	-0.630
BGH3_HUMAN	-0.539	-0.380	-0.703	-0.647	-0.537	-0.850	-0.609
LPP_HUMAN	-0.763	-0.704	-0.710	-0.503	-0.390	-0.487	-0.593

DUT_HUMAN	-0.477	-0.510	-0.542	-0.645	-0.575	-0.671	-0.570
UFO_HUMAN	-0.501	-0.621	-0.513	-0.525	-0.541	-0.661	-0.560
PPM1B_HUMAN	-0.499	-0.421	-0.416	-0.490	-0.556	-0.941	-0.554
TMM33_HUMAN	-0.433	-0.531	-0.522	-0.530	-0.653	-0.580	-0.542
BAZ1B_HUMAN	-0.643	-0.789	-0.450	-0.403	-0.439	-0.302	-0.504
NOB1_HUMAN	-0.382	-0.527	-0.301	-0.564	-0.638	-0.578	-0.498
TXLNA_HUMAN	-0.617	-0.555	-0.607	-0.468	-0.331	-0.354	-0.489
ABLM1_HUMAN	-0.571	-0.655	-0.500	-0.541	-0.350	-0.308	-0.487
MDN1_HUMAN	-0.323	-0.410	-0.406	-0.675	-0.550	-0.527	-0.482
HN1L_HUMAN	-0.537	-0.459	-0.435	-0.581	-0.432	-0.431	-0.479
SAR1A_HUMAN	-0.304	-0.356	-0.467	-0.441	-0.648	-0.632	-0.474
OGFD1_HUMAN	-0.319	-0.410	-0.446	-0.635	-0.443	-0.557	-0.468
CHD1_HUMAN	-0.306	-0.392	-0.517	-0.356	-0.583	-0.653	-0.468
OAT_HUMAN	-0.500	-0.463	-0.379	-0.453	-0.540	-0.450	-0.464
PA1B2_HUMAN	-0.492	-0.586	-0.433	-0.363	-0.572	-0.282	-0.455
SDCB1_HUMAN	-0.339	-0.453	-0.421	-0.476	-0.527	-0.513	-0.454
CDK1_HUMAN	-0.268	-0.334	-0.369	-0.656	-0.583	-0.516	-0.454
G3BP2_HUMAN	-0.344	-0.516	-0.706	-0.315	-0.465	-0.357	-0.450
WBS22_HUMAN	-0.242	-0.405	-0.469	-0.596	-0.494	-0.388	-0.432
PNO1_HUMAN	-0.483	-0.245	-0.483	-0.433	-0.470	-0.464	-0.429
KIME_HUMAN	-0.546	-0.540	-0.369	-0.514	-0.182	-0.411	-0.427
EIF1_HUMAN	-0.238	-0.370	-0.379	-0.461	-0.480	-0.547	-0.412
CAPR1_HUMAN	-0.291	-0.363	-0.390	-0.475	-0.523	-0.393	-0.406
BZW1_HUMAN	-0.278	-0.529	-0.474	-0.319	-0.421	-0.356	-0.396
STAU1_HUMAN	-0.374	-0.507	-0.531	-0.347	-0.254	-0.252	-0.377
DDX5_HUMAN	-0.213	-0.277	-0.387	-0.406	-0.448	-0.515	-0.375
RCC2_HUMAN	-0.185	-0.297	-0.330	-0.513	-0.510	-0.406	-0.374
UCK2_HUMAN	-0.305	-0.426	-0.361	-0.390	-0.402	-0.354	-0.373
DDX47_HUMAN	-0.395	-0.497	-0.514	-0.216	-0.282	-0.327	-0.372
SMC3_HUMAN	-0.231	-0.411	-0.355	-0.400	-0.407	-0.407	-0.369
LMNB1_HUMAN	-0.451	-0.413	-0.417	-0.349	-0.230	-0.314	-0.362
WBP11_HUMAN	-0.402	-0.364	-0.378	-0.317	-0.348	-0.336	-0.358
ABCF2_HUMAN	-0.323	-0.322	-0.441	-0.248	-0.423	-0.372	-0.355
ANXA1_HUMAN	-0.381	-0.322	-0.389	-0.370	-0.353	-0.298	-0.352
IF4G1_HUMAN	-0.473	-0.377	-0.341	-0.278	-0.355	-0.283	-0.351
IQGA3_HUMAN	-0.324	-0.281	-0.401	-0.390	-0.294	-0.403	-0.349
RAB18_HUMAN	-0.333	-0.415	-0.236	-0.372	-0.354	-0.348	-0.343
HSP13_HUMAN	-0.356	-0.306	-0.203	-0.523	-0.255	-0.393	-0.339
CKAP5_HUMAN	-0.361	-0.223	-0.176	-0.423	-0.475	-0.371	-0.338
DDX3X_HUMAN	-0.246	-0.294	-0.249	-0.460	-0.357	-0.365	-0.329
CERS2_HUMAN	-0.203	-0.253	-0.380	-0.420	-0.370	-0.330	-0.326
IF4A3_HUMAN	-0.154	-0.296	-0.244	-0.339	-0.467	-0.413	-0.319
YBOX1_HUMAN	-0.193	-0.276	-0.206	-0.410	-0.444	-0.365	-0.316

STAG2_HUMAN	-0.251	-0.218	-0.322	-0.367	-0.342	-0.389	-0.315
LRC40_HUMAN	-0.260	-0.294	-0.184	-0.391	-0.273	-0.451	-0.309
TCTP_HUMAN	-0.129	-0.238	-0.316	-0.314	-0.402	-0.362	-0.293
IPO7_HUMAN	-0.234	-0.296	-0.328	-0.236	-0.350	-0.278	-0.287
PRPS1_HUMAN	-0.216	-0.431	-0.351	-0.271	-0.221	-0.214	-0.284
BUB3_HUMAN	-0.263	-0.311	-0.332	-0.220	-0.354	-0.201	-0.280
SPT5H_HUMAN	-0.333	-0.292	-0.281	-0.228	-0.225	-0.321	-0.280
CHRD1_HUMAN	-0.376	-0.236	-0.199	-0.211	-0.283	-0.342	-0.274
SNW1_HUMAN	-0.331	-0.169	-0.337	-0.279	-0.233	-0.276	-0.271
TM41B_HUMAN	-0.398	-0.184	-0.210	-0.188	-0.329	-0.311	-0.270
RIC8A_HUMAN	-0.212	-0.373	-0.348	-0.257	-0.224	-0.180	-0.266
RAGP1_HUMAN	-0.192	-0.290	-0.324	-0.267	-0.221	-0.281	-0.263
NOG1_HUMAN	-0.239	-0.299	-0.176	-0.227	-0.320	-0.304	-0.261
ORML1_HUMAN	-0.394	-0.160	-0.232	-0.211	-0.273	-0.278	-0.258
TCEA1_HUMAN	-0.271	-0.348	-0.278	-0.230	-0.190	-0.223	-0.257
EIF3F_HUMAN	-0.297	-0.214	-0.226	-0.229	-0.244	-0.294	-0.251
IF4B_HUMAN	-0.231	-0.233	-0.238	-0.240	-0.267	-0.284	-0.249
SMC4_HUMAN	-0.226	-0.167	-0.153	-0.245	-0.323	-0.379	-0.249
PQBP1_HUMAN	-0.181	-0.285	-0.156	-0.345	-0.273	-0.245	-0.248
CBX3_HUMAN	-0.234	-0.275	-0.259	-0.187	-0.174	-0.332	-0.244
PIPNB_HUMAN	-0.271	-0.273	-0.212	-0.174	-0.311	-0.215	-0.243
CTND1_HUMAN	-0.379	-0.186	-0.164	-0.168	-0.263	-0.248	-0.235
IF4A1_HUMAN	-0.130	-0.195	-0.194	-0.260	-0.323	-0.251	-0.226
NP1L1_HUMAN	-0.281	-0.258	-0.248	-0.172	-0.165	-0.139	-0.211
RFC4_HUMAN	-0.143	-0.143	-0.211	-0.210	-0.237	-0.282	-0.204
CAND1_HUMAN	-0.189	-0.183	-0.262	-0.162	-0.177	-0.204	-0.196
ATLA3_HUMAN	-0.246	-0.198	-0.240	-0.201	-0.150	-0.134	-0.195
MCM7_HUMAN	-0.110	-0.226	-0.275	-0.193	-0.198	-0.153	-0.192
SK2L2_HUMAN	-0.125	-0.192	-0.184	-0.205	-0.208	-0.236	-0.191
PABP1_HUMAN	-0.166	-0.186	-0.171	-0.194	-0.213	-0.171	-0.183
RB6I2_HUMAN	-0.216	-0.146	-0.249	-0.090	-0.182	-0.190	-0.179
PCNA_HUMAN	-0.109	-0.175	-0.154	-0.262	-0.169	-0.181	-0.175
SNX12_HUMAN	-0.176	-0.074	-0.179	-0.192	-0.229	-0.189	-0.173
RL10_HUMAN	-0.116	-0.140	-0.132	-0.197	-0.208	-0.242	-0.173
TBB2B_HUMAN	-0.213	-0.219	-0.196	-0.169	-0.163	-0.058	-0.170
LRC59_HUMAN	-0.220	-0.109	-0.105	-0.224	-0.183	-0.140	-0.163
EIF3M_HUMAN	-0.189	-0.088	-0.142	-0.134	-0.177	-0.248	-0.163
RL40_HUMAN	-0.133	-0.103	-0.138	-0.226	-0.175	-0.161	-0.156
MCM3_HUMAN	-0.103	-0.149	-0.173	-0.158	-0.136	-0.216	-0.156
UB2V1_HUMAN	-0.221	-0.187	-0.076	-0.139	-0.156	-0.147	-0.155
FUS_HUMAN	-0.172	-0.140	-0.203	-0.096	-0.151	-0.160	-0.154
MCM6_HUMAN	-0.135	-0.227	-0.201	-0.122	-0.089	-0.129	-0.151
TBB6_HUMAN	-0.099	-0.122	-0.121	-0.182	-0.198	-0.173	-0.149

MCM4_HUMAN	-0.094	-0.195	-0.188	-0.113	-0.109	-0.135	-0.139
EHD1_HUMAN	-0.074	-0.184	-0.153	-0.164	-0.107	-0.143	-0.137
EIF3E_HUMAN	-0.118	-0.076	-0.124	-0.114	-0.214	-0.146	-0.132
TBCB_HUMAN	-0.158	-0.176	-0.101	-0.153	-0.053	-0.124	-0.127
EF2_HUMAN	-0.077	-0.109	-0.117	-0.136	-0.173	-0.115	-0.121
EMC1_HUMAN	-0.100	-0.154	-0.147	-0.065	-0.091	-0.101	-0.110
SEPT7_HUMAN	-0.072	-0.133	-0.102	-0.131	-0.110	-0.102	-0.108
RSSA_HUMAN	-0.066	-0.105	-0.107	-0.153	-0.129	-0.084	-0.107
PSD11_HUMAN	-0.106	-0.076	-0.069	-0.124	-0.139	-0.126	-0.107
RS3_HUMAN	-0.056	-0.096	-0.070	-0.111	-0.146	-0.130	-0.102
PFKAP_HUMAN	-0.025	-0.083	-0.086	-0.071	-0.060	-0.058	-0.064
HNRC2_HUMAN	0.050	0.060	0.070	0.083	0.078	0.117	0.076
NEUL_HUMAN	0.072	0.115	0.105	0.049	0.105	0.075	0.087
MPCP_HUMAN	0.073	0.157	0.098	0.084	0.136	0.067	0.102
PTBP1_HUMAN	0.074	0.118	0.109	0.105	0.148	0.095	0.108
SYFA_HUMAN	0.088	0.158	0.095	0.160	0.079	0.128	0.118
SPTB2_HUMAN	0.172	0.087	0.137	0.085	0.143	0.129	0.126
PHF5A_HUMAN	0.103	0.127	0.154	0.122	0.128	0.132	0.128
SNX3_HUMAN	0.109	0.077	0.095	0.172	0.154	0.162	0.128
PROF1_HUMAN	0.092	0.095	0.150	0.173	0.175	0.146	0.138
ATPO_HUMAN	0.122	0.114	0.115	0.175	0.246	0.138	0.151
RU17_HUMAN	0.186	0.116	0.103	0.157	0.154	0.201	0.153
PARP1_HUMAN	0.146	0.179	0.173	0.144	0.169	0.111	0.154
ALG5_HUMAN	0.115	0.191	0.127	0.202	0.185	0.108	0.155
HNRPM_HUMAN	0.196	0.174	0.171	0.142	0.141	0.158	0.164
KPYM_HUMAN	0.166	0.131	0.103	0.218	0.182	0.185	0.164
TOP2B_HUMAN	0.077	0.154	0.174	0.188	0.224	0.184	0.167
PEBP1_HUMAN	0.187	0.227	0.220	0.145	0.071	0.171	0.170
CAZA2_HUMAN	0.217	0.084	0.179	0.161	0.213	0.170	0.170
NNRE_HUMAN	0.107	0.229	0.226	0.165	0.138	0.166	0.172
RADI_HUMAN	0.103	0.136	0.132	0.193	0.224	0.245	0.172
MOES_HUMAN	0.152	0.222	0.160	0.140	0.207	0.172	0.176
GSHB_HUMAN	0.169	0.175	0.145	0.221	0.264	0.100	0.179
VDAC1_HUMAN	0.137	0.222	0.232	0.089	0.203	0.218	0.184
DHB4_HUMAN	0.109	0.205	0.149	0.176	0.214	0.250	0.184
XPO7_HUMAN	0.128	0.278	0.226	0.210	0.118	0.173	0.189
ECHA_HUMAN	0.150	0.161	0.164	0.186	0.230	0.252	0.191
1433E_HUMAN	0.131	0.238	0.221	0.197	0.200	0.161	0.191
PGRC1_HUMAN	0.089	0.183	0.208	0.232	0.207	0.237	0.193
LSM6_HUMAN	0.119	0.201	0.261	0.155	0.174	0.248	0.193
PTPA_HUMAN	0.116	0.219	0.148	0.297	0.220	0.178	0.196
M2OM_HUMAN	0.197	0.271	0.214	0.166	0.221	0.113	0.197
ARF1_HUMAN	0.184	0.206	0.252	0.141	0.225	0.176	0.197

DIC_HUMAN	0.199	0.218	0.153	0.220	0.154	0.247	0.198
RB11A_HUMAN	0.110	0.213	0.186	0.261	0.219	0.202	0.199
ADT1_HUMAN	0.169	0.217	0.244	0.170	0.205	0.193	0.200
ECHB_HUMAN	0.141	0.173	0.199	0.227	0.210	0.256	0.201
SYDC_HUMAN	0.146	0.250	0.309	0.138	0.165	0.227	0.206
TPIS_HUMAN	0.191	0.205	0.211	0.233	0.190	0.210	0.207
UFC1_HUMAN	0.169	0.158	0.158	0.321	0.262	0.202	0.212
ACOC_HUMAN	0.151	0.164	0.171	0.252	0.244	0.291	0.212
AP1B1_HUMAN	0.102	0.203	0.192	0.312	0.265	0.231	0.217
FUBP2_HUMAN	0.191	0.297	0.229	0.257	0.165	0.167	0.218
NRBP_HUMAN	0.131	0.176	0.146	0.286	0.272	0.312	0.221
SUMF2_HUMAN	0.198	0.344	0.152	0.135	0.246	0.259	0.222
PYGL_HUMAN	0.221	0.133	0.196	0.333	0.195	0.283	0.227
ILF3_HUMAN	0.137	0.305	0.239	0.241	0.233	0.217	0.229
PDC6I_HUMAN	0.309	0.205	0.194	0.213	0.244	0.218	0.230
STOM_HUMAN	0.316	0.191	0.092	0.232	0.298	0.260	0.232
UCRI_HUMAN	0.106	0.231	0.318	0.283	0.207	0.267	0.236
QCR7_HUMAN	0.133	0.202	0.266	0.281	0.266	0.268	0.236
PGM1_HUMAN	0.191	0.286	0.199	0.222	0.233	0.295	0.238
TM9S3_HUMAN	0.245	0.155	0.396	0.176	0.246	0.286	0.251
AIFM1_HUMAN	0.178	0.276	0.263	0.343	0.187	0.262	0.251
CALU_HUMAN	0.181	0.377	0.329	0.186	0.268	0.170	0.252
MRCKB_HUMAN	0.193	0.335	0.276	0.240	0.196	0.283	0.254
ECI1_HUMAN	0.118	0.281	0.213	0.315	0.334	0.266	0.255
HINT1_HUMAN	0.241	0.303	0.333	0.230	0.182	0.240	0.255
NIPS2_HUMAN	0.210	0.348	0.284	0.327	0.133	0.257	0.260
GALT2_HUMAN	0.327	0.207	0.264	0.213	0.189	0.380	0.263
GDIA_HUMAN	0.236	0.350	0.358	0.229	0.221	0.188	0.264
PLIN3_HUMAN	0.313	0.203	0.197	0.331	0.243	0.301	0.265
HNRL1_HUMAN	0.163	0.244	0.191	0.355	0.296	0.343	0.265
1433B_HUMAN	0.151	0.258	0.251	0.302	0.297	0.346	0.268
FUMH_HUMAN	0.270	0.251	0.289	0.240	0.339	0.219	0.268
BAF_HUMAN	0.213	0.367	0.372	0.193	0.256	0.214	0.269
UBA1_HUMAN	0.273	0.259	0.257	0.321	0.271	0.273	0.276
AN32A_HUMAN	0.174	0.315	0.349	0.153	0.383	0.282	0.276
FKB1A_HUMAN	0.299	0.296	0.380	0.279	0.234	0.171	0.277
CHSP1_HUMAN	0.308	0.278	0.137	0.290	0.306	0.343	0.277
1433G_HUMAN	0.207	0.409	0.284	0.196	0.343	0.248	0.281
MIF_HUMAN	0.268	0.204	0.245	0.337	0.322	0.317	0.282
GBB1_HUMAN	0.336	0.380	0.374	0.184	0.176	0.285	0.289
RT34_HUMAN	0.173	0.335	0.420	0.214	0.279	0.323	0.290
FLNB_HUMAN	0.115	0.251	0.314	0.381	0.367	0.365	0.299
NIBL1_HUMAN	0.227	0.389	0.334	0.294	0.265	0.285	0.299

RBM14_HUMAN	0.274	0.299	0.376	0.232	0.344	0.309	0.306
ETFA_HUMAN	0.210	0.455	0.367	0.220	0.301	0.289	0.307
KAP2_HUMAN	0.268	0.450	0.383	0.226	0.352	0.187	0.311
ABC3C_HUMAN	0.241	0.250	0.319	0.316	0.345	0.416	0.315
PHP14_HUMAN	0.322	0.374	0.331	0.291	0.334	0.265	0.319
PYGB_HUMAN	0.238	0.423	0.469	0.242	0.274	0.294	0.323
PA1B3_HUMAN	0.217	0.407	0.306	0.312	0.337	0.404	0.330
THIL_HUMAN	0.212	0.422	0.442	0.273	0.328	0.346	0.337
TRAP1_HUMAN	0.302	0.488	0.464	0.244	0.281	0.262	0.340
ITB6_HUMAN	0.216	0.334	0.390	0.313	0.375	0.449	0.346
DAAF5_HUMAN	0.282	0.266	0.297	0.425	0.363	0.447	0.347
HXK1_HUMAN	0.396	0.255	0.208	0.502	0.311	0.414	0.348
RB22A_HUMAN	0.221	0.301	0.287	0.439	0.384	0.498	0.355
CLIC4_HUMAN	0.163	0.408	0.334	0.375	0.418	0.435	0.356
ARF4_HUMAN	0.378	0.283	0.308	0.352	0.439	0.402	0.360
MYO1B_HUMAN	0.380	0.460	0.394	0.366	0.174	0.416	0.365
ETFB_HUMAN	0.218	0.509	0.496	0.330	0.372	0.281	0.368
HNRH2_HUMAN	0.384	0.253	0.284	0.462	0.431	0.481	0.382
RAB5B_HUMAN	0.347	0.361	0.329	0.396	0.487	0.463	0.397
PREP_HUMAN	0.406	0.330	0.394	0.543	0.285	0.474	0.405
GNA11_HUMAN	0.329	0.477	0.557	0.230	0.367	0.519	0.413
AP2A1_HUMAN	0.403	0.256	0.304	0.551	0.501	0.475	0.415
KCY_HUMAN	0.362	0.499	0.329	0.383	0.552	0.458	0.431
HCFC1_HUMAN	0.469	0.323	0.402	0.508	0.472	0.615	0.465
SQRD_HUMAN	0.428	0.653	0.721	0.384	0.340	0.414	0.490
TERA_HUMAN	0.428	0.514	0.499	0.535	0.524	0.459	0.493
ERG28_HUMAN	0.233	0.557	0.632	0.467	0.452	0.632	0.496
SH3G1_HUMAN	0.489	0.700	0.477	0.467	0.596	0.327	0.509
KATL2_HUMAN	0.387	0.493	0.595	0.496	0.579	0.617	0.528
DNPH1_HUMAN	0.469	0.568	0.528	0.721	0.482	0.475	0.541
RFA1_HUMAN	0.600	0.747	0.665	0.395	0.539	0.413	0.560
KPCA_HUMAN	0.662	0.599	0.477	0.548	0.540	0.631	0.576
VPS4B_HUMAN	0.453	0.668	0.445	0.699	0.643	0.645	0.592
RPTOR_HUMAN	0.697	0.818	0.597	0.495	0.546	0.586	0.623
AL9A1_HUMAN	0.888	0.869	0.855	0.817	0.698	0.689	0.803
CADM1_HUMAN	0.830	1.124	1.129	0.857	0.836	0.927	0.950
HKDC1_HUMAN	1.146	1.275	1.158	1.113	0.678	0.796	1.028
PDCD4_HUMAN	0.906	1.045	1.170	1.235	1.355	1.356	1.178
SCAM1_HUMAN	1.078	1.341	1.532	1.237	1.300	1.447	1.322

This page has been intentionally left blank.

10. REFERENCES

1. Bray, F., et al., *Global cancer statistics 2018: GLOBOCAN estimates of incidence and mortality worldwide for 36 cancers in 185 countries.* CA Cancer J Clin, 2018. **68**(6): p. 394-424.
2. El-Serag, H.B., *Hepatocellular carcinoma.* N Engl J Med, 2011. **365**(12): p. 1118-27.
3. Farazi, P.A. and R.A. DePinho, *Hepatocellular carcinoma pathogenesis: from genes to environment.* Nat Rev Cancer, 2006. **6**(9): p. 674-87.
4. Njei, B., et al., *Emerging trends in hepatocellular carcinoma incidence and mortality.* Hepatology, 2015. **61**(1): p. 191-9.
5. Jemal, A., et al., *Global cancer statistics.* CA Cancer J Clin, 2011. **61**(2): p. 69-90.
6. Sanyal, A.J., S.K. Yoon, and R. Lencioni, *The etiology of hepatocellular carcinoma and consequences for treatment.* Oncologist, 2010. **15 Suppl 4**: p. 14-22.
7. Zoller, H. and H. Tilg, *Nonalcoholic fatty liver disease and hepatocellular carcinoma.* Metabolism, 2016. **65**(8): p. 1151-60.
8. Marengo, A., C. Rosso, and E. Bugianesi, *Liver Cancer: Connections with Obesity, Fatty Liver, and Cirrhosis.* Annu Rev Med, 2016. **67**: p. 103-17.
9. Balogh, J., et al., *Hepatocellular carcinoma: a review.* J Hepatocell Carcinoma, 2016. **3**: p. 41-53.
10. Dhanasekaran, R., S. Bandoh, and L.R. Roberts, *Molecular pathogenesis of hepatocellular carcinoma and impact of therapeutic advances.* F1000Res, 2016. **5**.
11. Adachi, Y., et al., *AFP-producing gastric carcinoma: multivariate analysis of prognostic factors in 270 patients.* Oncology, 2003. **65**(2): p. 95-101.
12. Sato, Y., T. Sekine, and S. Ohwada, *Alpha-fetoprotein-producing rectal cancer: calculated tumor marker doubling time.* J Surg Oncol, 1994. **55**(4): p. 265-8.
13. Forner, A., J.M. Llovet, and J. Bruix, *Hepatocellular carcinoma.* Lancet, 2012. **379**(9822): p. 1245-55.
14. Bruix, J., M. Sherman, and D. American Association for the Study of Liver, *Management of hepatocellular carcinoma: an update.* Hepatology, 2011. **53**(3): p. 1020-2.
15. European Association For The Study Of The, L., R. European Organisation For, and C. Treatment Of, *EASL-EORTC clinical practice guidelines: management of hepatocellular carcinoma.* J Hepatol, 2012. **56**(4): p. 908-43.
16. Spangenberg, H.C., R. Thimme, and H.E. Blum, *Targeted therapy for hepatocellular carcinoma.* Nat Rev Gastroenterol Hepatol, 2009. **6**(7): p. 423-32.
17. Bruix, J., et al., *Regorafenib for patients with hepatocellular carcinoma who progressed on sorafenib treatment (RESORCE): a randomised, double-blind, placebo-controlled, phase 3 trial.* Lancet, 2017. **389**(10064): p. 56-66.
18. Pestana, R.C., et al., *Clinical and prognostic significance of circulating levels of angiopoietin-1 and angiopoietin-2 in hepatocellular carcinoma.* Oncotarget, 2018. **9**(102): p. 37721-37732.
19. Crick, F.H., *On protein synthesis.* Symp Soc Exp Biol, 1958. **12**: p. 138-63.
20. RajBhandary, U.L. and C. Kohrer, *Early days of tRNA research: discovery, function, purification and sequence analysis.* J Biosci, 2006. **31**(4): p. 439-51.

21. Palade, G.E., *A small particulate component of the cytoplasm.* J Biophys Biochem Cytol, 1955. **1**(1): p. 59-68.
22. Dreyfuss, G., L. Philipson, and I.W. Mattaj, *Ribonucleoprotein particles in cellular processes.* J Cell Biol, 1988. **106**(5): p. 1419-25.
23. Weinberg, R.A. and S. Penman, *Small molecular weight monodisperse nuclear RNA.* J Mol Biol, 1968. **38**(3): p. 289-304.
24. Maxwell, E.S. and M.J. Fournier, *The small nucleolar RNAs.* Annu Rev Biochem, 1995. **64**: p. 897-934.
25. Guerrier-Takada, C., et al., *The RNA moiety of ribonuclease P is the catalytic subunit of the enzyme.* Cell, 1983. **35**(3 Pt 2): p. 849-57.
26. Kruger, K., et al., *Self-splicing RNA: autoexcision and autocyclization of the ribosomal RNA intervening sequence of Tetrahymena.* Cell, 1982. **31**(1): p. 147-57.
27. Djebali, S., et al., *Landscape of transcription in human cells.* Nature, 2012. **489**(7414): p. 101-8.
28. Jonas, S. and E. Izaurralde, *Towards a molecular understanding of microRNA-mediated gene silencing.* Nat Rev Genet, 2015. **16**(7): p. 421-33.
29. Winter, J., et al., *Many roads to maturity: microRNA biogenesis pathways and their regulation.* Nat Cell Biol, 2009. **11**(3): p. 228-34.
30. Mercer, T.R., M.E. Dinger, and J.S. Mattick, *Long non-coding RNAs: insights into functions.* Nat Rev Genet, 2009. **10**(3): p. 155-9.
31. Ponting, C.P., P.L. Oliver, and W. Reik, *Evolution and functions of long noncoding RNAs.* Cell, 2009. **136**(4): p. 629-41.
32. Zhang, K., et al., *The ways of action of long non-coding RNAs in cytoplasm and nucleus.* Gene, 2014. **547**(1): p. 1-9.
33. Ulitsky, I. and D.P. Bartel, *lincRNAs: genomics, evolution, and mechanisms.* Cell, 2013. **154**(1): p. 26-46.
34. Derrien, T., et al., *The GENCODE v7 catalog of human long noncoding RNAs: analysis of their gene structure, evolution, and expression.* Genome Res, 2012. **22**(9): p. 1775-89.
35. Chen, Z.Z., et al., *LncSox4 promotes the self-renewal of liver tumour-initiating cells through Stat3-mediated Sox4 expression.* Nat Commun, 2016. **7**: p. 12598.
36. Wang, Y., et al., *The long noncoding RNA lncTCF7 promotes self-renewal of human liver cancer stem cells through activation of Wnt signaling.* Cell Stem Cell, 2015. **16**(4): p. 413-25.
37. Yang, F., et al., *Repression of the long noncoding RNA-LET by histone deacetylase 3 contributes to hypoxia-mediated metastasis.* Mol Cell, 2013. **49**(6): p. 1083-96.
38. Wang, X., et al., *Long non-coding RNA DILC regulates liver cancer stem cells via IL-6/STAT3 axis.* J Hepatol, 2016. **64**(6): p. 1283-94.
39. Mikkelsen, T.S., et al., *Genome-wide maps of chromatin state in pluripotent and lineage-committed cells.* Nature, 2007. **448**(7153): p. 553-60.
40. Guttman, M., et al., *Chromatin signature reveals over a thousand highly conserved large non-coding RNAs in mammals.* Nature, 2009. **458**(7235): p. 223-7.
41. Khalil, A.M., et al., *Many human large intergenic noncoding RNAs associate with chromatin-modifying complexes and affect gene expression.* Proc Natl Acad Sci U S A, 2009. **106**(28): p. 11667-72.

42. Sati, S., et al., *Genome-wide analysis reveals distinct patterns of epigenetic features in long non-coding RNA loci.* Nucleic Acids Res, 2012. **40**(20): p. 10018-31.
43. Consortium, E.P., *An integrated encyclopedia of DNA elements in the human genome.* Nature, 2012. **489**(7414): p. 57-74.
44. Mercer, T.R., et al., *Specific expression of long noncoding RNAs in the mouse brain.* Proc Natl Acad Sci U S A, 2008. **105**(2): p. 716-21.
45. Cabili, M.N., et al., *Integrative annotation of human large intergenic noncoding RNAs reveals global properties and specific subclasses.* Genes Dev, 2011. **25**(18): p. 1915-27.
46. Geisler, S. and J. Coller, *RNA in unexpected places: long non-coding RNA functions in diverse cellular contexts.* Nat Rev Mol Cell Biol, 2013. **14**(11): p. 699-712.
47. Batista, P.J. and H.Y. Chang, *Long noncoding RNAs: cellular address codes in development and disease.* Cell, 2013. **152**(6): p. 1298-307.
48. Gupta, R.A., et al., *Long non-coding RNA HOTAIR reprograms chromatin state to promote cancer metastasis.* Nature, 2010. **464**(7291): p. 1071-6.
49. Wang, J., et al., *CREB up-regulates long non-coding RNA, HULC expression through interaction with microRNA-372 in liver cancer.* Nucleic Acids Res, 2010. **38**(16): p. 5366-83.
50. Yuan, J.H., et al., *A long noncoding RNA activated by TGF-beta promotes the invasion-metastasis cascade in hepatocellular carcinoma.* Cancer Cell, 2014. **25**(5): p. 666-81.
51. Taft, R.J., M. Pheasant, and J.S. Mattick, *The relationship between non-protein-coding DNA and eukaryotic complexity.* Bioessays, 2007. **29**(3): p. 288-99.
52. Pang, K.C., M.C. Frith, and J.S. Mattick, *Rapid evolution of noncoding RNAs: lack of conservation does not mean lack of function.* Trends Genet, 2006. **22**(1): p. 1-5.
53. Lee, J.T. and M.S. Bartolomei, *X-inactivation, imprinting, and long noncoding RNAs in health and disease.* Cell, 2013. **152**(6): p. 1308-23.
54. Wang, K.C. and H.Y. Chang, *Molecular mechanisms of long noncoding RNAs.* Mol Cell, 2011. **43**(6): p. 904-14.
55. Klingenberg, M., et al., *Non-coding RNA in hepatocellular carcinoma: Mechanisms, biomarkers and therapeutic targets.* J Hepatol, 2017. **67**(3): p. 603-618.
56. Hanahan, D. and R.A. Weinberg, *The hallmarks of cancer.* Cell, 2000. **100**(1): p. 57-70.
57. Hanahan, D. and R.A. Weinberg, *Hallmarks of cancer: the next generation.* Cell, 2011. **144**(5): p. 646-74.
58. Gutschner, T. and S. Diederichs, *The hallmarks of cancer: a long non-coding RNA point of view.* RNA Biol, 2012. **9**(6): p. 703-19.
59. Li, M., et al., *An Apela RNA-Containing Negative Feedback Loop Regulates p53-Mediated Apoptosis in Embryonic Stem Cells.* Cell Stem Cell, 2015. **16**(6): p. 669-83.
60. Mourtada-Maarabouni, M., et al., *GAS5, a non-protein-coding RNA, controls apoptosis and is downregulated in breast cancer.* Oncogene, 2009. **28**(2): p. 195-208.
61. Puvvula, P.K., et al., *Long noncoding RNA PANDA and scaffold-attachment-factor SAFA control senescence entry and exit.* Nat Commun, 2014. **5**: p. 5323.
62. Takayama, K., et al., *Androgen-responsive long noncoding RNA CTBP1-AS promotes prostate cancer.* EMBO J, 2013. **32**(12): p. 1665-80.
63. Tseng, Y.Y., et al., *PVT1 dependence in cancer with MYC copy-number increase.* Nature, 2014. **512**(7512): p. 82-6.

64. Rinn, J.L., et al., *Functional demarcation of active and silent chromatin domains in human HOX loci by noncoding RNAs.* Cell, 2007. **129**(7): p. 1311-23.
65. Montes, M., et al., *The lncRNA MIR31HG regulates p16(INK4A) expression to modulate senescence.* Nat Commun, 2015. **6**: p. 6967.
66. Yoon, J.H., et al., *LincRNA-p21 suppresses target mRNA translation.* Mol Cell, 2012. **47**(4): p. 648-55.
67. Liu, B., et al., *A cytoplasmic NF-kappaB interacting long noncoding RNA blocks IkappaB phosphorylation and suppresses breast cancer metastasis.* Cancer Cell, 2015. **27**(3): p. 370-81.
68. Flockhart, R.J., et al., *BRAFV600E remodels the melanocyte transcriptome and induces BANCR to regulate melanoma cell migration.* Genome Res, 2012. **22**(6): p. 1006-14.
69. Gutschner, T., et al., *The noncoding RNA MALAT1 is a critical regulator of the metastasis phenotype of lung cancer cells.* Cancer Res, 2013. **73**(3): p. 1180-9.
70. Lu, Z., et al., *Long non-coding RNA HULC promotes tumor angiogenesis in liver cancer by up-regulating sphingosine kinase 1 (SPHK1).* Oncotarget, 2016. **7**(1): p. 241-54.
71. Ji, P., et al., *MALAT-1, a novel noncoding RNA, and thymosin beta4 predict metastasis and survival in early-stage non-small cell lung cancer.* Oncogene, 2003. **22**(39): p. 8031-41.
72. Pandey, G.K., et al., *The risk-associated long noncoding RNA NBAT-1 controls neuroblastoma progression by regulating cell proliferation and neuronal differentiation.* Cancer Cell, 2014. **26**(5): p. 722-37.
73. Flynn, R.L., et al., *TERRA and hnRNPA1 orchestrate an RPA-to-POT1 switch on telomeric single-stranded DNA.* Nature, 2011. **471**(7339): p. 532-6.
74. Kretz, M., et al., *Control of somatic tissue differentiation by the long non-coding RNA TINCR.* Nature, 2013. **493**(7431): p. 231-5.
75. Su, D.N., et al., *HOTAIR, a long non-coding RNA driver of malignancy whose expression is activated by FOXC1, negatively regulates miRNA-1 in hepatocellular carcinoma.* Oncol Lett, 2016. **12**(5): p. 4061-4067.
76. Yang, L., et al., *The long noncoding RNA HOTAIR activates autophagy by upregulating ATG3 and ATG7 in hepatocellular carcinoma.* Mol Biosyst, 2016. **12**(8): p. 2605-12.
77. Gao, J.Z., et al., *Long non-coding RNA HOTAIR is a marker for hepatocellular carcinoma progression and tumor recurrence.* Oncol Lett, 2016. **11**(3): p. 1791-1798.
78. Xiong, D., et al., *LINC00052 regulates the expression of NTRK3 by miR-128 and miR-485-3p to strengthen HCC cells invasion and migration.* Oncotarget, 2016. **7**(30): p. 47593-47608.
79. Wang, X., et al., *LINC01225 promotes occurrence and metastasis of hepatocellular carcinoma in an epidermal growth factor receptor-dependent pathway.* Cell Death Dis, 2016. **7**: p. e2130.
80. Li, T., et al., *Upregulation of long noncoding RNA ZEB1-AS1 promotes tumor metastasis and predicts poor prognosis in hepatocellular carcinoma.* Oncogene, 2016. **35**(12): p. 1575-84.
81. Jin, W., et al., *Long non-coding RNA TUC338 is functionally involved in sorafenib-sensitized hepatocarcinoma cells by targeting RASAL1.* Oncol Rep, 2017. **37**(1): p. 273-280.

82. Yuan, P., et al., *The HIF-2alpha-MALAT1-miR-216b axis regulates multi-drug resistance of hepatocellular carcinoma cells via modulating autophagy.* Biochem Biophys Res Commun, 2016. **478**(3): p. 1067-73.
83. Yu, J., et al., *The long noncoding RNAs PVT1 and uc002mbe.2 in sera provide a new supplementary method for hepatocellular carcinoma diagnosis.* Medicine (Baltimore), 2016. **95**(31): p. e4436.
84. Peng, W. and H. Fan, *Long noncoding RNA CCHE1 indicates a poor prognosis of hepatocellular carcinoma and promotes carcinogenesis via activation of the ERK/MAPK pathway.* Biomed Pharmacother, 2016. **83**: p. 450-455.
85. Ma, X., et al., *DANCR Acts as a Diagnostic Biomarker and Promotes Tumor Growth and Metastasis in Hepatocellular Carcinoma.* Anticancer Res, 2016. **36**(12): p. 6389-6398.
86. Chen, Z., et al., *LncRNA CRNDE promotes hepatic carcinoma cell proliferation, migration and invasion by suppressing miR-384.* Am J Cancer Res, 2016. **6**(10): p. 2299-2309.
87. Zhang, T., et al., *SNHG3 correlates with malignant status and poor prognosis in hepatocellular carcinoma.* Tumour Biol, 2016. **37**(2): p. 2379-85.
88. Zhang, J.H., H.W. Wei, and H.G. Yang, *Long noncoding RNA SNHG15, a potential prognostic biomarker for hepatocellular carcinoma.* Eur Rev Med Pharmacol Sci, 2016. **20**(9): p. 1720-4.
89. Zhang, D., et al., *Up-regulation of LncRNA SNHG20 Predicts Poor Prognosis in Hepatocellular Carcinoma.* J Cancer, 2016. **7**(5): p. 608-17.
90. Wang, F., et al., *Long non-coding RNA CARLo-5 expression is associated with disease progression and predicts outcome in hepatocellular carcinoma patients.* Clin Exp Med, 2017. **17**(1): p. 33-43.
91. Ma, W., et al., *Downregulation of long non-coding RNAs JPX and XIST is associated with the prognosis of hepatocellular carcinoma.* Clin Res Hepatol Gastroenterol, 2017. **41**(2): p. 163-170.
92. Chang, L., et al., *Decreased expression of long non-coding RNA GAS5 indicates a poor prognosis and promotes cell proliferation and invasion in hepatocellular carcinoma by regulating vimentin.* Mol Med Rep, 2016. **13**(2): p. 1541-50.
93. Sui, C.J., et al., *Long noncoding RNA GIHCG promotes hepatocellular carcinoma progression through epigenetically regulating miR-200b/a/429.* J Mol Med (Berl), 2016. **94**(11): p. 1281-1296.
94. Wang, T., et al., *Long noncoding RNA ZNFX1-AS1 suppresses growth of hepatocellular carcinoma cells by regulating the methylation of miR-9.* Onco Targets Ther, 2016. **9**: p. 5005-14.
95. Tang, J., et al., *Bidirectional transcription of Linc00441 and RB1 via H3K27 modification-dependent way promotes hepatocellular carcinoma.* Cell Death Dis, 2017. **8**(3): p. e2675.
96. Xu, Y., et al., *Long non-coding RNA CCAT2 is associated with poor prognosis in hepatocellular carcinoma and promotes tumor metastasis by regulating Snail2-mediated epithelial-mesenchymal transition.* Onco Targets Ther, 2017. **10**: p. 1191-1198.
97. Battistelli, C., et al., *The Snail repressor recruits EZH2 to specific genomic sites through the enrollment of the lncRNA HOTAIR in epithelial-to-mesenchymal transition.* Oncogene, 2017. **36**(7): p. 942-955.

98. Bo, C., et al., *Long noncoding RNA uc.338 promotes cell proliferation through association with BMI1 in hepatocellular carcinoma.* Hum Cell, 2016. **29**(4): p. 141-7.
99. Lan, T., et al., *Long non-coding RNA small nucleolar RNA host gene 12 (SNHG12) promotes tumorigenesis and metastasis by targeting miR-199a/b-5p in hepatocellular carcinoma.* J Exp Clin Cancer Res, 2017. **36**(1): p. 11.
100. Wu, M., et al., *HULC cooperates with MALAT1 to aggravate liver cancer stem cells growth through telomere repeat-binding factor 2.* Sci Rep, 2016. **6**: p. 36045.
101. Ortega, S., M. Malumbres, and M. Barbacid, *Cyclin D-dependent kinases, INK4 inhibitors and cancer.* Biochim Biophys Acta, 2002. **1602**(1): p. 73-87.
102. Pujol, M.J., et al., *Differential association of p21Cip1 and p27Kip1 with cyclin E-CDK2 during rat liver regeneration.* J Hepatol, 2000. **33**(2): p. 266-74.
103. Ilyin, G.P., et al., *Regulation and role of p21 and p27 cyclin-dependent kinase inhibitors during hepatocyte differentiation and growth.* Am J Physiol Gastrointest Liver Physiol, 2003. **285**(1): p. G115-27.
104. Albrecht, J.H., et al., *Involvement of p21 and p27 in the regulation of CDK activity and cell cycle progression in the regenerating liver.* Oncogene, 1998. **16**(16): p. 2141-50.
105. Uehara, T., et al., *Molecular mechanisms of fibrosis-associated promotion of liver carcinogenesis.* Toxicol Sci, 2013. **132**(1): p. 53-63.
106. Zucman-Rossi, J., et al., *Differential effects of inactivated Axin1 and activated beta-catenin mutations in human hepatocellular carcinomas.* Oncogene, 2007. **26**(5): p. 774-80.
107. van Malenstein, H., J. van Pelt, and C. Verslype, *Molecular classification of hepatocellular carcinoma anno 2011.* Eur J Cancer, 2011. **47**(12): p. 1789-97.
108. El-Serag, H.B. and K.L. Rudolph, *Hepatocellular carcinoma: epidemiology and molecular carcinogenesis.* Gastroenterology, 2007. **132**(7): p. 2557-76.
109. Hayflick, L., *The Limited in Vitro Lifetime of Human Diploid Cell Strains.* Exp Cell Res, 1965. **37**: p. 614-36.
110. Kuilman, T., et al., *The essence of senescence.* Genes Dev, 2010. **24**(22): p. 2463-79.
111. Coppe, J.P., et al., *The senescence-associated secretory phenotype: the dark side of tumor suppression.* Annu Rev Pathol, 2010. **5**: p. 99-118.
112. Kuilman, T. and D.S. Peeper, *Senescence-messaging secretome: SMS-ing cellular stress.* Nat Rev Cancer, 2009. **9**(2): p. 81-94.
113. Acosta, J.C., et al., *A complex secretory program orchestrated by the inflammasome controls paracrine senescence.* Nat Cell Biol, 2013. **15**(8): p. 978-90.
114. Acosta, J.C., et al., *Chemokine signaling via the CXCR2 receptor reinforces senescence.* Cell, 2008. **133**(6): p. 1006-18.
115. Lee, M. and J.S. Lee, *Exploiting tumor cell senescence in anticancer therapy.* BMB Rep, 2014. **47**(2): p. 51-9.
116. Zhang, Y. and J.M. Yang, *The impact of cellular senescence in cancer therapy: is it true or not?* Acta Pharmacol Sin, 2011. **32**(10): p. 1199-207.
117. Ewald, J.A., et al., *Therapy-induced senescence in cancer.* J Natl Cancer Inst, 2010. **102**(20): p. 1536-46.
118. Lleonart, M.E., A. Artero-Castro, and H. Kondoh, *Senescence induction; a possible cancer therapy.* Mol Cancer, 2009. **8**: p. 3.

119. Pang, J.H. and K.Y. Chen, *A specific CCAAT-binding protein, CBP/tk, may be involved in the regulation of thymidine kinase gene expression in human IMR-90 diploid fibroblasts during senescence.* J Biol Chem, 1993. **268**(4): p. 2909-16.
120. Noda, A., et al., *Cloning of senescent cell-derived inhibitors of DNA synthesis using an expression screen.* Exp Cell Res, 1994. **211**(1): p. 90-8.
121. Hara, E., et al., *Regulation of p16CDKN2 expression and its implications for cell immortalization and senescence.* Mol Cell Biol, 1996. **16**(3): p. 859-67.
122. Weingartner, M., et al., *Expression of a nondegradable cyclin B1 affects plant development and leads to endomitosis by inhibiting the formation of a phragmoplast.* Plant Cell, 2004. **16**(3): p. 643-57.
123. Alcorta, D.A., et al., *Involvement of the cyclin-dependent kinase inhibitor p16 (INK4a) in replicative senescence of normal human fibroblasts.* Proc Natl Acad Sci U S A, 1996. **93**(24): p. 13742-7.
124. Salama, R., et al., *Cellular senescence and its effector programs.* Genes Dev, 2014. **28**(2): p. 99-114.
125. Reichard, P., *Interactions between deoxyribonucleotide and DNA synthesis.* Annu Rev Biochem, 1988. **57**: p. 349-74.
126. Zeman, M.K. and K.A. Cimprich, *Causes and consequences of replication stress.* Nat Cell Biol, 2014. **16**(1): p. 2-9.
127. Mathews, C.K., *DNA precursor metabolism and genomic stability.* FASEB J, 2006. **20**(9): p. 1300-14.
128. Gilkerson, R., *Commentary: Mitochondrial DNA damage and loss in diabetes.* Diabetes Metab Res Rev, 2016. **32**(7): p. 672-674.
129. Kunz, B.A., et al., *International Commission for Protection Against Environmental Mutagens and Carcinogens. Deoxyribonucleoside triphosphate levels: a critical factor in the maintenance of genetic stability.* Mutat Res, 1994. **318**(1): p. 1-64.
130. Aird, K.M. and R. Zhang, *Nucleotide metabolism, oncogene-induced senescence and cancer.* Cancer Lett, 2015. **356**(2 Pt A): p. 204-10.
131. Pai, C.C. and S.E. Kearsey, *A Critical Balance: dNTPs and the Maintenance of Genome Stability.* Genes (Basel), 2017. **8**(2).
132. Sigoillot, F.D., et al., *Cell cycle-dependent regulation of pyrimidine biosynthesis.* J Biol Chem, 2003. **278**(5): p. 3403-9.
133. Quemeneur, L., et al., *Differential control of cell cycle, proliferation, and survival of primary T lymphocytes by purine and pyrimidine nucleotides.* J Immunol, 2003. **170**(10): p. 4986-95.
134. Liu, Y.C., et al., *Global regulation of nucleotide biosynthetic genes by c-Myc.* PLoS One, 2008. **3**(7): p. e2722.
135. Wang, Y., et al., *Cross Talk between Nucleotide Synthesis Pathways with Cellular Immunity in Constraining Hepatitis E Virus Replication.* Antimicrob Agents Chemother, 2016. **60**(5): p. 2834-48.
136. Lane, A.N. and T.W. Fan, *Regulation of mammalian nucleotide metabolism and biosynthesis.* Nucleic Acids Res, 2015. **43**(4): p. 2466-85.
137. Moffatt, B.A. and H. Ashihara, *Purine and pyrimidine nucleotide synthesis and metabolism.* Arabidopsis Book, 2002. **1**: p. e0018.

138. Fairman, J.W., et al., *Structural basis for allosteric regulation of human ribonucleotide reductase by nucleotide-induced oligomerization.* Nat Struct Mol Biol, 2011. **18**(3): p. 316-22.
139. Nordlund, P. and P. Reichard, *Ribonucleotide reductases.* Annu Rev Biochem, 2006. **75**: p. 681-706.
140. Hakansson, P., A. Hofer, and L. Thelander, *Regulation of mammalian ribonucleotide reduction and dNTP pools after DNA damage and in resting cells.* J Biol Chem, 2006. **281**(12): p. 7834-41.
141. Pang, J.H. and K.Y. Chen, *Global change of gene expression at late G1/S boundary may occur in human IMR-90 diploid fibroblasts during senescence.* J Cell Physiol, 1994. **160**(3): p. 531-8.
142. Arner, E.S. and S. Eriksson, *Mammalian deoxyribonucleoside kinases.* Pharmacol Ther, 1995. **67**(2): p. 155-86.
143. Zhou, X., et al., *Progressive loss of mitochondrial DNA in thymidine kinase 2-deficient mice.* Hum Mol Genet, 2008. **17**(15): p. 2329-35.
144. Fox, J.T. and P.J. Stover, *Folate-mediated one-carbon metabolism.* Vitam Horm, 2008. **79**: p. 1-44.
145. Blount, B.C., et al., *Folate deficiency causes uracil misincorporation into human DNA and chromosome breakage: implications for cancer and neuronal damage.* Proc Natl Acad Sci U S A, 1997. **94**(7): p. 3290-5.
146. Yap, K.L., et al., *Molecular interplay of the noncoding RNA ANRIL and methylated histone H3 lysine 27 by polycomb CBX7 in transcriptional silencing of INK4a.* Mol Cell, 2010. **38**(5): p. 662-74.
147. Kotake, Y., et al., *Long non-coding RNA ANRIL is required for the PRC2 recruitment to and silencing of p15(INK4B) tumor suppressor gene.* Oncogene, 2011. **30**(16): p. 1956-62.
148. Kotake, Y., et al., *Oncogenic Ras influences the expression of multiple lncRNAs.* Cytotechnology, 2016. **68**(4): p. 1591-6.
149. Montes, M., et al., *The lncRNA MIR31HG regulates p16(INK4A) expression to modulate senescence.* Nat Commun, 2015. **6**: p. 6967.
150. Hu, X., et al., *A functional genomic approach identifies FAL1 as an oncogenic long noncoding RNA that associates with BMI1 and represses p21 expression in cancer.* Cancer Cell, 2014. **26**(3): p. 344-357.
151. Lazorthes, S., et al., *A vlincRNA participates in senescence maintenance by relieving H2AZ-mediated repression at the INK4 locus.* Nat Commun, 2015. **6**: p. 5971.
152. Wu, C.L., et al., *Senescence-associated Long Non-coding RNA (SALNR) Delays Oncogene-induced Senescence through NF90 Regulation.* J Biol Chem, 2015. **290**(50): p. 30175-92.
153. Tominaga-Yamanaka, K., et al., *NF90 coordinately represses the senescence-associated secretory phenotype.* Aging (Albany NY), 2012. **4**(10): p. 695-708.
154. Abdelmohsen, K., et al., *Regulation of senescence by microRNA biogenesis factors.* Ageing Res Rev, 2012. **11**(4): p. 491-500.
155. Kumar, P.P., et al., *Coordinated control of senescence by lncRNA and a novel T-box3 co-repressor complex.* Elife, 2014. **3**.
156. Yoon, J.H., et al., *Scaffold function of long non-coding RNA HOTAIR in protein ubiquitination.* Nat Commun, 2013. **4**: p. 2939.

157. Mazan-Mamczarz, K., et al., *RNA-binding protein HuR enhances p53 translation in response to ultraviolet light irradiation.* Proc Natl Acad Sci U S A, 2003. **100**(14): p. 8354-9.
158. Abdelmohsen, K., et al., *7SL RNA represses p53 translation by competing with HuR.* Nucleic Acids Res, 2014. **42**(15): p. 10099-111.
159. Castro, F., et al., *High-throughput SNP-based authentication of human cell lines.* Int J Cancer, 2013. **132**(2): p. 308-14.
160. Hannus, M., et al., *siPools: highly complex but accurately defined siRNA pools eliminate off-target effects.* Nucleic Acids Res, 2014. **42**(12): p. 8049-61.
161. Gagnon, K.T., et al., *Analysis of nuclear RNA interference in human cells by subcellular fractionation and Argonaute loading.* Nat Protoc, 2014. **9**(9): p. 2045-60.
162. Munschauer, M., et al., *The NORAD lncRNA assembles a topoisomerase complex critical for genome stability.* Nature, 2018. **561**(7721): p. 132-136.
163. Diamond, T.L., et al., *Macrophage tropism of HIV-1 depends on efficient cellular dNTP utilization by reverse transcriptase.* J Biol Chem, 2004. **279**(49): p. 51545-53.
164. Li, J., et al., *TANRIC: An Interactive Open Platform to Explore the Function of lncRNAs in Cancer.* Cancer Res, 2015. **75**(18): p. 3728-37.
165. Valianou, M., et al., *Pharmacological inhibition of Polo-like kinase 1 (PLK1) by BI-2536 decreases the viability and survival of hamartin and tuberin deficient cells via induction of apoptosis and attenuation of autophagy.* Cell Cycle, 2015. **14**(3): p. 399-407.
166. Yin, D., et al., *Pro-Angiogenic Role of LncRNA HULC in Microvascular Endothelial Cells via Sequestrating miR-124.* Cell Physiol Biochem, 2018. **50**(6): p. 2188-2202.
167. Parkhomchuk, D., et al., *Transcriptome analysis by strand-specific sequencing of complementary DNA.* Nucleic Acids Res, 2009. **37**(18): p. e123.
168. Lin, M.F., I. Jungreis, and M. Kellis, *PhyloCSF: a comparative genomics method to distinguish protein coding and non-coding regions.* Bioinformatics, 2011. **27**(13): p. i275-82.
169. Kong, L., et al., *CPC: assess the protein-coding potential of transcripts using sequence features and support vector machine.* Nucleic Acids Res, 2007. **35**(Web Server issue): p. W345-9.
170. Gandhi, M., M. Caudron-Herger, and S. Diederichs, *RNA motifs and combinatorial prediction of interactions, stability and localization of noncoding RNAs.* Nat Struct Mol Biol, 2018. **25**(12): p. 1070-1076.
171. Roth, A. and S. Diederichs, *Molecular biology: Rap and chirp about X inactivation.* Nature, 2015. **521**(7551): p. 170-1.
172. Paz, I., et al., *RBPmap: a web server for mapping binding sites of RNA-binding proteins.* Nucleic Acids Res, 2014. **42**(Web Server issue): p. W361-7.
173. Hon, C.C., et al., *An atlas of human long non-coding RNAs with accurate 5' ends.* Nature, 2017. **543**(7644): p. 199-204.
174. Andrews, S.J. and J.A. Rothnagel, *Emerging evidence for functional peptides encoded by short open reading frames.* Nat Rev Genet, 2014. **15**(3): p. 193-204.
175. Anderson, D.M., et al., *A micropeptide encoded by a putative long noncoding RNA regulates muscle performance.* Cell, 2015. **160**(4): p. 595-606.
176. Rui, L., *Energy metabolism in the liver.* Compr Physiol, 2014. **4**(1): p. 177-97.

177. Zhao, X., Y. Liu, and S. Yu, *Long noncoding RNA AWPPH promotes hepatocellular carcinoma progression through YBX1 and serves as a prognostic biomarker.* Biochim Biophys Acta Mol Basis Dis, 2017. **1863**(7): p. 1805-1816.
178. Liu, Y., et al., *lncRNA GAS5 enhances G1 cell cycle arrest via binding to YBX1 to regulate p21 expression in stomach cancer.* Sci Rep, 2015. **5**: p. 10159.
179. Peng, Z., et al., *The long noncoding RNA LINC00312 induces lung adenocarcinoma migration and vasculogenic mimicry through directly binding YBX1.* Mol Cancer, 2018. **17**(1): p. 167.
180. Zhang, E., et al., *A novel long noncoding RNA HOXC-AS3 mediates tumorigenesis of gastric cancer by binding to YBX1.* Genome Biol, 2018. **19**(1): p. 154.
181. Kosnopfel, C., et al., *YB-1 Expression and Phosphorylation Regulate Tumorigenicity and Invasiveness in Melanoma by Influencing EMT.* Mol Cancer Res, 2018. **16**(7): p. 1149-1160.
182. Shibata, T., et al., *Y-box binding protein YBX1 and its correlated genes as biomarkers for poor outcomes in patients with breast cancer.* Oncotarget, 2018. **9**(98): p. 37216-37228.
183. Engstrom, Y., et al., *Cell cycle-dependent expression of mammalian ribonucleotide reductase. Differential regulation of the two subunits.* J Biol Chem, 1985. **260**(16): p. 9114-6.
184. Bester, A.C., et al., *Nucleotide deficiency promotes genomic instability in early stages of cancer development.* Cell, 2011. **145**(3): p. 435-46.
185. Boss, G.R. and J.E. Seegmiller, *Genetic defects in human purine and pyrimidine metabolism.* Annu Rev Genet, 1982. **16**: p. 297-328.
186. Ammann, A.J., *Purine nucleotide imbalance in immunodeficiency disorders.* Basic Life Sci, 1985. **31**: p. 487-502.
187. Burhans, W.C. and M. Weinberger, *DNA replication stress, genome instability and aging.* Nucleic Acids Res, 2007. **35**(22): p. 7545-56.
188. Kimura, T., et al., *Impaired function of p53R2 in Rrm2b-null mice causes severe renal failure through attenuation of dNTP pools.* Nat Genet, 2003. **34**(4): p. 440-5.
189. Dobrovolsky, V.N., et al., *Mice deficient for cytosolic thymidine kinase gene develop fatal kidney disease.* Mol Genet Metab, 2003. **78**(1): p. 1-10.
190. Pitceathly, R.D., et al., *Adults with RRM2B-related mitochondrial disease have distinct clinical and molecular characteristics.* Brain, 2012. **135**(Pt 11): p. 3392-403.
191. El-Hattab, A.W. and F. Scaglia, *Mitochondrial DNA depletion syndromes: review and updates of genetic basis, manifestations, and therapeutic options.* Neurotherapeutics, 2013. **10**(2): p. 186-98.
192. Weinberg, G., B. Ullman, and D.W. Martin, Jr., *Mutator phenotypes in mammalian cell mutants with distinct biochemical defects and abnormal deoxyribonucleoside triphosphate pools.* Proc Natl Acad Sci U S A, 1981. **78**(4): p. 2447-51.
193. Meuth, M., *The molecular basis of mutations induced by deoxyribonucleoside triphosphate pool imbalances in mammalian cells.* Exp Cell Res, 1989. **181**(2): p. 305-16.
194. Chang, L., et al., *Chromosomal instability triggered by Rrm2b loss leads to IL-6 secretion and plasmacytic neoplasms.* Cell Rep, 2013. **3**(5): p. 1389-97.
195. Chabosseau, P., et al., *Pyrimidine pool imbalance induced by BLM helicase deficiency contributes to genetic instability in Bloom syndrome.* Nat Commun, 2011. **2**: p. 368.

196. Mannava, S., et al., *Ribonucleotide reductase and thymidylate synthase or exogenous deoxyribonucleosides reduce DNA damage and senescence caused by C-MYC depletion.* Aging (Albany NY), 2012. **4**(12): p. 917-22.
197. Chang, Z.F. and D.Y. Huang, *Regulation of thymidine kinase expression during cellular senescence.* J Biomed Sci, 2001. **8**(2): p. 176-83.
198. Mannava, S., et al., *Depletion of deoxyribonucleotide pools is an endogenous source of DNA damage in cells undergoing oncogene-induced senescence.* Am J Pathol, 2013. **182**(1): p. 142-51.
199. Aird, K.M., et al., *Suppression of nucleotide metabolism underlies the establishment and maintenance of oncogene-induced senescence.* Cell Rep, 2013. **3**(4): p. 1252-65.
200. Eriksson, S. and L. Thelander, *Allosteric regulation of calf thymus ribonucleotide reductase.* Ciba Found Symp, 1978(68): p. 165-75.
201. Endo, H., et al., *Enhanced expression of long non-coding RNA HOTAIR is associated with the development of gastric cancer.* PLoS One, 2013. **8**(10): p. e77070.
202. Leucci, E., et al., *Melanoma addiction to the long non-coding RNA SAMMSON.* Nature, 2016. **531**(7595): p. 518-22.
203. Diermeier, S.D. and D.L. Spector, *Antisense Oligonucleotide-mediated Knockdown in Mammary Tumor Organoids.* Bio Protoc, 2017. **7**(16).
204. Arun, G., et al., *Differentiation of mammary tumors and reduction in metastasis upon Malat1 lncRNA loss.* Genes Dev, 2016. **30**(1): p. 34-51.
205. Galmarini, C.M., J.R. Mackey, and C. Dumontet, *Nucleoside analogues and nucleobases in cancer treatment.* Lancet Oncol, 2002. **3**(7): p. 415-24.
206. Munoz-Pinedo, C., N. El Mjiyad, and J.E. Ricci, *Cancer metabolism: current perspectives and future directions.* Cell Death Dis, 2012. **3**: p. e248.
207. Manegold, C., et al., *Gemcitabine in non-small cell lung cancer (NSCLC).* Invest New Drugs, 2000. **18**(1): p. 29-42.
208. Amrutkar, M. and I.P. Gladhaug, *Pancreatic Cancer Chemoresistance to Gemcitabine.* Cancers (Basel), 2017. **9**(11).
209. Aye, Y. and J. Stubbe, *Clofarabine 5'-di and -triphosphates inhibit human ribonucleotide reductase by altering the quaternary structure of its large subunit.* Proc Natl Acad Sci U S A, 2011. **108**(24): p. 9815-20.
210. Aye, Y., et al., *Clofarabine targets the large subunit (alpha) of human ribonucleotide reductase in live cells by assembly into persistent hexamers.* Chem Biol, 2012. **19**(7): p. 799-805.
211. Pfisterer, J., et al., *Combination therapy with gemcitabine and carboplatin in recurrent ovarian cancer.* Int J Gynecol Cancer, 2005. **15 Suppl 1**: p. 36-41.
212. DeBerardinis, R.J. and N.S. Chandel, *Fundamentals of cancer metabolism.* Sci Adv, 2016. **2**(5): p. e1600200.
213. Levin, V.A., *The place of hydroxyurea in the treatment of primary brain tumors.* Semin Oncol, 1992. **19**(3 Suppl 9): p. 34-9.
214. Hehlmann, R., et al., *Randomized comparison of busulfan and hydroxyurea in chronic myelogenous leukemia: prolongation of survival by hydroxyurea. The German CML Study Group.* Blood, 1993. **82**(2): p. 398-407.

215. Sterkers, Y., et al., *Acute myeloid leukemia and myelodysplastic syndromes following essential thrombocythemia treated with hydroxyurea: high proportion of cases with 17p deletion.* Blood, 1998. **91**(2): p. 616-22.
216. Vitiello, M., A. Tuccoli, and L. Poliseno, *Long non-coding RNAs in cancer: implications for personalized therapy.* Cell Oncol (Dordr), 2015. **38**(1): p. 17-28.
217. Pavco, P.A., et al., *Antitumor and antimetastatic activity of ribozymes targeting the messenger RNA of vascular endothelial growth factor receptors.* Clin Cancer Res, 2000. **6**(5): p. 2094-103.
218. Mizrahi, A., et al., *Development of targeted therapy for ovarian cancer mediated by a plasmid expressing diphtheria toxin under the control of H19 regulatory sequences.* J Transl Med, 2009. **7**: p. 69.
219. Miller, J.C., et al., *An improved zinc-finger nuclease architecture for highly specific genome editing.* Nat Biotechnol, 2007. **25**(7): p. 778-85.
220. Takahashi, H. and P. Carninci, *Widespread genome transcription: new possibilities for RNA therapies.* Biochem Biophys Res Commun, 2014. **452**(2): p. 294-301.
221. Tsushima, Y., et al., *Uric acid secretion from adipose tissue and its increase in obesity.* J Biol Chem, 2013. **288**(38): p. 27138-49.
222. Kunjara, S., et al., *Pyrimidine nucleotide synthesis in the rat kidney in early diabetes.* Biochem Med Metab Biol, 1991. **46**(2): p. 215-25.
223. Choi, Y.J., et al., *Orotic acid induces hypertension associated with impaired endothelial nitric oxide synthesis.* Toxicol Sci, 2015. **144**(2): p. 307-17.
224. Floyd, S., et al., *The insulin-like growth factor-I-mTOR signaling pathway induces the mitochondrial pyrimidine nucleotide carrier to promote cell growth.* Mol Biol Cell, 2007. **18**(9): p. 3545-55.
225. Ben-Sahra, I., et al., *mTORC1 induces purine synthesis through control of the mitochondrial tetrahydrofolate cycle.* Science, 2016. **351**(6274): p. 728-733.
226. Ben-Sahra, I., et al., *Stimulation of de novo pyrimidine synthesis by growth signaling through mTOR and S6K1.* Science, 2013. **339**(6125): p. 1323-8.
227. Sun, B. and M. Karin, *Obesity, inflammation, and liver cancer.* J Hepatol, 2012. **56**(3): p. 704-13.
228. Pillwein, K., et al., *Insulin regulatory effects on purine- and pyrimidine metabolism in alloxan diabetic rat liver.* Padiatr Padol, 1988. **23**(2): p. 135-44.
229. Zhang, X., et al., *Fine-tuning BMP7 signalling in adipogenesis by UBE2O/E2-230K-mediated monoubiquitination of SMAD6.* EMBO J, 2013. **32**(7): p. 996-1007.
230. Mashtalir, N., et al., *Autodeubiquitination protects the tumor suppressor BAP1 from cytoplasmic sequestration mediated by the atypical ubiquitin ligase UBE2O.* Mol Cell, 2014. **54**(3): p. 392-406.
231. Zhang, X., et al., *UBE2O negatively regulates TRAF6-mediated NF-kappaB activation by inhibiting TRAF6 polyubiquitination.* Cell Res, 2013. **23**(3): p. 366-77.
232. Vila, I.K., et al., *A UBE2O-AMPKalpha2 Axis that Promotes Tumor Initiation and Progression Offers Opportunities for Therapy.* Cancer Cell, 2017. **31**(2): p. 208-224.
233. Hardie, D.G., *An Oncogenic Role for the Ubiquitin Ligase UBE2O by Targeting AMPK-alpha2 for Degradation.* Cancer Cell, 2017. **31**(2): p. 163-165.

DECLARATION

I hereby declare that this doctoral thesis titled, "Long non-coding RNA *lincNMR* in regulation of nucleotide metabolism in liver cancer" is the result of my work. I have not used any other sources or materials than those explicitly indicated and cited. This work was carried out in the division of "RNA Biology and Cancer" at German Cancer Research Center (DKFZ) in Heidelberg under the mentorship of Prof. Dr. Sven Diederichs. Contributions from colleagues in form of scientific collaborations are explicitly referenced in the text. I further declare that this work has not been submitted at any other institution in order to obtain a degree.

_____ _____

Place: Heidelberg, Germany (Minakshi Gandhi)

Date: 23rd May 2019 PhD Student